Computational Modelling of shrinkage in repaired concrete

Mohammed Asad

Civil Engineering

December 1995

Abstract

This study aims at development of a computational model and experimental study of moisture diffusion and shrinkage in cementitious repair materials to evaluate the suitability of a cementitious repair mortar for shrinkage performance. Time-dependent moisture loss in a cementitious repair materials was modeled using moisture diffusion theory. The problem of moisture diffusion is highly non-linear with the diffusion theory. The problem of moisture diffusion is highly non-linear with the diffucivity Kc depending on the moisture content C. Two finite element codes MSTDIFF1 and MSTDIFF2 have been developed which handle one- and two-dimentional moisture diffusion through cementitious materials, respectively. The relationship between the diffusivity Kc and moisture content C, required for the predictin of moisture loss, was established using experimental data of changes in moisture content C at different depths from the drying surface for different drying times. Free shrinkage strains esh in the repair material were determined experimentally and related to the moisture loss M. The relationship established between free shrinkage strains esh and moisture loss M can be used to determine the free shrinkage strains for different values of moisture loss in the repair material.

Free shrinkage strains esh were fed into a finite element based stress analysis program STRSRSYS developed to predict the shrinkage stresses in the repair overlay/substrate concrete system. The suitability of a cementitious repair material for shrinkage performance was evaluated by comparing the stresses developed in the repair material with the premissible maximum stresses. The results of this study show that use of a moisture dependent diffusivity Kc simulates the problem of moisture diffusion through the material more accurately. Free shrinkage strains were noted not to vary linearly with moisture loss, rendering the practice of solving directly the shrinkage diffusion equation questionable. The commercial repair material used yielded high free shrinkage strains resulting in high tensile and shear stresses. The ultimate free shrinkage strain of the repair material had the most significant effect on the level of induced stresses in the repair overlay/substrate concrete system. The restraint provided by the concrete substrate as well as the elastic modulus of the repair material had a significant effect on the level of induced stresses.

Computational Modelling of Shrinkage In Repaired Concrete

by

Mohammed Asad

A Thesis Presented to the

FACULTY OF THE COLLEGE OF GRADUATE STUDIES

KING FAHD UNIVERSITY OF PETROLEUM & MINERALS

DHAHRAN, SAUDI ARABIA

In Partial Fulfillment of the
Requirements for the Degree of

MASTER OF SCIENCE

In

CIVIL ENGINEERING

December, 1995

COMPUTATIONAL MODELLING OF SHRINKAGE IN REPAIRED CONCRETE

BY

MOHAMMED ASAD

A Thesis Presented to the

FACULTY OF THE COLLEGE OF GRADUATE STUDIES

KING FAHD UNIVERSITY OF PETROLEUM & MINERALS

DHAHRAN, SAUDI ARABIA

In Partial Fulfillment of the
Requirements for the Degree of

MASTER OF SCIENCE

In

CIVIL ENGINEERING

December, 1995

KING FAHD UNIVERSITY OF PETROLEUM AND MINERALS

DHAHRAN, SAUDI ARABIA

COLLEGE OF GRADUATE STUDIES

This thesis, written by

Mohammed Asad

under the direction of his Thesis Advisor, and approved by his Thesis committee, has been presented to and accepted by the Dean, College of Graduate Studies, in partial fulfillment of the requirements for the degree of

MASTER OF SCIENCE IN CIVIL ENGINEERING (STRUCTURES)

Thesis Committee:

Dr. Mohammed H. Baluch (Chairman)

Dr. Ali H. Al-Gadhib (Member)

Dr. O. S. B. Al-Amoudi (Member)

Dr. Saeid A. Al-Ghamdi (Member)

Dr. Al-Farabi Sharief
Department Chairman

Dr. Ala H. Al-Rabeh
Dean, College of Graduate Studies

Date : 11.2.91

Dedicated to

my beloved parents

whose prayers, inspiration and love led to this

accomplishment

ACKNOWLEDGEMENT

In the name of Allah, Most Gracious, Most Merciful. Read in the name of thy Lord and Cherisher, Who Created man from a {*leech-like* } clot. Read and thy Lord is Most Bountiful. He Who taught {the use of} the pen. Taught man that which he knew not. Nay, but man doth transgress all bounds. In that he looketh upon himself as self-sufficient. Verily, to thy Lord is the return {of all }. (The Holy Quran, Surah Al-A'alaq, No.96)

First and foremost, all praise to Allah, *subhanahu-wa-ta-Aala*, the Almighty, Who gave me an opportunity, courage and patience to carry out this work. I seek His mercy, favor, and forgiveness. I feel priviledged to glorify His name in the sincerest way through this small accomplishment. May He, *subhanahu-wa-ta-Aaala*, guide me and the whole humanity to the right path *(Aameen)*.

Acknowledgement is due to King Fahd University of Petroleum & Minerals for having given me an opportunity to pursue my graduate study here and for the support provided to this research work.

I am extremely thankful and deeply indebted to my thesis chairman, Dr. Mohammed H. Baluch for his help and advice. I acknowledge him for his valuable time, encouragement and guidance during all stages of this work. Working with him was indeed a learning experience.

I am grateful to my thesis committee member Dr. Ali H. Al-Gadhib, and Dr. O. S. B. Al-Amoudi for their interest, constructive criticism and personal un-

derstanding. Thanks are also due to my thesis committee member, Dr. Saeid. A. Al-Ghamdi for his comments and critical review of the thesis.

I am also thankful to the department chairman, Dr. Alfarabi M. Sharif and other faculty members for their cooperation.

I express my sincere appreciation and thanks to Mr. Ibrahim Asi for his help throughout this work. Thanks to Mr. Omar, Mr. Nahash, Mr. Hasan Zakariya and other staff of the civil engineering laboratories for their help during various stages of this work. I would also like to express my thanks to Mr. Younus of the workshop for fabricating the demec studs used for strain measurement.

I am very much thankful to all my friends in the campus who provided a wonderful company.

Last but not the least, thanks are due to the members of my family for their emotional and moral support throughout my academic career. No personal development could ever take place without the proper guidance of parents. This work is dedicated to my parents for taking pains to fulfill my personal and academic pursuits and shaping my personality.

Contents

List of Tables

List of Figures

ABSTRACT

Name: Mohammed Asad
Title: Computational Modelling of Shrinkage in Repaired Concrete
Major Field: Civil Engineering (Structures)
Date of Degree: December 1995

This study aims at development of a computational model and experimental study of moisture diffusion and shrinkage in cementitious repair materials to evaluate the suitability of a cementitious repair mortar for shrinkage performance. Time-dependent moisture loss in a cementitious repair material was modeled using moisture diffusion theory. The problem of moisture diffusion is highly non-linear with the diffusivity K_c depending on the moisture content C. Two finite element codes MSTDIFF1 and MSTDIFF2 have been developed which handle one- and two-dimensional moisture diffusion through cementitious materials, respectively. The relationship between the diffusivity K_c and moisture content C, required for the prediction of moisture loss, was established using experimental data of changes in moisture content C at different depths from the drying surface for different drying times. Free shrinkage strains ϵ_{sh} in the repair material were determined experimentally and related to the moisture loss M. The relationship established between free shrinkage strains ϵ_{sh} and moisture loss M can be used to determine the free shrinkage strains for different values of moisture loss in the repair material.

Free shrinkage strains ϵ_{sh} were fed into a finite element based stress analysis program STRSRSYS developed to predict the shrinkage stresses in the repair overlay/substrate concrete system. The suitability of a cementitious repair material for shrinkage performance was evaluated by comparing the stresses developed in the repair material with the permissible maximum stresses. The results of this study show that use of a moisture dependent diffusivity K_c simulates the problem of moisture diffusion through the material more accurately. Free shrinkage strains were noted not to vary linearly with moisture loss, rendering the practice of solving directly the shrinkage diffusion equation questionable. The commercial repair material used yielded high free shrinkage strains resulting in high tensile and shear stresses. The ultimate free shrinkage strain of the repair material had the most significant effect on the level of induced stresses in the repair overlay/substrate concrete system. The restraint provided by the concrete substrate as well as the elastic modulus of the repair material had a significant effect on the level of induced stresses.

MASTER OF SCIENCE DEGREE
KING FAHD UNIVERSITY OF PETROLEUM AND MINERALS
Dhahran, Saudi Arabia

ABSTRACT (Arabic)

ملخص

الإسم : محمد أسد

العنوان : موديل رياضي لإنكماش الخرسانة المرممة

التخصص : هندسة مدنية (إنشاءات)

التاريخ : ديسمبر ١٩٩٥ م

تهدف هذه الدراسة إلى تطوير موديل رياضي ودراسة مخبرية لإنتشار السوائل وكذلك إنكماش المواد الإسمنتية المستخدمة كمواد ترميم وذلك لتقييم أداء هذه المواد من حيث ملائمتها في أدائها الإنكماشي . تم عمل موديل لمعرفة كمية فقدان الماء من مواد الترميم الأسمنتية مع الوقت بإستخدام نظرية نفاذية السوائل . من جهة نفادية السوائل هناك علاقة غير خطية بين معامل النفاذية (Kc) ونسبة السوائل . تم تطوير برنامجين (MSTDIFF1) و (MSTDIFF2) بإستخدام طريقة العناصر المحدودة لمعرفة نفاذية السوائل بإتجاه واحد وبإتجاهين . كما تم تطوير العلاقة بين النفاذية ونسبة إحتواء السائل لإستخدامها في حساب كمية فقدان المواد للسوائل . وقد أعتمد في تطوير تلك العلاقة على المعلومات المخبرية لتغير نسبة السوائل عند أعماق مختلفة من سطح العينة في أوقات مختلفة . وإستخدم من قوة الشد الناتجة عن الإنكماش في مواد الترميم والتي تم قياسها مخبرياً في بناء علاقة مع السائل المفقود . ويمكن إستخدام تلك العلاقة في إيجاد قوى الشد الإنكماشي عند فقدان نسب مختلفة من السوائل في مواد الترميم .

تم إستخدام قوى الشد الإنكماشي في برنامج العناصر المحدودة لتحليل الإجهاد (STRSRSYS) والذي تم تطويره لإيجاد قوى الشد الإنكماشية في نظام الخرسانة المرممة في طبقات الترميم والطبقات السفلية . تم تحديد ملائمة مواد الترميم من ناحية أدائها في الإنكماش وذلك بمقارنة قوى الشد الناتجة من مواد الترميم مع القوى القصوى المسموح بها . بينت نتائج هذه الدراسة أن معامل النفاذية يمثل نفاذية السائل خلال المواد بدقة أكبر كما ظهر عدم وجود علاقة خطية بين قوى الشد الإنكماشي ونسبة فقدان المياه . أظهرت المواد التجارية المستخدمة في ترميم الخرسانة قوى شد إنكماشية وقوى قص عالية . ولقوى الشد الإنكماشي القصوى أكبر التأثير على القوى المؤثرة على نظام الخرسانة المرممة . وتلعب القوى الناتجة من الطبقات التي تم ترميمها وكذلك معامل الليونة لمواد الترميم الدور الأساسي في إيجاد قوى الشد في الخرسانة المرممة .

ماجستير في علوم الهندسة

جامعة الملك فهد للبترول والمعادن

الظهران ، المملكة العربية السعودية

Chapter 1

INTRODUCTION

1.1 General

The low durability performance of concrete structures in the Arabian Gulf region has resulted in deterioration problems imposing significant challenge to the construction industry. As a result, the repair and rehabilitation of concrete structures has increased rapidly in recent years and is considered to be the growth sector of the 1990s construction industry.

Concrete members damaged as a result of harsh environment are reinstated by suitable repairs. However, the service life of the concrete repair itself depends on the correct choice and proper use of repair materials. Mistakes in design, selection of materials and construction practices will certainly lead to incompatibility between the repair and the existing concrete substrate. Despite the existence of large and expanding repair and rehabilitation market in the Arabian Gulf region and worldwide, little research has been done to establish performance criteria for repair materials and to study the implications of incompatibility between repair

materials and existing concrete substrate.

Most of the literature reported in the field of concrete repair [1, 2, 3, 4, 5, 6, 7] reveals that dimensional incompatibility, in particular drying shrinkage, is one of the major problems of concrete repair. The problem of drying shrinkage in repair materials is even more critical in the Arabian Gulf region because of the severe service environment characterized by adverse climatic conditions, typified by the large fluctuations in diurnal and seasonal temperature and humidity regimes with the temperature varying as much as $30°C$ during a typical summer day, and the relative humidity ranging from 40 to 100% over a period of 24 hours. These sudden and continuous variations in temperature and humidity create cycles of expansion/contraction and hydration/dehydration in the constrained layer of the repair section which induces thermal and shrinkage stresses leading to cracking and debonding at the interface of the repair layer with the concrete substrate.

Drying shrinkage in cementitious repair materials is brought about by drying and the associated decrease in moisture content. Therefore, it is necessary to estimate the moisture loss as accurately as possible in order to study drying shrinkage in repair materials.

A growing realization of the impact of shrinkage in concrete repair is being translated into a demand for low shrinkage repair materials. This demand, in turn, emphasizes the need to study the shrinkage characteristics of repair materials and to provide the designer with the necessary guidelines to obtain durable concrete repairs.

1.2 Literature Review

In this review of the literature, recent references on the problems associated with the concrete repairs were reviewed first. Literature review was performed on the subject of properties of repair materials necessary for successful concrete repairs. Thereafter, the literature on shrinkage characteristics of repair materials was reviewed. Literature was then reviewed for the analytical and numerical methods used for shrinkage prediction in concrete. Finally, the literature on the prediction of moiture loss in concrete and other cementitious materials was reviewed.

1.2.1 Problems Associated with Concrete Repairs

Emmons and Vaysburd [1] have recently presented their point of view on the current state of knowledge on concrete repair and the methodology for the design and production of long lasting repairs. In the discussion focussing on the factors affecting the durability of concrete repair system (Figure 1.1), compatibility of the repair materials with the existing substrate is identified as the key element in ensuring a successful repair. The factors which govern compatibility, as given in Figure 1.1, are service and exposure conditions of the repair system, loading conditions of composite system and properties of substrate materials. The other factors affecting the durability of concrete repair system, as given in Figure 1.1, are properties of repair materials, repair process which includes surface preparation, application method,

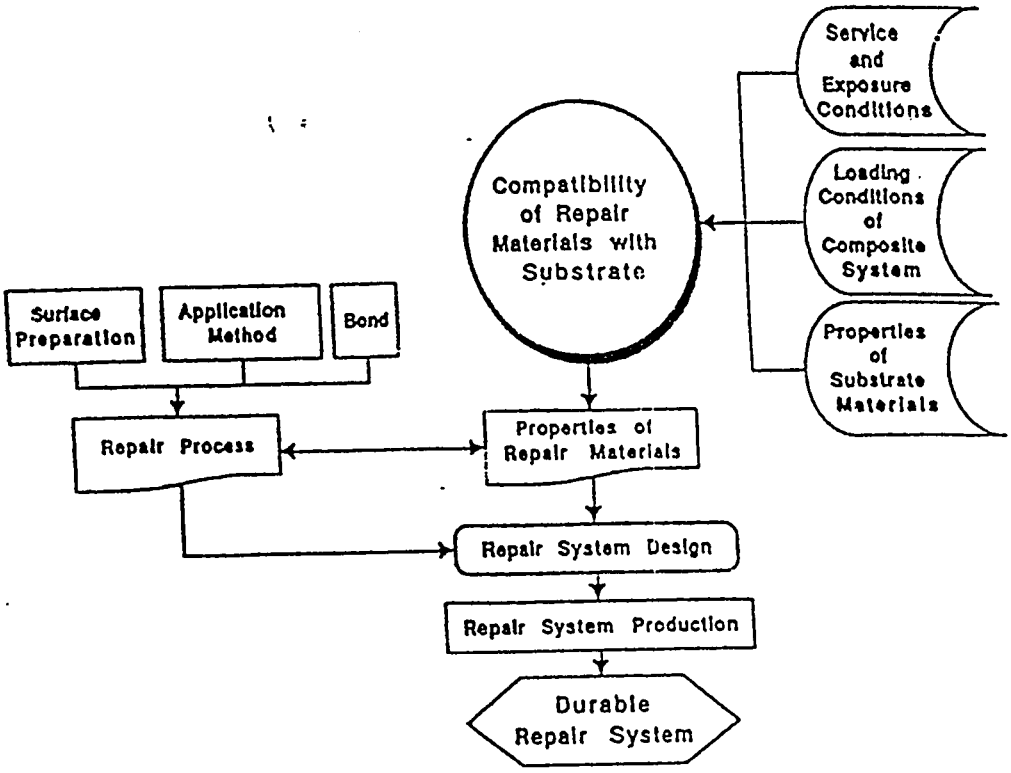

Figure 1.1: Factors Affecting the Durability of Concrete Repair System [1]

and bond between repair material and existing concrete substrate; repair system design, and repair system production.

In their viewpoint, for practical application of repair materials, the emphasis in many cases has to be shifted from compressive strength and/or low permeability to other properties or combinations of properties of the repair material, collectively called compatibility with the existing substrate. They defined compatibility as the balance of physical, chemical, and electrochemical properties and dimensions between repair materials and existing substrates that ensures that a repair can withstand all stresses induced by volume changes, chemical and electrochemical effects without exhibiting distress and deterioration in a specified environment over a designed period of time.

The factors affecting compatibility of repair materials are identified as dimensional compatibility, chemical compatibility, electrochemical compatibility and permeability compatibility [1]. The dimensional compatibility was found to be further affected by drying shrinkage, thermal expansion, creep and modulus of elasticity (Figure 1.2). Emmons and Vaysburd [1] emphasize that drying shrinkage is the most important factor which influences dimensional compatiblity.

Emphasis is placed on the need for complete information on the characteristics of the environment and how these may control the needed properties of repair [1]. It has been found that in many cases, undesired cracking and delamination of repairs were the results of improper choice in matching the repair material specfied

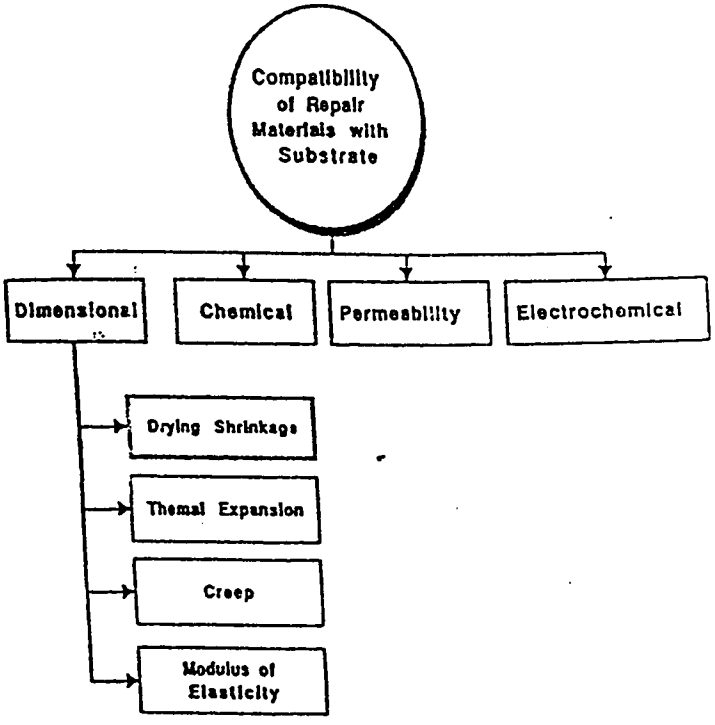

Figure 1.2: Factors Affecting Compatibility of Repair Materials [1]

and selected for use in a given environment with the characteristics of that environment. It is concluded that in order to design the repair for durability, the effect of the environment on the repair; *per se*, as well as the effect of the same environment on the existing substrate and the interface between the two phases should be considered.

1.2.2 Properties of Repair Materials for Successful Concrete Repairs

Emberson and Mays [8] carried out a study to identify the mechanical and physical properties of mortars for patch repair which might be of significance to the subsequent structural behaviour of the repaired member. These properties include strength, modulus of elasticity, coefficient of thermal expansion, tensile adhesion, Poisson's ratio, early curing shrinkage, long term creep and shrinkage. The available test methods to measure these properties were examined and the authors found that many of the tests were deficient or provided unrealistic results. They revised and developed new test methods for which results were questionable. They discussed all the test methods used for measuring the above properties and used nine patch repair systems representing the range of generically different systems available in the market which included resin mortars, polymer modified cementtious mortars and cementitious mortars. The test results revealed a wide range of values for each property. Emberson and Mays [8] concluded that each of the property values and their interaction will be an important consideration in the selection of a repair

system and in the design of a successful patch repair.

Edward and Martin [9] discussed the properties necessary for successful concrete repair materials. The properties included adhesion/bond; shrinkage, thermal movement and cracking; permeability; chemical passivity of embedded steel; mechanical strength; and ease of application. The methods used by the manufacturers (of the repair materials) for testing these characteristics were also described briefly. The test methods described for assessing shrinkage characteristics are the prism test (ASTM C 157), light test (ASTM C 827), micrometer-bridge test (CRD C 621) and shrinkage ring test. Edward and Martin concluded that the selection of a repair material for a particular situation must be on the basis of the properties described [9].

Yuan and Marosszeky [4] investigated the major factors, including the properties of the repair concrete, which affect the performance of serviceability of a repaired beam. Three groups of test beams were repaired by three types of polymer cement concrete to investigate the long-term performance of structural repair. The early age properties of the repair material, such as tensile strength, modulus of elasticity, shrinkage and creep, were investigated under the same environmental conditions as the beams. They also carried out simulation analyses to support this experimental study. From the results of the experiments and analyses [4], the authors found that restrained shrinkage has a quite significant effect on the seviceability. They concluded that early age tensile strain, free shrinkage, creep coefficient and tensile strength are the major factors influencing the performance of structural repair. In

addition to the above factors, they found the stiffness of section and moment redistribution in an indeterminate structure to be the major factors influencing the performance of structural repair.

1.2.3 Shrinkage Characteristics of Repair Materials

Emmons, et al. [2] emphasize the dimensional incompatibility of the repair materials as the major problem of concrete repairs. The focus is on drying shrinkage as the most significant property affecting the dimensional compatibility and the shrinkage characteristics of various repair materials. The authors presented the details of a study conducted by The Alberta Transportation and Utilities in 1987 for concrete patching materials. In that study, 46 different repair materials were evaluated for various properties, one of which was drying shrinkage. The ASTM C 157 shrinkage test was used to determine the shrinkage values. They found that the shrinkage of the majority of the repair materials far exceeded the shrinkage value of a normal concrete, 0.05 percent at 30 days (Figure 1.3). Only seven repair materials out of the 46 tested materials exhibited a shrinkage value less than that of plain concrete. This indicated that many manufacturers of the repair products are not designing their products to minimize shrinkage despite the fact that they claim that their materials to be non-expansive, non-shrinking, or shrinkage-compensating. Moreover, it was found that only limited information on the properties is available from manufacturers' data sheets. Information regarding shrinkage was not even

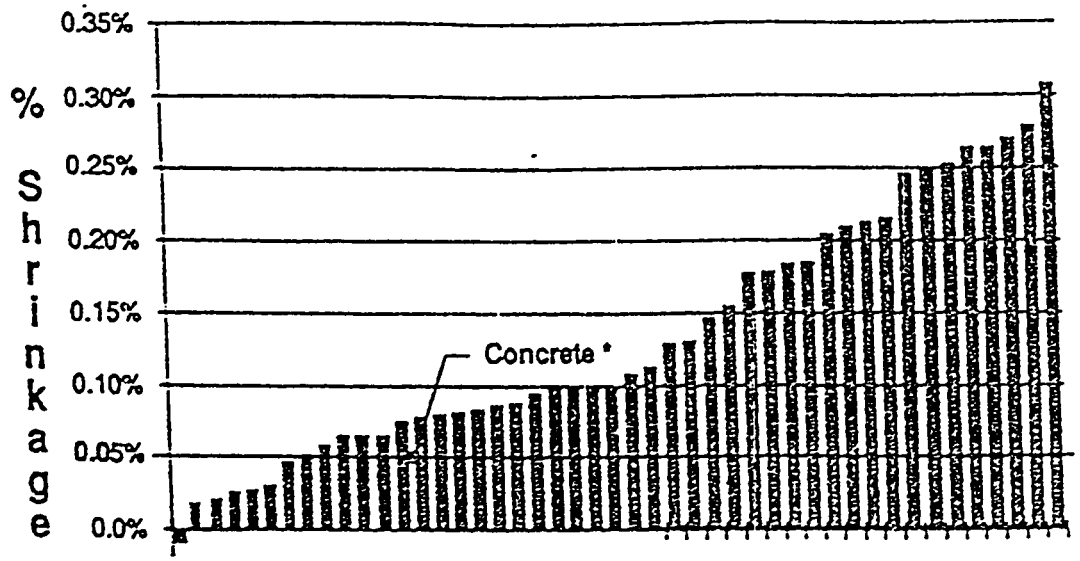

Figure 1.3: Shrinkage Test Results [2]

listed on some of them.

It has been reported that the industry cannot limit the manufacturers of repair materials to a certain maximum shrinkage value because the basis for an acceptable shrinkage value has not been established. ASTM C 928, which provides physical requirements for packaged cementitious concrete repair materials, recommends that shrinkage should not exceed 0.15 percent. This is three times the shrinkage of normal concrete. Thus, the repair materials which satsify the above criterion will be highly susceptible to excessive drying shrinkage stress, cracking, delamination, and failure.

It has been found that there is no standard method of testing the repair materials because different manufacturers use different test methods and standards to evaluate the performance of their products. The most commonly used shrinkage tests by materials manufacturers are ASTM C 157, ASTM C 490, ASTM C 596, CRD C 621-82A, Ring Modified and DIN 52450.

The authors [2] conclude that there is a need to integrate our knowledge and understanding of the compatibility of repair materials with existing concrete and to develop perfomance criteria to provide the engineer with a methodology of modeling for repair durability under various conditions of repair-environment interaction. Since the existing test methods and practices do not produce comparative shrinkage measurements due to variations in techniques and test conditions, an exigent need exists for the industry to choose or develop a test method that will assure reliable

test results for predicting field performance of materials.

Emberson and Mays [3] also emphasized the significance of property mismatch in the patch repair of structural concrete. They measured the mechanical and physical properties of the various repair materials available in the market. The repair materials were categorized as resinous materials, polymer-modified cementitious materials and cementitious materials. Each category had three different types of material, so there were a total of nine types of repair materials. The properties measured were strength, elastic modulus, Poisson's ratio, coefficient of thermal expansion, tensile adhesion, early curing shrinkage, long-term creep and shrinkage. The test methods and specimens used to measure the above properties were discussed briefly. A comparison of the properties measured was made for the nine representative products.

To measure the long-term shrinkage of unrestrained prisms (40mm square by 160mm long) made with mortar were used. Strain gauges were used to measure the shrinkage. The specimens were stored in a room, in which the temperature and humidity varied from 12^{o} to $22^{o}C$ and from 55 to 95%, respectively. Test results indicated that the total shrinkage strains were greatest for the polyester mortar and the vinylacetate modified cementitious mortar. The epoxy and acrylic resin systems had particularly low values of total shrinkage and the magnesium phosphate system is expansive. Shrinkage strains increased with time for all types due to continued drying.

Yuan and Marosszeky [5] presented a computer-based method to analyse corrosion-damaged reinforced concrete elements for repair. The method can estimate the ultimate strength, ductility and stress distribution before and after repair. Also time-dependent analysis can be performed to predict the tensile stress and cracking induced by restrained shrinkage in repaired structural member during hardening, curing and aging of the repair material. They evaluated four different commercial repair materials for the necessary properties . They concluded that it is important to evaluate some material properties such as free shrinkage strain, creep coefficient and modulus of elasticity at an early age, to predict the development of stress and cracking in that period.

1.2.4 Prediction of Shrinkage in Concrete

Shrinkage in concrete has been predicted since long time by solving the shrinkage diffusion equation. Shrinkage was assumed to be directly proportional to the moisture loss and the moisture flow within the concrete was assumed to obey the moisture diffusion equation. These two assumptions led to the shrinkage diffusion equation with shrinkage as the unknown. The following are the references which solved the shrinkage diffusion equation to predict the time-dependent shrinkage in concrete.

Carlson [10] described the application of diffusion principles to compute drying shrinkage in concrete. In his study of distribution of moisture in concrete,

Carlson assumed that the diffusion equation can be used to express the diffusion of moisture from the interior matrix of concrete towards the drying surface.

Pickett [11] derived the theoretical expressions for deformations and distribution of shrinkage stresses in concrete beams and slabs that occur during the course of drying, using an analytical approach for the solution of the boundary value problem governing the diffusion of moisture. It was assumed that, if the flow of water were entirely by vapor diffusion, if the vapor pressure of water in the concrete were proportional to the moisture content, and if the permeability were independent of the moisture content, then the flow of water could be expressed by the diffusion equation. It was further assumed that if the shrinkage tendency of each elemental volume were linearly related to the moisture-content, the unrestrained shrinkage could also be expressed by the diffusion equation.

The three cases considered by Pickett [11] were slab or beam drying from one face only, slab or beam drying from two opposite faces, and prism drying from four faces. Tables and curves were given from which the theoretical shrinkages, stresses, etc., may be obtained, at any point in the specimen after any period of drying, for various values of physical properties, diffusivity, surface factor, ultimate shrinkage, and dimensions of the specimen.

Pickett also considered the applicability of the equations to diffusion of moisture in concrete. It was shown that the shortening of prisms as computed by the theoretical equations was in good agreement with experimental values. Further-

more, it was shown that from a test on one prism, the shortening versus period of drying of other prisms of the same material but differing in size and number of sides exposed to drying can be predicted with fair accuracy if the differences in size were not too great.

Becker and Macinnis [12] presented a theoretical method for predicting the shrinkage of concrete, based on the linear diffusion theory. They assumed that the shrinkage of concrete is a linear function of the average moisture loss over the cross-section. The equations were derived for the slabs drying from one or both sides, rectangular beams drying from four sides and circular columns drying from their circumference.

Graphical solutions for the equations were presented and applied to a wide variety of published experimental data. The proposed theory was used to describe accurately the shrinkage of concrete regardless of the cement composition or fineness, the specimen size and shape, the mix composition, or the ambient relative humidity.

Iding and Bresler [13] presented a finite element approach for predicting the shrinkage stresses and deformations in concrete members. Nonuniform, time-dependent free shrinkage in structural concrete members was modelled by the shrinkage diffusion equation. The effects of ambient relative humidity, surface conditions, and material characteristics of concrete on shrinkage were discussed.

1.2.5 Prediction of Moisture Content in Concrete

Sakata [14] studied the time-dependent phenomenon of moisture diffusion and distribution of water in concrete using the nonlinear diffusion theory. The finite element technique was used to solve the moisture diffusion equation. The diffusion coefficient was determined as a function of moisture content at each time step by the experiment. He showed that the diffusion coefficient was strongly dependent on the relative moisture content at the beginning of drying. The author also found that the moisture loss rate is almost linearly related to the shrinkage strain.

Penev and Kawamura [15] studied the moisture diffusion in soil-cement mixtures and compacted lean concrete. They used the nonlinear moisture diffusion equation along with the appropriate initial and boundary conditions. They derived expressions for the diffusion coefficent as a function of a combined variable of time and space. Moisture losses predicted with the nonlinear theory were in good agreement, especially after drying of 50% of the evaporable water. The diffusion coefficients of lean concretes and soil-cement mixtures were found to be much higher than those in usual concrete. The diffusion coefficients of the lean concrete are larger than those of soil-cements. The difference in diffusion coefficients was attributed to the difference in their pore size distributions. They found that the relation between drying rate and shrinkage strain for the materials studied is not linear. In the soil-cement, the rate of shrinkage surpasses the rate of moisture loss, whereas there was

an opposite trend in lean concretes.

The above review of the literature indicates that the dimensional compatibility between repair materials and the existing concrete substrate is essential for long-lasting of concrete repairs. It also indicates that drying shrinkage is the most important factor influencing dimensional compatibility of concrete repair. No work has yet been identified in the literature which studied the time dependent moisture diffusion in cementitious repair materials. Furthermore, the tests performed by the manufacturers (of the repair materials) for measuring shrinkage in repair materials do not simulate the actual field conditions. The tests reported in the literature are performed on repair materials alone and not on the repaired concrete system.

1.3 Scope and Objectives

The scope of this study was to develop computational models to predict the moisture loss in cementitious repair materials and to predict the stresses induced by the drying shrinkage of the repair material in the repaired concrete system.

The model for moisture loss prediction was based upon the application of the diffusion theory to the problem of computing moisture loss in repair materials. It was assumed that the moisture flow within the repair material obeys the moisture diffusion equation. The moisture diffusion equation is a time-dependent, non-linear equation. The nonlinearity is induced due to the dependence of the diffusivity on

the moisture content. The stress prediction model was based on two-dimensional plane stress formulation with free shrinkage strain of the repair material as the input data.

In addition to the numerical analysis, an experimental determination of moisture loss and drying shrinkage of a typical repair material was carried out. Drying shrinkage data included free shrinkage and restrained shrinkage strains. Restrained shrinkage data was obtained from the specimens in which a repair layer representative of a typically available commercial material was cast over a hardened base concrete.

The main objectives of this study were:

1. Development of a finite element driven computational model to predict moisture loss in cementitious materials, based on both one- and two- dimensional moisture diffusion equations.

2. Execution of an experimental program to determine moisture loss and generate shrinkage data for the repair material.

3. Experimental determination of diffusivity as a function of moisture content.

4. Establishing a relationship between moisture loss and free shrinkage.

5. Development of a finite element based computational model to predict shrinkage stresses in the repair overlay/substrate concrete system.

The flow chart shown in Figure 1.4 depicts the overall numerical and experimental model for the evaluation of repair materials for shrinkage performance.

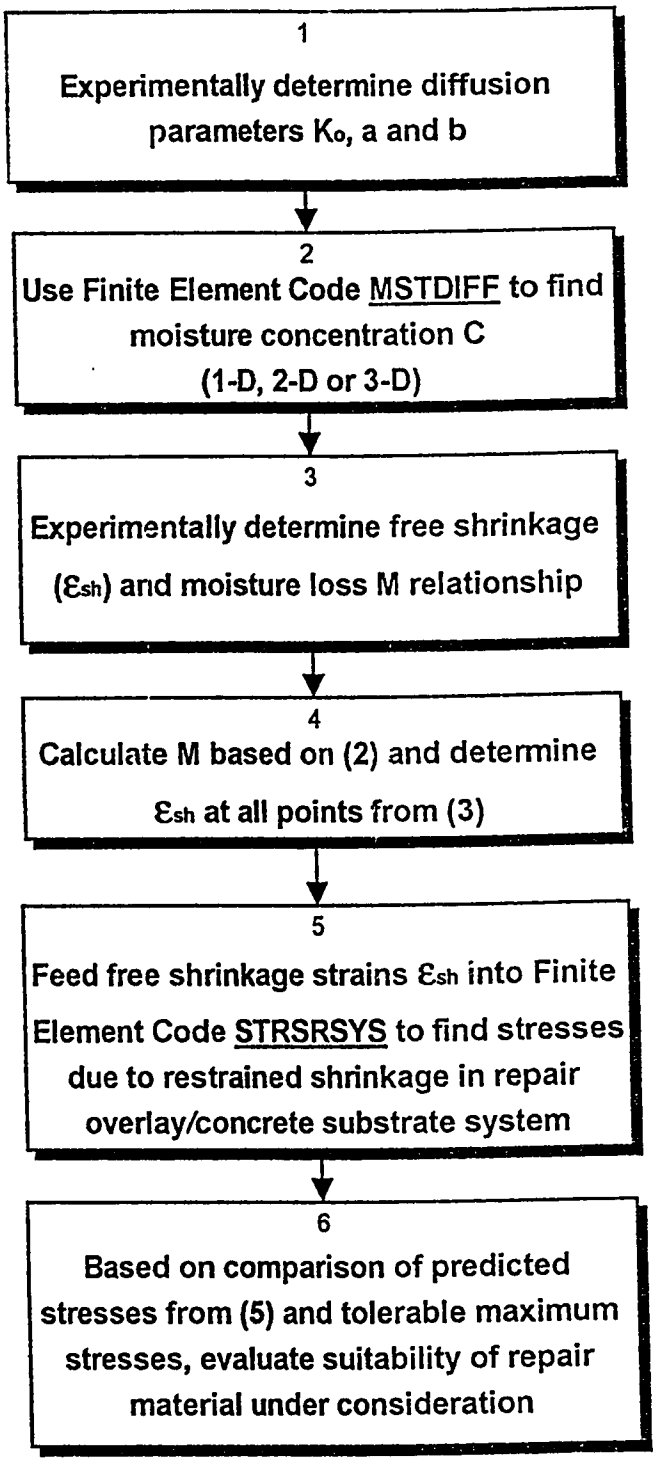

Figure 1.4: Hybrid Numerical/Experimental Model Flow Sequence for Shrinkage Evaluation of Repair Materials

Chapter 2

MOISTURE DIFFUSION AND DRYING SHRINKAGE

2.1 Moisture Diffusion Phenomenon

It is believed that moisture in concrete flows partly as liquid in capillaries, partly as vapour, and partly as adsorbed liquid on the surface of the colloidal products of hydration [10]. The moisture in the interior of drying concrete drifts towards the surface as a vapour. The concentration or humidity of the moisture vapour increases with depth below a concrete surface. While the drying progresses, the vapour pressure of the water remaining in the region losing water decreases progressively with the moisture content. It is this tendency of the vapour pressure to equalize that causes the slow drift of moisture toward the drying surface. Therefore, the shrinkage process starts at the surface that is exposed to drying and gradually penetrates into the concrete [10].

2.2 Drying Shrinkage

Drying shrinkage may be defined as the reduction in volume of concrete caused by the chemical and physical loss of water during the hardening and subsequent exposure to unsaturated air [16]. Drying shrinkage occurs initially at a high rate, and slows down with time, as concrete ages. As a result of the reduction in volume in a constrained member, tensile stresses are produced that may cause cracks thereby affecting the performance of concrete. The mechanism of the formation of cracks in concrete is somewhat complex, largely because of time dependent factors [16].

2.2.1 Drying Shrinkage in Concrete

Consider an unstressed element of concrete under certain conditions of moisture and temperature as shown in Figure. 2.1. If the concrete is dried, provided it is free from restraint, it will reduce in length and no cracks will develop. This contraction of the element when there is no constraint on its movement is termed as 'free shrinkage'.

If, however, the ends of the element are fixed in such a way that the original length is maintained, then a tensile stress will develop in the concrete which is equal to the stress that would be required to pull the free element back to its original length. In practice, the restraint may not be external; in large elements the core of

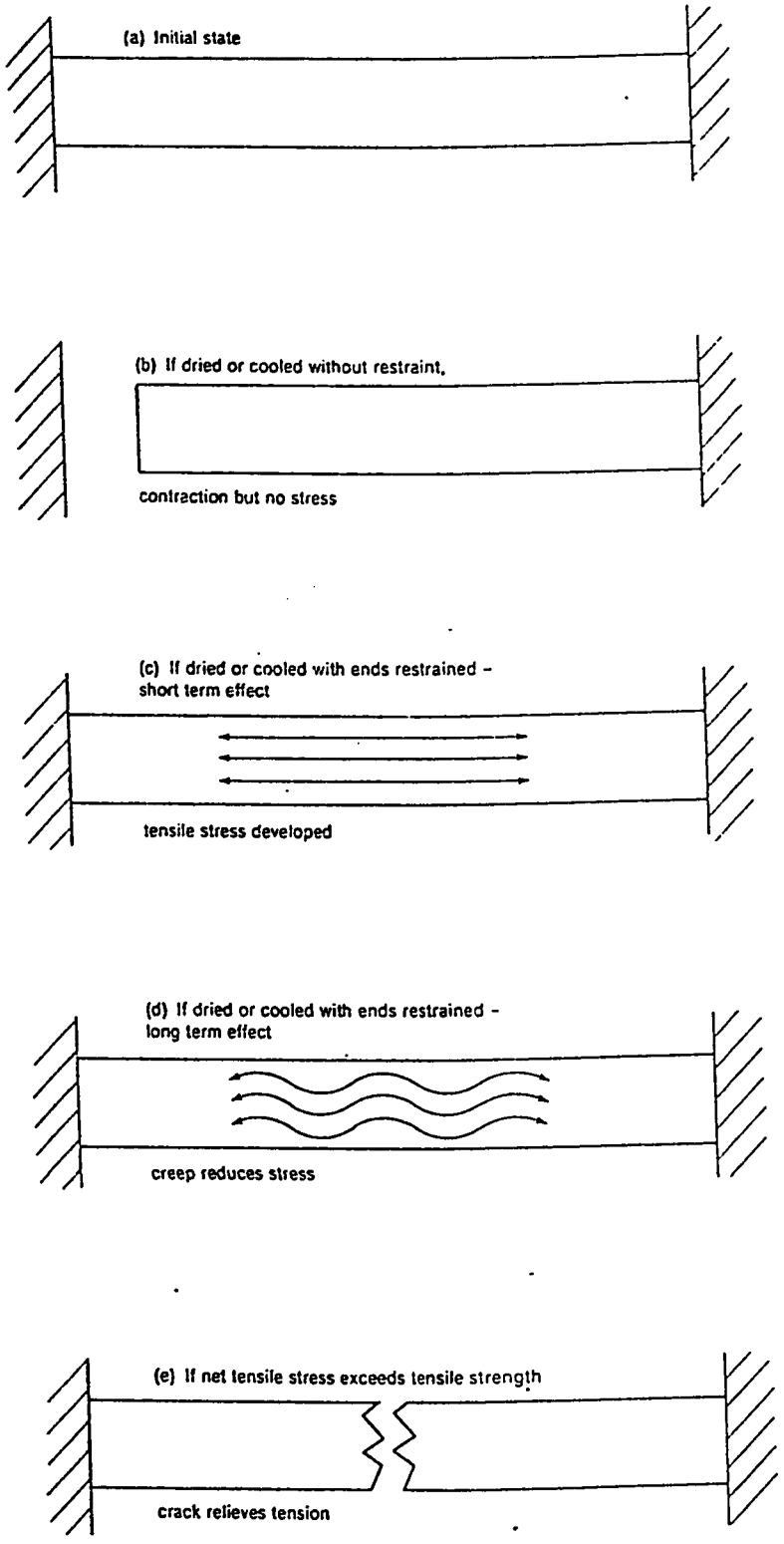

Figure 2.1: Free and Restrained Shrinkage [16]

the concrete may be warmer and wetter than the external surfaces and thus cause internal restraint [16]. The contraction of an element under internal restraint is called as 'apparent shrinkage'. Apparent shrinkage is defined as the experimentally measurable movement within a specimen which includes not only free shrinkage strain but stress-related strain as well [13].

In most simple terms, the concrete will crack when the tensile stress exceeds its tensile strength. However, several time dependent factors must be considred. First, assuming that hydration continues with time (*i.e.* the concrete matures), the 'mechanical' properties of the concrete change. In particular the modulus of elasticity increases and thus the stresses induced by a given strain also increase [16].

A more important factor is that of creep, which causes the stresses induced by a sustained strain to reduce with time as shown in Figure. 2.2. It is only when the net tensile stress exceeds the tensile strength that cracks form. The reduction of stress with time is sometimes called 'relaxation' and has a major effect on reducing the incidence of cracking in concrete. The effect of creep reduces with age of loading; therefore, it is significant in the context of plastic cracks and early thermal contraction cracks. On the other hand, the rate of straining is also important and this tends to be most significant in long-term drying shrinkage cracks [16].

2.2.2 Drying Shrinkage in Patch Repairs

Drying shrinkage of hardened cementitious repair mortar is much more critical

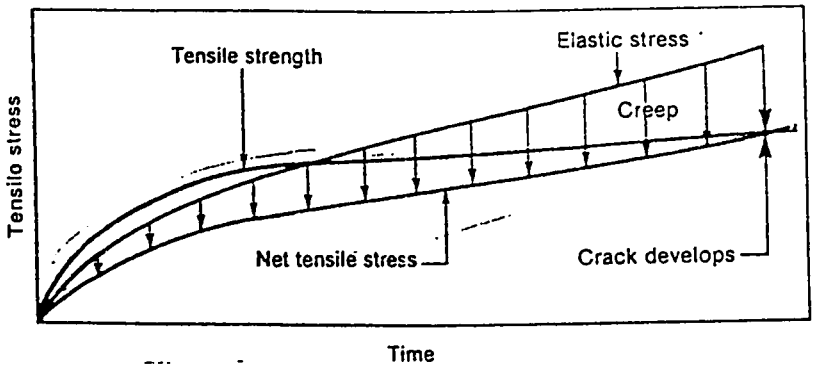

Figure 2.2: Effect of Creep on Net Tensile Strength [16]

than in the case of normal mortars. This is so because of the role it plays in ensuring the longevity of the repair system [17]. In patch repairs, shrinkage of repair mortar is restrained by the existing substrate concrete and this shrinkage of the repair mortar under restraint is termed as 'restrained shrinkage'. Restrained shrinkage induces tensile and shear stresses in the repair material as illustrated in Figure. 2.3, and these stresses increase with the increase in drying shrinkage. Once the tensile and shear strengths are exceeded, these increasing tensile and shear stresses may lead to crack initiation and propagation, debonding and distress along the interfaces between the repair and the substrate. Figure. 2.4 is a photographic evidence of cracking and delamination which occured in a patch repair. The interface is natural plane of weakness and is very susceptible to premature cracking and stress concentration. Figure. 2.5 shows the possible zones of cracking and debonding under tensile and shear stresses respectively, in a patch repair.

If the induced stresses are high then creep plays its role and reduces the stresses with time. Specially, in patch repairs if the rate of straining is high then the effect of creep becomes significant in long-term drying shrinkage cracks.

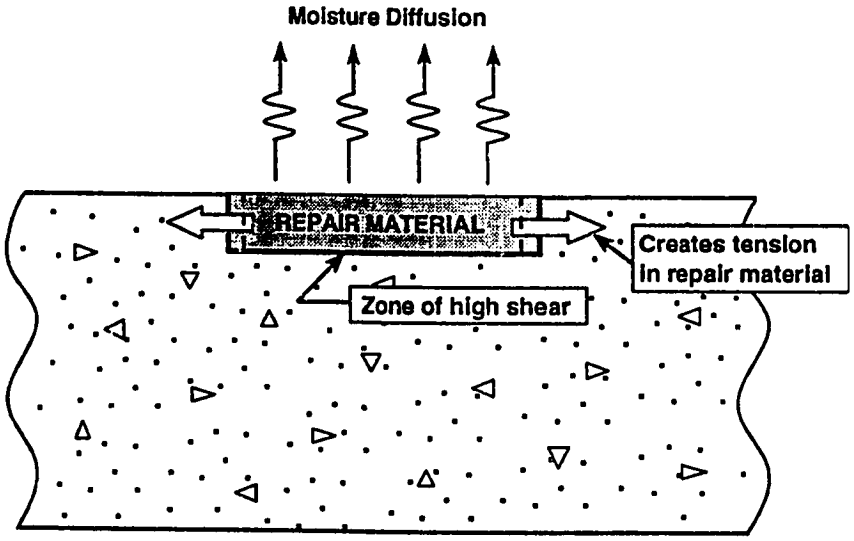

Figure 2.3: Stresses in Patch Repair due to Drying Shrinkage

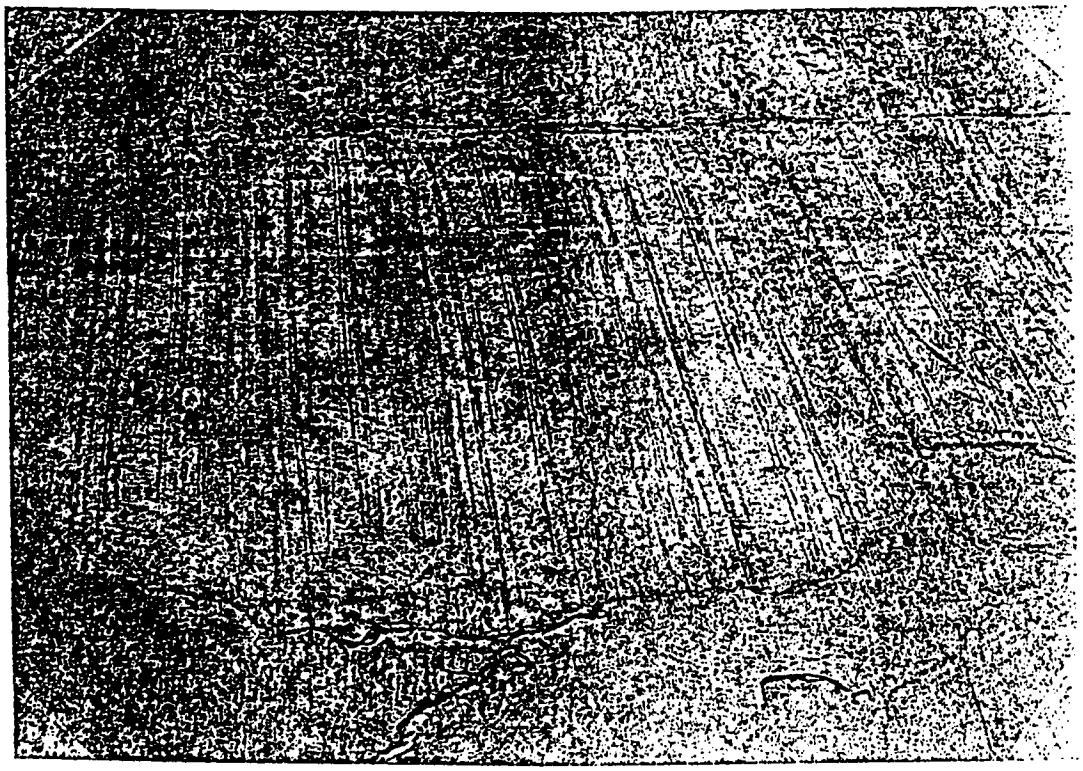

Figure 2.4: Cracking and Delamination in a Patch Repair due to Drying Shrinkage

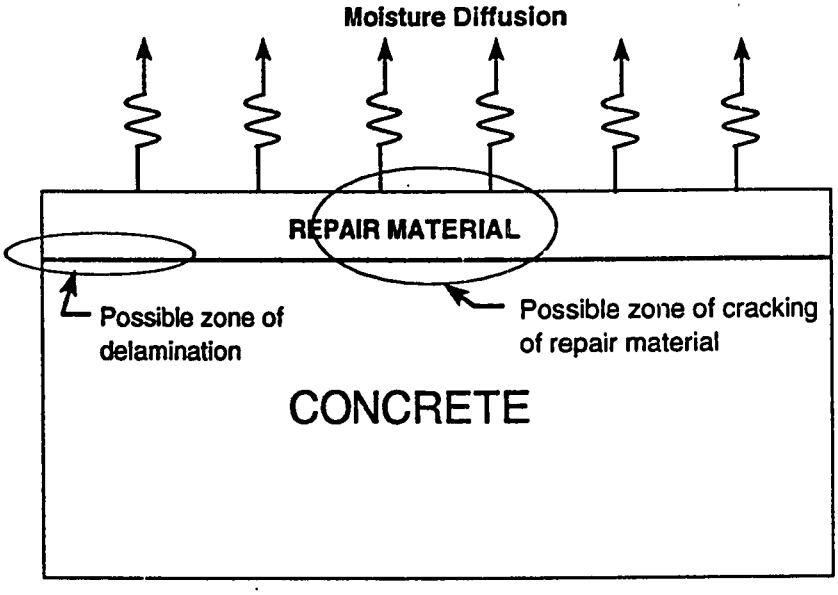

Figure 2.5: Possible Zones of Cracking and Debonding in a Patch Repair

Chapter 3

FORMULATION OF MOISTURE DIFFUSION PROBLEM

3.1 Mathematical Model for Moisture Diffusion

The mathematical model for moisture diffusion is based on the assumption that moisture flow within a cementitious material obeys the moisture diffusion equation [11]. The diffusion equation which is the governing differential equation for moisture flow in porous materials is given by Fick's second law as

$$\frac{\partial C}{\partial t} = \frac{\partial}{\partial x}\left[K_c(C)\frac{\partial C}{\partial x}\right] + \frac{\partial}{\partial y}\left[K_c(C)\frac{\partial C}{\partial y}\right] + \frac{\partial}{\partial z}\left[K_c(C)\frac{\partial C}{\partial z}\right] \qquad (3.1)$$

where $C(x, y, z, t)$ is the moisture content, K_c is the moisture diffusivity and t is the time from start of diffusion process.

The moisture diffusivity K_c is a material property and can be defined as the rate at which the moisture flows through the material when there exists a unit moisture gradient. The diffusivity K_c is highly moisture dependent which renders

the moisture diffusion problem through any porous medium nonlinear.

3.1.1 Initial and Boundary Conditions

The initial condition is

$$C(x, y, z, 0) = C_o(x, y, z) \tag{3.2}$$

where C_o is the initial distribution of moisture content in the moisture flow region.

The boundary conditions at the boundary of moisture flow region and surrounding environment may be a combination of the following:

(a) No-flow boundary

$$\frac{\partial C}{\partial n} = 0 \tag{3.3}$$

(b) Prescribed surface moisture boundary

$$C(x, y, z, t) = C_b(x, y, z, t) \tag{3.4}$$

(c) Surface evaporation boundary

$$K_c(C)\frac{\partial C}{\partial n} = f(C_e - C_s) \tag{3.5}$$

where $\partial C/\partial n$ is the moisture gradient at the drying surface identified by a unit normal n, C_b is the prescribed moisture content at the boundary, f is the surface moisture transfer coefficient or surface factor, C_e is the ultimate or equilibrium moisture content that an element would reach when it reaches steady state equilibrium

with the environmental moisture conditions. It is both a material property depending on mix proportions and a forcing function depending on relative humidity of environment. C_s is the moisture content at the drying surface.

3.2 Finite Element Formulation of One Dimensional Problem

The diffusion equation in one-dimensional form, including domain evaporation as shown in Figure 3.1, is given by

$$\frac{\partial C}{\partial t} = \frac{\partial}{\partial x}\left[K_c(C)\frac{\partial C}{\partial x}\right] - GC + Q \tag{3.6}$$

where $G = fP/A$, $Q = fPC_e/A$, A is the cross sectional area and P is the perimeter around the cross section.

Equation. 3.6 can be transformed to finite element form by the use of the Galerkin's weighted residual method as outlined in [11]. The Galerkin's weighted residual method requires that

$$\int_0^L W_i(x)R(x)dx = 0 \tag{3.7}$$

The residual $R(x)$ is multiplied by a weighting function $W_i(x)$, and the integral of the product is required to be zero. Rewriting Eqn. 3.6 in the form

$$\frac{\partial}{\partial x}\left[K_c(C)\frac{\partial C}{\partial x}\right] - GC + Q - \frac{\partial C}{\partial t} = 0 \tag{3.8}$$

The element contribution to the Galerkin residual equation is given by

$$\left\{R^{(e)}\right\} = -\int_{x_i}^{x_j}[W]^T\left(\frac{\partial}{\partial x}\left[K_c(C)\frac{\partial C}{\partial x}\right] - GC + Q - \frac{\partial C}{\partial t}\right)dx \tag{3.9}$$

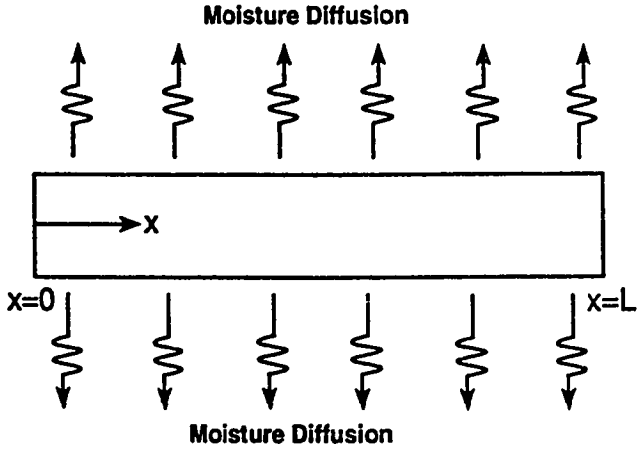

Figure 3.1: One-Dimensional Body with Domain Evaporation

where $[W]^T$ contains the Galerkin weighting functions. Integrating by parts in order to reduce the highest ordered derivative of C in Eqn. 3.9 (since one anticipates use of interpolation functions requiring continuity only of C at nodes)

$$\left\{R^{(e)}\right\} = -\left(K_c(C)[W]^T\frac{\partial C}{\partial x}\right)\Bigg|_{x_i}^{x_j} + \int_{x_i}^{x_j}\left[K_c(C)\frac{\partial [W]^T}{\partial x}\frac{\partial C}{\partial x}\right]dx +$$

$$\int_{x_i}^{x_j}\left[[W]^T GC\right]dx - \int_{x_i}^{x_j}\left[[W]^T Q\right]dx + \int_{x_i}^{x_j}\left[[W]^T\frac{\partial C}{\partial t}\right]dx \qquad (3.10)$$

Within each element, the unknown moisture content, C, is determined by interpolation or shape functions N_i as

$$C = \sum_{i=1}^{n} N_i C_i$$

or

$$C^{(e)} = [N]\left\{C^{(e)}\right\} \qquad (3.11)$$

in which n is the number of nodes associated with each element. In the Galerkin process, the number of weighting functions must equal the number of unknown nodes and therefore choosing $W_i = N_i$, we get $[W]^T = [N]^T$.

Substituting for C from Eqn. 3.11 and selecting $[W]^T = [N]^T$, Eqn. 3.10 becomes

$$\left\{R^{(e)}\right\} = -\left(K_c(C)[N]^T\frac{\partial C}{\partial x}\right)\Bigg|_{x_i}^{x_j} + \left(\int_{x_i}^{x_j}\left[K_c(C)\frac{\partial [N]^T}{\partial x}\frac{\partial [N]}{\partial x}\right]dx\right)\left\{C^{(e)}\right\} +$$

$$\left(\int_{x_i}^{x_j}\left[G[N]^T[N]\right]dx\right)\left\{C^{(e)}\right\} - \int_{x_i}^{x_j}\left[Q[N]^T\right]dx + \left(\int_{x_i}^{x_j}\left[[N]^T[N]\right]dx\right)\left\{\dot{C}^{(e)}\right\} \qquad (3.12)$$

which has the general form

$$\left\{R^{(e)}\right\} = \left\{I^{(e)}\right\} + \left[K^{(e)}\right]\left\{C^{(e)}\right\} + \left[L^{(e)}\right]\left\{\dot{C}^{(e)}\right\} - \left\{F^{(e)}\right\} \tag{3.13}$$

where

$$\left\{I^{(e)}\right\} = -\left(K_c(C)[N]^T\frac{\partial C}{\partial x}\right)\Bigg|_{x_i}^{x_j} \tag{3.14}$$

or

$$\left\{I^{(e)}\right\} = \begin{Bmatrix} K_c(C)\frac{\partial C}{\partial x}\Big|_{x=x_i} \\ -K_c(C)\frac{\partial C}{\partial x}\Big|_{x=x_j} \end{Bmatrix} \tag{3.15}$$

since the shape functions are either zero or one at the respective nodes. Also

$$\left[K^{(e)}\right] = \int_{x_i}^{x_j}\left[K_c(C)\frac{\partial[N]^T}{\partial x}\frac{\partial[N]}{\partial x}\right]dx + \int_{x_i}^{x_j}\left[G[N]^T[N]\right]dx \tag{3.16}$$

$$\left[L^{(e)}\right] = \int_{x_i}^{x_j}\left[[N]^T[N]\right]dx \tag{3.17}$$

and

$$\left\{F^{(e)}\right\} = \int_{x_i}^{x_j}\left[Q[N]^T\right]dx \tag{3.18}$$

The matrix $\left[K^{(e)}\right]$ can be written as

$$\left[K^{(e)}\right] = \left[K_D^{(e)}\right] + \left[K_G^{(e)}\right] \tag{3.19}$$

in which

$$\left[K_D^{(e)}\right] = \int_{x_i}^{x_j}\left[K_c(C)\frac{\partial[N]^T}{\partial x}\frac{\partial N}{\partial x}\right]dx \tag{3.20}$$

or

$$\left[K_D^{(e)}\right] = \int_{x_i}^{x_j}\left[K_c(C)[B]^T[B]\right]dx \tag{3.21}$$

where $[B]$ is the matrix containing the derivatives of the shape functions, and is given by

$$[B] = \begin{bmatrix} \frac{\partial N_i}{\partial x} & \frac{\partial N_j}{\partial x} \end{bmatrix} \tag{3.22}$$

The matrix $\left[K_G^{(e)}\right]$ is

$$\left[K_G^{(e)}\right] = \int_{x_i}^{x_j} \left[G[N]^T[N]\right] dx \tag{3.23}$$

The vector $\left\{I^{(e)}\right\}$ is an interelement vector and, at the boundary, it has to be evaluated using the boundary conditions given in Equations 3.3, 3.4 and 3.5. For the boundary with surface evaporating condition, the part of the vector $\left\{I^{(e)}\right\}$ associated with the boundary condition becomes (for the right boundary)

$$\left\{I^{(e)}\right\} = \begin{Bmatrix} 0 \\ f(C_s - C_e) \end{Bmatrix} = \begin{Bmatrix} 0 \\ fC_j \end{Bmatrix} - \begin{Bmatrix} 0 \\ fC_e \end{Bmatrix} \tag{3.24}$$

since C_s is the same as the moisture content associated with the right node 'j', C_j, Eqn. 3.24 is equivalent to

$$\begin{aligned} \left\{I^{(e)}\right\} &= \begin{bmatrix} 0 & 0 \\ 0 & f \end{bmatrix} \begin{Bmatrix} C_i \\ C_j \end{Bmatrix} - \begin{Bmatrix} 0 \\ fC_e \end{Bmatrix} \\ &= \left[K_M^{(e)}\right] \left\{C^{(e)}\right\} - \left\{f_s^{(e)}\right\} \end{aligned} \tag{3.25}$$

where

$$\left[K_M^{(e)}\right] = \begin{bmatrix} 0 & 0 \\ 0 & f \end{bmatrix} \tag{3.26}$$

and

$$\left\{f_s^{(e)}\right\} = \left\{ \begin{array}{c} 0 \\ \\ fC_e \end{array} \right\} \tag{3.27}$$

The matrix $\left[K_M^{(e)}\right]$ adds to $\left[K^{(e)}\right]$ and the vector $\left\{f_s^{(e)}\right\}$ adds to $\left\{F^{(e)}\right\}$. Assembly of all element contributions given by Eqn. 3.13, on equating to zero results in the following matrix equation

$$[K]\{C\} + [L]\{\dot{C}\} = \{F\} \tag{3.28}$$

where $[K]$ represents the moisture diffusivity matrix, $[L]$ the moisture velocity matrix, $\{F\}$ the external moisture flow vector, $\{C\}$ the nodal moisture content and $\{\dot{C}\}$ the rate of change of nodal moisture content.

3.2.1 Element Stiffness Matrices

The element stiffness matrices are derived using numerical integration. To facilitate numerical integration, the shape functions N_i are expressed in terms of the natural coordinate ξ shown in Fig. 3.2.

For the two noded element, the shape functions are given by

$$N_i = \frac{1}{2}(1-\xi)$$

$$N_j = \frac{1}{2}(1+\xi) \tag{3.29}$$

In order to use numerical integration, Eqn. 3.12 must be transformed into the ξ-coordinate system. For the isoparametric representation, the coordinates for any

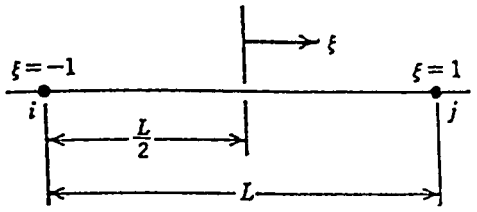

Figure 3.2: Natural Coordinate System for One Dimensional Element

point inside the element can be interpolated using the same shape functions as those that govern variation of moisture C within the element (see Eqn. 3.29), that is

$$x = \sum_{i=1}^{n} N_i x_i \tag{3.30}$$

The Cartesian shape function derivatives needed in Eqn. 3.22 are given as

$$\frac{dN_i}{dx} = \frac{dN_i}{d\xi}\frac{d\xi}{dx} \tag{3.31}$$

or

$$\frac{dN_i}{dx} = [J]^{-1}\frac{dN_i}{d\xi} \tag{3.32}$$

where

$$[J] = \frac{dx}{d\xi}$$

is the Jacobian of the coordinate transformation and

$$[J]^{-1} = \frac{d\xi}{dx}$$

is the inverse of the Jacobian.

Therefore, for a two-noded element Eqns. 3.29 and 3.30 give

$$[J] = \frac{dx}{d\xi} = \sum_{i=1}^{2} \frac{dN_i}{d\xi} x_i = \frac{L}{2} \tag{3.33}$$

and dx needed in Eqn. 3.12 is given as

$$dx = |J| d\xi = \frac{L}{2} d\xi \tag{3.34}$$

The integration to obtain the element matrices can now be performed in ξ-coordinate system. The element matrix $\left[K_D^{(e)}\right]$ in ξ-coordinate system is

$$\left[K_D^{(e)}\right] = \int_{-1}^{+1} \left[K_c(C)[B]^T[B]\right] |J| d\xi \tag{3.35}$$

which on simplification becomes

$$\left[K_D^{(e)}\right] = \frac{1}{2L} \begin{bmatrix} 1 & -1 \\ -1 & 1 \end{bmatrix} \int_{-1}^{+1} K_c(C) d\xi \tag{3.36}$$

The above matrix can further be integrated if the diffusivity K_c is expressed as a function of moisture content C. In this study the diffusivity $K_c(C)$ obtained from experimental investigation (see Section 6.2) is

$$K_c(C) = K_o + a \left(\frac{C}{1-C}\right)^b \tag{3.37}$$

where K_o is the diffusivity at $C = 0\%$ and a and b are regression parameters. Substituting Eqn. 3.11 into Eqn. 3.37 yields

$$K_c(C) = K_o + a \left(\frac{\sum_{i=1}^{2} N_i C_i}{1 - \sum_{i=1}^{2} N_i C_i}\right)^b \tag{3.38}$$

Numerical integration is performed in order to evaluate $\left[K_D^{(e)}\right]$ using one-point integration, with Eqn. 3.36 taking the form

$$\left[K_D^{(e)}\right] = \frac{1}{2L}\begin{bmatrix} 1 & -1 \\ -1 & 1 \end{bmatrix} \sum_{i=1}^{1} f(\xi_i) W_i \tag{3.39}$$

where W_i is the Gauss weighting factor at the sampling point ξ.

Using $f(\xi_i) = K_o + a\left(\frac{\sum_{i=1}^{2} N_i C_i}{1-\sum_{i=1}^{2} N_i C_i}\right)^b$ and simplifying Eqn. 3.39 results in the following

$$\left[K_D^{(e)}\right] = \frac{1}{L}\begin{bmatrix} 1 & -1 \\ -1 & 1 \end{bmatrix} \left[K_o + a\left(\frac{C_1 + C_2}{2 - (C_1 + C_2)}\right)^b\right] \tag{3.40}$$

The matrix $\left[K_G^{(e)}\right]$ can be expressed in ξ-coordinate system as

$$\left[K_G^{(e)}\right] = \frac{GL}{2}\int_{-1}^{+1} \left[[N]^T[N]\right] d\xi \tag{3.41}$$

Evaluation of the integral in Eqn. 3.41 results in

$$\left[K_G^{(e)}\right] = \frac{GL}{6}\begin{bmatrix} 2 & 1 \\ 1 & 2 \end{bmatrix} \tag{3.42}$$

The matrix $\left[K_M^{(e)}\right]$ which is the contribution of the moisture transfer at the element's end, to the matrix $\left[K^{(e)}\right]$ is given as

$$\left[K_M^{(e)}\right] = f\begin{bmatrix} 0 & 0 \\ 0 & 1 \end{bmatrix} \tag{3.43}$$

for evaporation at the right boundary and

$$\left[K_M^{(e)}\right] = f\begin{bmatrix} 1 & 0 \\ 0 & 0 \end{bmatrix} \tag{3.44}$$

for evaporation at the left boundary.

The moisture velocity matrix $\left[L^{(e)}\right]$ in ξ-coordinate system is

$$\left[L^{(e)}\right] = \frac{L}{2}\int_{-1}^{+1}\left[[N]^T[N]\right]d\xi \tag{3.45}$$

which on simplification becomes

$$\left[L^{(e)}\right] = \frac{L}{6}\begin{bmatrix} 2 & 1 \\ 1 & 2 \end{bmatrix} \tag{3.46}$$

The above formulation of the moisture velocity matrix $\left[L^{(e)}\right]$ is called the consistent formulation. The lumped formulation gives the matrix in a diagonal form as follows [18].

$$\left[L^{(e)}\right] = \frac{L}{2}\begin{bmatrix} 1 & 0 \\ 0 & 1 \end{bmatrix} \tag{3.47}$$

The vector $\left\{F^{(e)}\right\}$ which is the load vector due to moisture evaporation into the surrounding environment, is given as

$$\left\{F^{(e)}\right\} = \left\{f_Q^{(e)}\right\} + \left\{f_s^{(e)}\right\} \tag{3.48}$$

The vector $\left\{f_Q^{(e)}\right\}$ is the contribution of the moisture evaporation from the element's perimeter into the environment (referred to as domain evaporation), which in ξ-coordinate system is

$$\left\{f_Q^{(e)}\right\} = \frac{L}{2}\int_{-1}^{+1}\left[Q[N]^T\right]d\xi \tag{3.49}$$

and on simplification becomes

$$\left\{f_Q^{(e)}\right\} = \frac{QL}{2}\begin{Bmatrix} 1 \\ 1 \end{Bmatrix} \tag{3.50}$$

The vector $\left\{f_s^{(e)}\right\}$ is the contribution of the moisture evaporation from the element's end into the environment, and is given as

$$\left\{f_s^{(e)}\right\} = fC_e\begin{Bmatrix} 0 \\ 1 \end{Bmatrix} \tag{3.51}$$

for evaporation at the right boundary and

$$\left\{f_s^{(e)}\right\} = fC_e\begin{Bmatrix} 1 \\ 0 \end{Bmatrix} \tag{3.52}$$

for evaporation at the left boundary.

3.3 Finite Element Formulation of Two Dimensional Problem

The two-dimensional moisture diffusion equation, inclusive of domain evaporation as shown in Fig. 3.3, is

$$\frac{\partial C}{\partial t} = \frac{\partial}{\partial x}\left[K_c(C)\frac{\partial C}{\partial x}\right] + \frac{\partial}{\partial y}\left[K_c(C)\frac{\partial C}{\partial y}\right] - GC + Q \tag{3.53}$$

where $G = 2f/t$, $Q = 2fC_e/t$ and t is the thickness of the body. Rewriting Eqn. 3.53 in the form

$$\frac{\partial}{\partial x}\left[K_c(C)\frac{\partial C}{\partial x}\right] + \frac{\partial}{\partial y}\left[K_c(C)\frac{\partial C}{\partial y}\right] - GC + Q - \frac{\partial C}{\partial t} = 0 \tag{3.54}$$

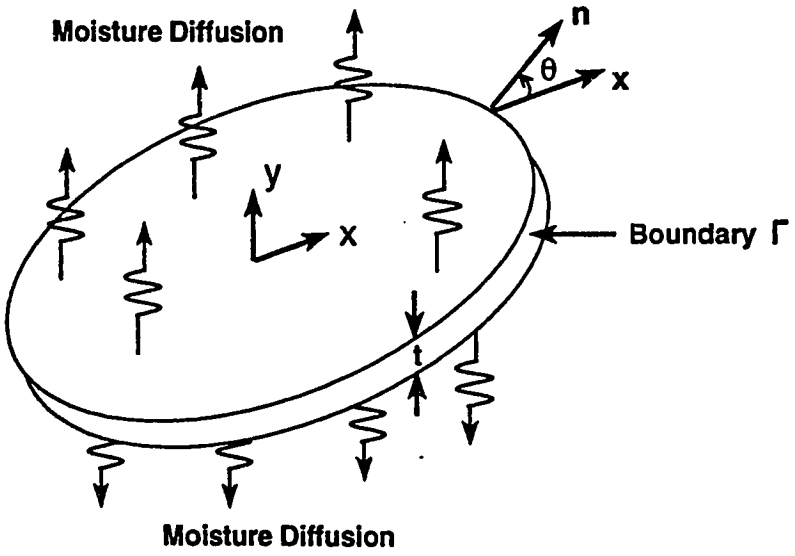

Figure 3.3: Two-Dimensional Body with Domain Evaporation

Using Galerkin's method, the residual integral for each element is

$$\left\{R^{(e)}\right\} = -\int_A [N]^T \left[\frac{\partial}{\partial x}\left[K_c(C)\frac{\partial C}{\partial x}\right] + \frac{\partial}{\partial y}\left[K_c(C)\frac{\partial C}{\partial y}\right] - GC + Q - \frac{\partial C}{\partial t}\right] dA \tag{3.55}$$

where $[N]$ is the row vector containing element shape functions.

Applying Green's theorem for reduction of Eqn. 3.55 to a lower order form results in

$$\begin{aligned}\left\{R^{(e)}\right\} = &-\int_\Gamma [N]^T \left(K_{cx}(C)\frac{\partial C}{\partial x}cos\theta + K_{cy}(C)\frac{\partial C}{\partial y}sin\theta\right) d\Gamma + \\ &\int_A \left(K_{cx}(C)\frac{\partial [N]^T}{\partial x}\frac{\partial C}{\partial x} + K_{cy}(C)\frac{\partial [N]^T}{\partial y}\frac{\partial C}{\partial y}\right) dA + \\ &\int_A \left[[N]^T GC\right] dA - \int_A \left[[N]^T Q\right] dA + \int_A \left[[N]^T \frac{\partial C}{\partial t}\right] dA\end{aligned} \tag{3.56}$$

where θ is the angle between the outward normal n and positive x-axis, measured positive counterclockwise and Γ is the element boundary(see Fig. 3.3).

Element shape functions vector $[N]$ are introduced in order to express $C^{(e)}$ in terms of nodal moisture values, $\left\{C^{(e)}\right\}$

$$C^{(e)} = [N]\left\{C^{(e)}\right\} \tag{3.57}$$

and substitution into Eqn. 3.56 results in

$$\begin{aligned}\left\{R^{(e)}\right\} = &-\int_\Gamma [N]^T \left(K_{cx}(C)\frac{\partial C}{\partial x}cos\theta + K_{cy}(C)\frac{\partial C}{\partial y}sin\theta\right) d\Gamma + \\ &\left(\int_A \left(K_{cx}(C)\frac{\partial [N]^T}{\partial x}\frac{\partial [N]}{\partial x} + K_{cy}(C)\frac{\partial [N]^T}{\partial y}\frac{\partial [N]}{\partial y}\right) dA\right) \left\{C^{(e)}\right\} + \\ &\left(\int_A \left[G[N]^T[N]\right] dA\right)\left\{C^{(e)}\right\} - \int_A \left[Q[N]^T\right] dA + \left(\int_A \left[[N]^T[N]\right] dA\right)\left\{\dot{C}^{(e)}\right\}\end{aligned} \tag{3.58}$$

which has the general form

$$\left\{R^{(e)}\right\} = \left\{I^{(e)}\right\} + \left[K^{(e)}\right]\left\{C^{(e)}\right\} + \left[L^{(e)}\right]\left\{\dot{C}^{(e)}\right\} - \left\{F^{(e)}\right\} \tag{3.59}$$

where

$$\left\{I^{(e)}\right\} = -\int_{\Gamma}[N]^T\left(K_{cx}(C)\frac{\partial C}{\partial x}cos\theta + K_{cy}(C)\frac{\partial C}{\partial y}sin\theta\right)d\Gamma \tag{3.60}$$

$$\left[K^{(e)}\right] = \int_A\left(K_{cx}(C)\frac{\partial[N]^T}{\partial x}\frac{\partial[N]}{\partial x} + K_{cy}(C)\frac{\partial[N]^T}{\partial y}\frac{\partial[N]}{\partial y}\right)dA + \int_A\left[G[N]^T[N]\right]dA \tag{3.61}$$

$$\left[L^{(e)}\right] = \int_A\left[[N]^T[N]\right]dA \tag{3.62}$$

and

$$\left\{F^{(e)}\right\} = \int_A\left[Q[N]^T\right]dA \tag{3.63}$$

The matrix $\left[K^{(e)}\right]$ can be written as

$$\left[K^{(e)}\right] = \int_A\left[[B]^T[K_c][B]\right]dA + \int_A\left[G[N]^T[N]\right]dA \tag{3.64}$$

where $[K_c]$ is a matrix defined as

$$[K_c] = \begin{bmatrix} K_{cx}(C) & 0 \\ 0 & K_{cy}(C) \end{bmatrix} \tag{3.65}$$

and $[B]$ is the matrix containing derivatives of shape fuctions which is given as

$$[B] = \begin{bmatrix} \frac{\partial[N]}{\partial x} \\ \frac{\partial[N]}{\partial y} \end{bmatrix} \tag{3.66}$$

The individual integrals in Eqn. 3.64 are denoted as $\left[K_D^{(e)}\right]$ and $\left[K_G^{(e)}\right]$, therefore

$$\left[K^{(e)}\right] = \left[K_D^{(e)}\right] + \left[K_G^{(e)}\right] \tag{3.67}$$

The vector $\left\{I^{(e)}\right\}$ is an interelement vector and at the boundary it has to be evaluated using the boundary condition

$$K_{cx}(C)\frac{\partial C}{\partial x}cos\theta + K_{cy}(C)\frac{\partial C}{\partial y}sin\theta = -MC_s + S \tag{3.68}$$

where M, S are specified parameters. For insulated or impermeable boundaries or along axes of symmetry

$$K_{cx}(C)\frac{\partial C}{\partial x}cos\theta + K_{cy}(C)\frac{\partial C}{\partial y}sin\theta = 0 \tag{3.69}$$

since both $M = S = 0$. For the boundary with surface evaporation condition, we have $M = f$ and $S = fC_e$ and the vector $\left\{I^{(e)}\right\}$ becomes

$$\left\{I^{(e)}\right\} = \int_\Gamma \left[[N]^T(MC_s - S)\right] d\Gamma \tag{3.70}$$

Substituting Eqn. 3.57 into Eqn. 3.70 produces

$$\left\{I^{(e)}\right\} = \int_\Gamma \left[[N]^T\left(M[N]\left\{C^{(e)}\right\} - S\right)\right] d\Gamma \tag{3.71}$$

which can be separated into

$$\left\{I^{(e)}\right\} = \left(\int_\Gamma \left[M[N]^T[N]\right] d\Gamma\right)\left\{C^{(e)}\right\} - \int_\Gamma \left[S[N]^T\right] d\Gamma \tag{3.72}$$

The first integral in Eqn. 3.72 adds to $\left[K^{(e)}\right]$ and the second integral adds to $\left\{F^{(e)}\right\}$. These two integrals are defined as

$$\left\{I^{(e)}\right\} = \left[K_M^{(e)}\right]\left\{C^{(e)}\right\} - \left\{f_s^{(e)}\right\} \tag{3.73}$$

where

$$\left[K_M^{(e)}\right] = \int_\Gamma \left[M[N]^T[N]\right] d\Gamma \tag{3.74}$$

and

$$\left\{f_s^{(e)}\right\} = \int_\Gamma \left[S[N]^T\right] d\Gamma \tag{3.75}$$

Assembly of all element contributions given by Eqn. 3.59, on equating to zero results in the following matrix equation

$$[K]\{C\} + [L]\{\dot{C}\} = \{F\} \tag{3.76}$$

where the matrices $[K]$, $[L]$, $\{F\}$, $\{C\}$ and $\{\dot{C}\}$ are defined in the same manner as in one-dimensional formulation.

3.3.1 Element Stiffness Matrices

The element stiffness matrices are derived using numerical integration. To facilitate numerical integration, the shape functions N_i are expressed in terms of the natural coordinates (ξ, η).

For the four noded element (Figure 3.4), the shape functions are given as

$$N_1 = \frac{1}{4}(1-\xi)(1-\eta), \qquad N_2 = \frac{1}{4}(1+\xi)(1-\eta)$$

$$N_3 = \frac{1}{4}(1+\xi)(1+\eta), \qquad N_4 = \frac{1}{4}(1-\xi)(1+\eta) \tag{3.77}$$

for the eight noded Serendipity element (Figure 3.4),

$$N_i = \frac{1}{4}(1+\xi\xi_i)(1+\eta\eta_i)(\xi\xi_i + \eta\eta_i - 1) \qquad i = 1,3,5,7$$

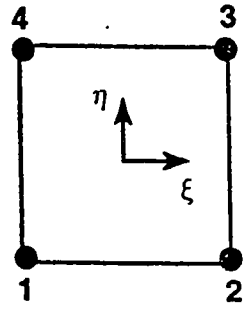

(a) Four-noded element

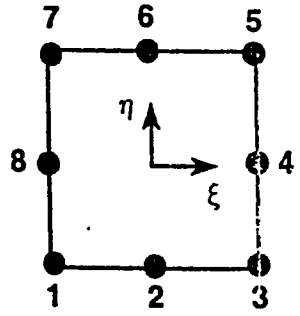

(b) Eight-noded Serendipity element

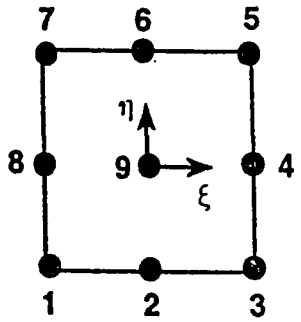

(c) Nine-noded Lagarangian element

Figure 3.4: Two Dimensional Elements

$$N_i = \frac{\xi_i^2}{2}(1+\xi\xi_i)(1-\eta^2) + \frac{\eta_i^2}{2}(1+\eta\eta_i)(1-\xi^2) \qquad i = 2,4,6,8 \qquad (3.78)$$

and for the nine noded Lagarangian element (Figure 3.4),

$$\begin{aligned} N_i &= \frac{1}{4}(\xi^2+\xi\xi_i)(\eta^2+\eta\eta_i) && i = 1,3,5,7 \\ N_i &= \frac{\eta_i^2}{2}(\eta^2+\eta\eta_i)(1-\xi^2) + \frac{\xi_i^2}{2}(\xi^2+\xi\xi_i)(1-\eta^2) && i = 2,4,6,8 \\ N_i &= (1-\xi^2)(1-\eta^2) && i = 9 \end{aligned} \qquad (3.79)$$

To facilitate the use of numerical integration, the elemental area dA in Equations 3.62, 3.63 and 3.64 as well as the matrix $[B]$ in Eqn. 3.66 must be transformed into the natural coordinates(ξ, η) system. For isoparametric representation, as is employed in this study, the coordinates for any point inside the element can be interpolated using similar shape functions as given in Equations 3.77, 3.78 and 3.79, that is

$$\begin{Bmatrix} x \\ y \end{Bmatrix} = \sum_{i=1}^{n} \begin{bmatrix} N_i & 0 \\ 0 & N_i \end{bmatrix} \begin{Bmatrix} x_i \\ y_i \end{Bmatrix} \qquad (3.80)$$

The Cartesian shape function derivatives needed in Eqn. 3.66 can be found by starting with the fact that

$$\begin{aligned} \frac{\partial N_i}{\partial \xi} &= \frac{\partial N_i}{\partial x}\frac{\partial x}{\partial \xi} + \frac{\partial N_i}{\partial y}\frac{\partial y}{\partial \xi} \\ \frac{\partial N_i}{\partial \eta} &= \frac{\partial N_i}{\partial x}\frac{\partial x}{\partial \eta} + \frac{\partial N_i}{\partial y}\frac{\partial y}{\partial \eta} \end{aligned} \qquad (3.81)$$

or

$$\begin{Bmatrix} \frac{\partial N_i}{\partial \xi} \\ \frac{\partial N_i}{\partial \eta} \end{Bmatrix} = \begin{bmatrix} \frac{\partial x}{\partial \xi} & \frac{\partial y}{\partial \xi} \\ \frac{\partial x}{\partial \eta} & \frac{\partial y}{\partial \eta} \end{bmatrix} \begin{Bmatrix} \frac{\partial N_i}{\partial x} \\ \frac{\partial N_i}{\partial y} \end{Bmatrix} = [J] \begin{Bmatrix} \frac{\partial N_i}{\partial x} \\ \frac{\partial N_i}{\partial y} \end{Bmatrix} \qquad (3.82)$$

where

$$J = \begin{bmatrix} \frac{\partial x}{\partial \xi} & \frac{\partial y}{\partial \xi} \\ \frac{\partial x}{\partial \eta} & \frac{\partial y}{\partial \eta} \end{bmatrix} = \begin{bmatrix} \sum_{i=1}^{n} \frac{\partial N_i}{\partial \xi} x_i & \sum_{i=1}^{n} \frac{\partial N_i}{\partial \xi} y_i \\ \sum_{i=1}^{n} \frac{\partial N_i}{\partial \eta} x_i & \sum_{i=1}^{n} \frac{\partial N_i}{\partial \eta} y_i \end{bmatrix} \tag{3.83}$$

is the Jacobian of the coordinate transformation.

Therefore the Cartesian derivatives in Eqn. 3.82 are given as

$$\begin{pmatrix} \frac{\partial N_i}{\partial x} \\ \frac{\partial N_i}{\partial y} \end{pmatrix} = [J]^{-1} \begin{pmatrix} \frac{\partial N_i}{\partial \xi} \\ \frac{\partial N_i}{\partial \eta} \end{pmatrix} \tag{3.84}$$

where the inverse of the Jacobian matrix can be shown to be

$$[J]^{-1} = \begin{bmatrix} \frac{\partial \xi}{\partial x} & \frac{\partial \eta}{\partial x} \\ \frac{\partial \xi}{\partial y} & \frac{\partial \eta}{\partial y} \end{bmatrix} = \frac{1}{|J|} \begin{bmatrix} \frac{\partial y}{\partial \eta} & -\frac{\partial y}{\partial \xi} \\ -\frac{\partial x}{\partial \eta} & \frac{\partial x}{\partial \xi} \end{bmatrix} \tag{3.85}$$

The elemental area dA becomes

$$dA = dxdy = |J| d\xi d\eta \tag{3.86}$$

where $|J|$ is the determinant of [J]. The integration to obtain the element stiffness matrices can now be performed in natural coordinates.

The element matrix $\left[K_D^{(e)}\right]$ now becomes

$$\left[K_D^{(e)}\right] = \int_{-1}^{+1} \int_{-1}^{+1} \left[[B]^T [K_c][B]\right] |J| d\xi d\eta \tag{3.87}$$

in which the submatrix $\left[K_D^{(e)}\right]_{ij}$ linking nodes i and j of the element is given as

$$\left[K_D^{(e)}\right]_{ij} = \int_{-1}^{+1} \int_{-1}^{+1} \left[[B]_i^T [K_c][B]_j\right] |J| d\xi d\eta \tag{3.88}$$

In this study the diffusivity $K_c(C)$ obtained from experimental investigation (see Section 6.2) is

$$K_{cx}(C) = K_o + a\left(\frac{C}{1-C}\right)^b \tag{3.89}$$

where K_o is diffusivity at $C = 0\%$ and a and b are regression parameters.

Substituting the relationship of Eqn. 3.57 in Eqn. 3.89, results in

$$K_{cx}(C) = K_o + a\left(\frac{\sum_{i=1}^{n} N_i C_i}{1-\sum_{i=1}^{n} N_i C_i}\right)^b \tag{3.90}$$

Assuming isotropic diffusion characteristics, *i.e.* $K_{cx}(C) = K_{cy}(C)$ and substituting Eqn. 3.90 in Eqn. 3.88 results in

$$\left[K_D^{(e)}\right]_{ij} = \int_{-1}^{+1}\int_{-1}^{+1}\left[\left(K_o + a\left(\frac{\sum_{i=1}^{n} N_i C_i}{1-\sum_{i=1}^{n} N_i C_i}\right)^b\right)[B]_i^T[B]_j\right]|J|d\xi d\eta$$

$$= \int_{-1}^{+1}\int_{-1}^{+1} f(\xi,\eta)d\xi d\eta \tag{3.91}$$

where $f(\xi,\eta) = \left[\left(K_o + a\left(\frac{\sum_{i=1}^{n} N_i C_i}{1-\sum_{i=1}^{n} N_i C_i}\right)^b\right)[B]_i^T[B]_j\right]|J|$.

Numerical integration is performed using two or three point integration rule depending upon the highest power of ξ and η in the element shape functions. Thus Eqn. 3.91 becomes

$$\left[K_D^{(e)}\right]_{ij} = \sum_{p=1}^{m}\sum_{q=1}^{n} f(\xi_p,\eta_q)W_pW_q \tag{3.92}$$

where W_p and W_q are the Guass weighting factors at the sampling points (ξ_p,η_q).

The element matrix $\left[K_G^{(e)}\right]$ in natural coodinates is

$$\left[K_G^{(e)}\right] = G\int_{-1}^{+1}\int_{-1}^{+1}\left[[N]^T[N]\right]|J|d\xi d\eta \tag{3.93}$$

in which the submatrix $\left[K_G^{(e)}\right]_{ij}$ is given as

$$\left[K_G^{(e)}\right]_{ij} = G\int_{-1}^{+1}\int_{-1}^{+1}\left[[N]_i^T[N]_j\right]|J|d\xi d\eta$$
$$= G\int_{-1}^{+1}\int_{-1}^{+1} f(\xi,\eta)d\xi d\eta \tag{3.94}$$

where $f(\xi,\eta) = \left[[N]_i^T[N]_j\right]|J|$.

The matrix $\left[K_M^{(e)}\right]$ can be written as

$$\left[K_M^{(e)}\right] = M\int_{-1}^{+1}\left[[N]^T[N]\right]\frac{L}{2}d\xi$$

for integration in ξ-direction and

$$\left[K_M^{(e)}\right] = M\int_{-1}^{+1}\left[[N]^T[N]\right]\frac{L}{2}d\eta \tag{3.95}$$

for integration in η-direction. The submatrix $\left[K_M^{(e)}\right]_{ij}$ for integration in ξ-direction is given as

$$\left[K_M^{(e)}\right]_{ij} = \frac{ML}{2}\int_{-1}^{+1}\left[[N]_i^T[N]_j\right]d\xi$$
$$= \frac{ML}{2}\int_{-1}^{+1} f(\xi,\eta)d\xi \tag{3.96}$$

and for integration in η-direction

$$\left[K_M^{(e)}\right]_{ij} = \frac{ML}{2}\int_{-1}^{+1}\left[[N]_i^T[N]_j\right]d\eta$$
$$= \frac{ML}{2}\int_{-1}^{+1} f(\xi,\eta)d\eta \tag{3.97}$$

where $f(\xi,\eta) = [N]_i^T[N]_j$.

The element matrix $\left[L^{(e)}\right]$ is given as

$$\left[L^{(e)}\right] = \int_{-1}^{+1}\int_{-1}^{+1}\left[[N]^T[N]\right]|J|d\xi d\eta \tag{3.98}$$

in which the submatrix $\left[L^{(e)}\right]_{ij}$ is

$$\left[L^{(e)}\right]_{ij} = \int_{-1}^{+1}\int_{-1}^{+1}\left[[N]_i^T[N]_j\right]|J|d\xi d\eta$$

$$= \int_{-1}^{+1}\int_{-1}^{+1} f(\xi,\eta)d\xi d\eta \tag{3.99}$$

where $f(\xi,\eta) = \left[[N]_i^T[N]_j\right]|J|$.

The vector $\left\{f_Q^{(e)}\right\}$ in natural coodinates is

$$\left\{f_Q^{(e)}\right\} = Q\int_{-1}^{+1}\int_{-1}^{+1}[N]^T|J|d\xi d\eta \tag{3.100}$$

in which each element $\left\{f_Q^{(e)}\right\}_i$ is given as

$$\left\{f_Q^{(e)}\right\}_i = Q\int_{-1}^{+1}\int_{-1}^{+1}[N]_i^T|J|d\xi d\eta$$

$$= Q\int_{-1}^{+1}\int_{-1}^{+1} f(\xi,\eta)d\xi d\eta \tag{3.101}$$

where $f(\xi,\eta) = [N]_i^T|J|$.

The vector $\left\{f_s^{(e)}\right\}$ can be written as

$$\left\{f_s^{(e)}\right\} = S\int_{-1}^{+1}[N]^T\frac{L}{2}d\xi$$

for integration in ξ-direction and

$$\left\{f_s^{(e)}\right\} = S\int_{-1}^{+1}[N]^T\frac{L}{2}d\eta \tag{3.102}$$

for integration in η-direction. The element $\left\{f_s^{(e)}\right\}_i$ for integration in ξ-direction is given as

$$\left\{f_s^{(e)}\right\}_i = \frac{SL}{2}\int_{-1}^{+1}[N]_i^T d\xi$$

$$= \frac{SL}{2} \int_{-1}^{+1} f(\xi, \eta) d\xi \tag{3.103}$$

and for integration in η-direction

$$\left\{ f_s^{(e)} \right\}_i = \frac{SL}{2} \int_{-1}^{+1} [N]_i^T d\eta$$

$$= \frac{SL}{2} \int_{-1}^{+1} f(\xi, \eta) d\eta \tag{3.104}$$

where $f(\xi, \eta) = [N]_i^T$.

3.4 Finite Difference Scheme for Time

For time-dependent problems, it is effective to employ numerical solutions in the time domain to get the solution of the differential equation. There are several procedures for numerically solving Equations 3.28 and 3.76. In this study, the finite difference method has been used to generate a numerical solution in the time domain [11].

The mean value theorem for differentiation gives

$$\frac{\partial \{C\}}{\partial t} = \frac{\{C\}^{t+\Delta t} - \{C\}^t}{\Delta t} \tag{3.105}$$

where Δt is the time step and $\{C\}^{t+\Delta t}$ and $\{C\}^t$ are the vectors containing nodal values of moisture contents at time $t + \Delta t$ and t, respectively.

The vector $\{C\}$ at time $t = t^*$ within the time step Δt is given as

$$\{C\} = (1 - \theta)\{C\}^t + \theta\{C\}^{t+\Delta t} \tag{3.106}$$

where θ is the ratio defined as

$$\theta = \frac{t^* - t}{\Delta t} \tag{3.107}$$

The vector $\{F\}$ is the same at times t and $t + \Delta t$. Equations 3.28 and 3.76 can now be written in terms of $\{C\}^t$ and $\{C\}^{t+\Delta t}$ by substituting Equations 3.105 and 3.106. The result is

$$([L] + \theta\Delta t[K])\{C\}^{t+\Delta t} = ([L] - (1-\theta)\Delta t[K])\{C\}^t + \Delta t\{F\} \tag{3.108}$$

Equation 3.108 gives nodal values $\{C\}^{t+\Delta t}$ in terms of a set of known values, $\{C\}$ and the ratio θ.

There are four different finite difference schemes depending upon the value of θ. The finite difference equation for each value of θ is as follows:

1. Forward difference method ($\theta = 0, \xi = t$)

$$[L]\{C\}^{t+\Delta t} = ([L] - \Delta t[K])\{C\}^t + \Delta t\{F\} \tag{3.109}$$

2. Central difference method ($\theta = \frac{1}{2}, \xi = \frac{\Delta t}{2}$)

$$\left([L] + \frac{\Delta t}{2}[K]\right)\{C\}^{t+\Delta t} = \left([L] - \frac{\Delta t}{2}[K]\right)\{C\}^t + \Delta t\{F\} \tag{3.110}$$

3. Galerkin's method ($\theta = \frac{2}{3}, \xi = \frac{2\Delta t}{3}$)

$$\left([L] + \frac{2\Delta t}{3}[K]\right)\{C\}^{t+\Delta t} = \left([L] - \frac{\Delta t}{3}[K]\right)\{C\}^t + \Delta t\{F\} \tag{3.111}$$

4. Backward difference method ($\theta = 1, \xi = t + \Delta t$)

$$([L] + \Delta t[K])\{C\}^{t+\Delta t} = [L]\{C\}^t + \Delta t\{F\} \tag{3.112}$$

The equations for all the four finite difference schemes has the following general form, regardless of the value of θ:

$$[A]\{C\}^{t+\Delta t} = [P]\{C\}^{t} + \{F^{*}\} \tag{3.113}$$

where $[A]$ and $[P]$ are combinations of $[L]$ and $[K]$ and are dependent on the time step Δt and since the diffusivity K_c is a function of moisture content $\{C\}$, it changes during the solution process and therefore $[A]$ and $[P]$ are re-evaluated for each time step.

The solution of Eqn. 3.108 for any value of θ has some stability problems such as numerical oscillations. However, it has been proven [18, 19] that the numerical solutions of Eqn. 3.108 are unconditionally stable when $\theta \geq \frac{1}{2}$. In this study, backward difference method is employed since it is unconditionally stable and the solution would not suffer from numerical oscillations [18].

3.5 Iterative Solution

For the case of non-linear problems, the solution has to be obtained iteratively for each time step because Eqn. 3.113 will not be satisfied and a residual vector $\{\Psi\}$ will exist, so that

$$\{\Psi\} = [A]\{C\}^{t+\Delta t} - [P]\{C\}^{t} - \{F^{*}\} \neq 0 \tag{3.114}$$

The iterations are continued till convergence is attained, *i.e* when a selected norm of the residual vector $\{\Psi\}$ becomes less than a specified level of tolerance.

Chapter 4

COMPUTER PROGRAM IMPLEMENTATION

4.1 Description of Moisture Diffusion Programs

Two different computer programs MSTDIFF1 and MSTDIFF2 were developed for computing the time-dependent moisture loss from a cementitious repair material. The code MSTDIFF1 handles the one-dimensional diffusion problem and the code MSTDIFF2 handles the two-dimensional diffusion problem. These codes were developed in FORTRAN programming language using the programming concepts described by Hinton and Owen [20, 21].

4.1.1 One-Dimensional Moisture Diffusion Program MSTDIFF1

The execution of the code MSTDIFF1 can be described as follows:

1. Reads the input data for description of geometry, material properties, boundary conditions, equillibrium moisture content, time step, and number of incre-

ments on time. It also computes the nodal forces $\{F\}$ for each element, due to domain evaporation and evaporation through sides.

2. Computes the element diffusivity matrices $[K]$ for the initial moisture content *i.e.* at time=0 and also computes the element moisture velocity matrices $[L]$, using either consistent formulation or lumped formulation.

3. Assembles all the element matrices to form global matrices.

4. Enters a loop for time increments.

5. Combines the matrices $[K]$, $[L]$ and $\{F\}$ according to a specified finite difference scheme. The options for finite difference scheme are forward difference, central difference, Galerkin's method and backward difference scheme.

6. Computes the moisture content $\{C\}$ by solving the matrix equation obtained in (5) using Guass reduction and back substitution.

7. Enters a loop for iterative solution.

8. Updates the element diffusivity matrices $[K]$ for the values of moisture content $\{C\}$ obtained in the previous iteration.

9. Assembles all element matrices and then combines the global matrices using the specified finite difference scheme.

10. Calculates the unbalanced residual moisture content vector $\{\Psi\}$ for this iteration.

11. Checks the solution for convergence based on the level of tolerance applied to the norm of residual vector $\{\Psi\}$.

12. If the solution converges, then it prints results of moisture content $\{C\}$ and moisture loss $\{M\} = \{I\} - \{C\}$, where $\{I\}$ is a vector whose entries are unity, for the particular time step. Otherwise, it solves the matrix equation obtained in (9) for moisture content values in this iteration and continues steps (8) to (11) till convergence.

13. Increments the time step and repeats steps (5) to (12) for the number of time increments specified.

Hence, finally we obtain the moisture content $\{C\}$ and moisture loss $\{M\}$ at different drying times. The flow chart of the computer program MSTDIFF1 is depicted in Figure 4.1. The input data to the code MSTDIFF1, for the one-dimensional moisture diffusion problem discussed in Section 6.3, is given in Appendix B.

4.1.2 Two-Dimensional Moisture Diffusion Program MSTDIFF2

The execution of the code MSTDIFF2 is as follows:

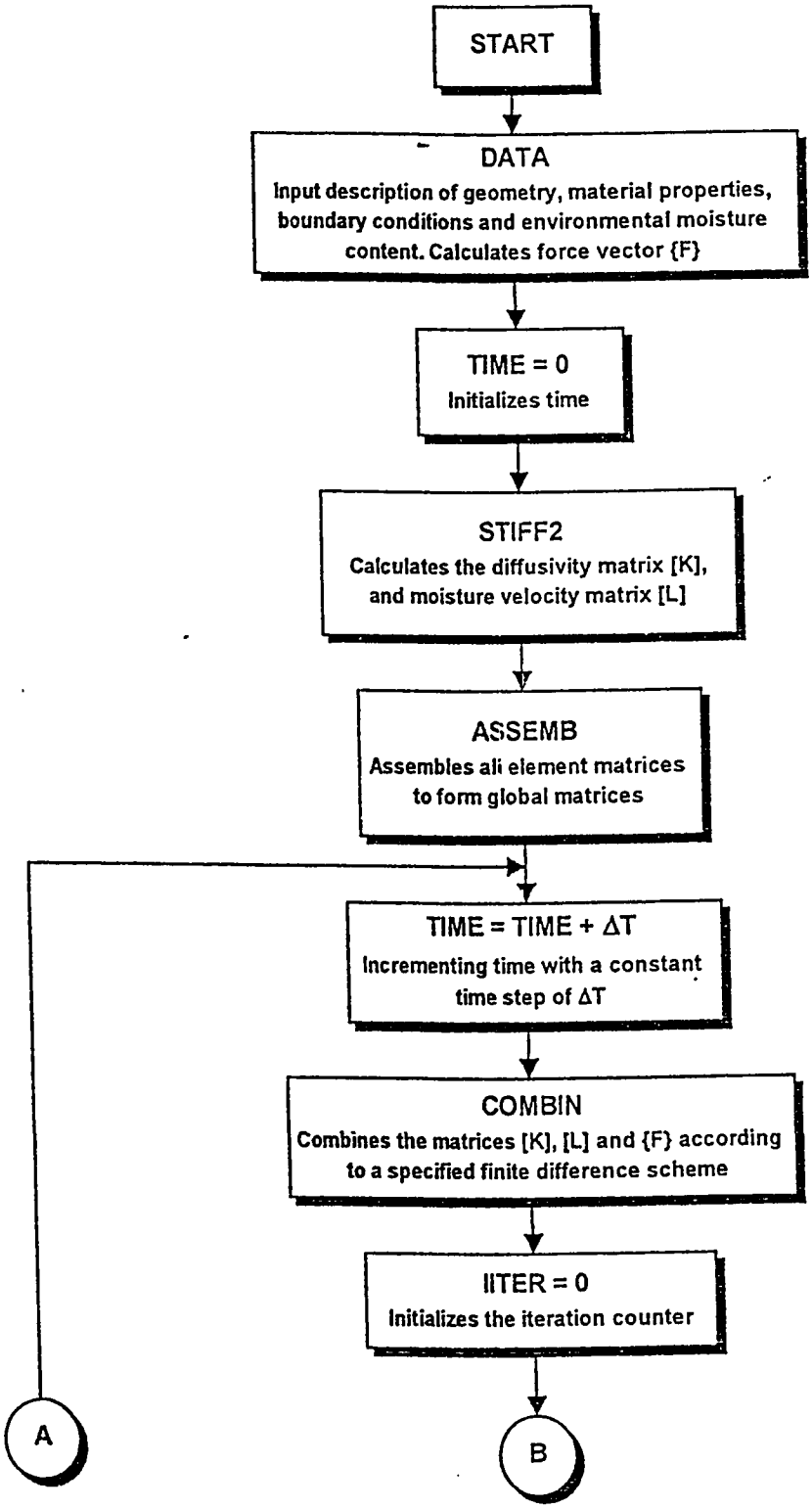

Figure 4.1: Flowchart of One-Dimensional Moisture Diffusion Program MSTDIFF1

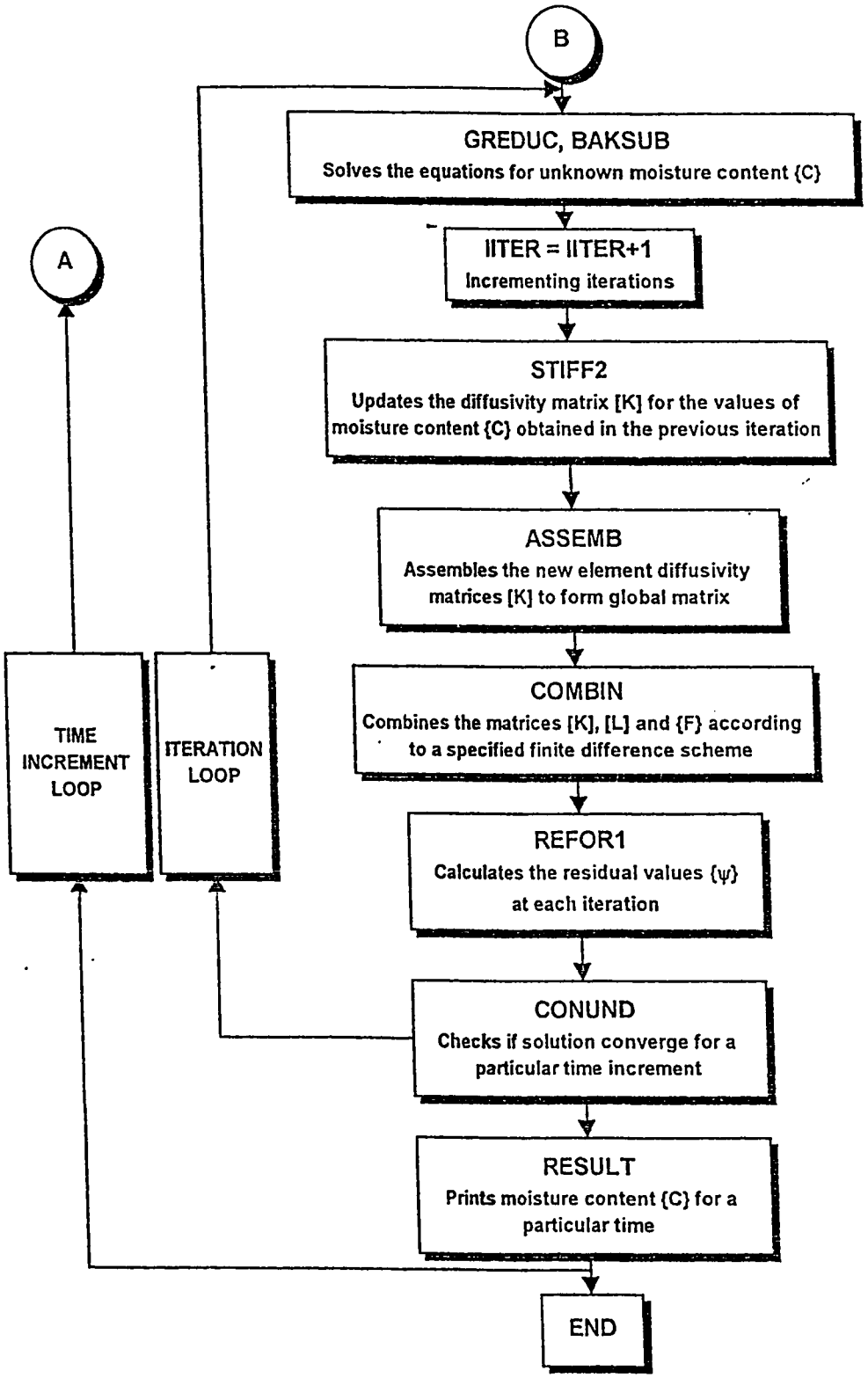

Figure 4.2: Flowchart of One-Dimensional Moisture Diffusion Program MSTDIFF1 (Continued)

1. Reads the input data for description of geometry, material properties, boundary conditions, equillibrium moisture content, time step, and number of increments on time.

2. Computes the nodal forces $\{f_Q\}$ for each element, which is the contribution of the domain evaporation to the element nodal forces $\{F\}$.

3. Computes the diffusivity matrix $[K_G]$ for each element, which is the contribution of the domain evaporation to the element diffusivity matrix $[K]$ and also computes the element moisture velocity matrices $[L]$, using either consistent formulation or lumped formulation.

4. Computes the diffusivity matrix $[K_M]$ and nodal forces $\{f_s\}$ for each edge with surface evaporation as boundary condition and associates them to the element diffusivity matrix $[K]$ and element nodal forces $\{F\}$ of the element associated with that edge.

5. Computes the element diffusivity matrices $[K_D]$ for the initial moisture content, *i.e.* at time=0 and adds them to the element matrices $[K]$.

6. Assembles all the element matrices to form global matrices.

7. Enters a loop for time increments.

8. Combines the matrices $[K]$, $[L]$ and $\{F\}$ according to a specified finite difference scheme. The options for finite difference scheme are forward difference,

central difference, Galerkin's method and backward difference scheme.

9. Computes the moisture content $\{C\}$ by solving the matrix equation obtained in (8) using Guass reduction and back substitution.

10. Enters a loop for iterative solution.

11. Updates the element diffusivity matrices $[K_D]$ for the values of moisture content $\{C\}$ obtained in the previous iteration.

12. Assembles all element matrices and then combines the global matrices using the specified finite difference scheme.

13. Calculates the unbalanced residual moisture content vector $\{\Psi\}$ for this iteration.

14. Checks the solution for convergence based on the level of tolerance applied to values of residual vector $\{\Psi\}$.

15. If the solution converges, then it prints results of moisture content $\{C\}$ and moisture loss $\{M\}$ for the particular time step, otherwise, it solves the matrix equation obtained in (12) for moisture content values in this iteration and continues steps (11) to (14) till convergence.

16. Increments the time step and repeats steps (8) to (15) for the number of time increments specified.

Hence, finally we obtain the moisture content $\{C\}$ and moisture loss $\{M\}$ at different drying times. The flowchart of the computer program MSTDIFF2 is depicted in Figure 4.3. The input data to the code MSTDIFF2, for the two-dimensional moisture diffusion problem discussed in Section 6.6 (Case II), is given in Appendix C.

4.2 Description of Shrinkage Stress Analysis Program

A computer program was developed to compute the stresses induced in a repair overlay/concrete substrate system, due to drying shrinkage of repair material. The code STRSRSYS (Stress in Repair System) is based on finite element formulation of two-dimensional plane stress problem. It allows for specifying in-plane free shrinkage strains in the elements representing repair material in the repaired system.

For two-dimensional shrinkage stress problem, the strain vector in terms of free shrinkage strains is given by [22]

$$\{\epsilon_S\} = \begin{Bmatrix} \epsilon_x \\ \epsilon_y \\ \epsilon_{xy} \end{Bmatrix} = \begin{Bmatrix} \epsilon_{sh} \\ 0 \\ 0 \end{Bmatrix} \tag{4.1}$$

where $\{\epsilon_{sh}\}$ is the free shrinakge strain in x-direction, shrinakge strain in y-direction is assumed as zero for thin patch repairs and shear strain is zero.

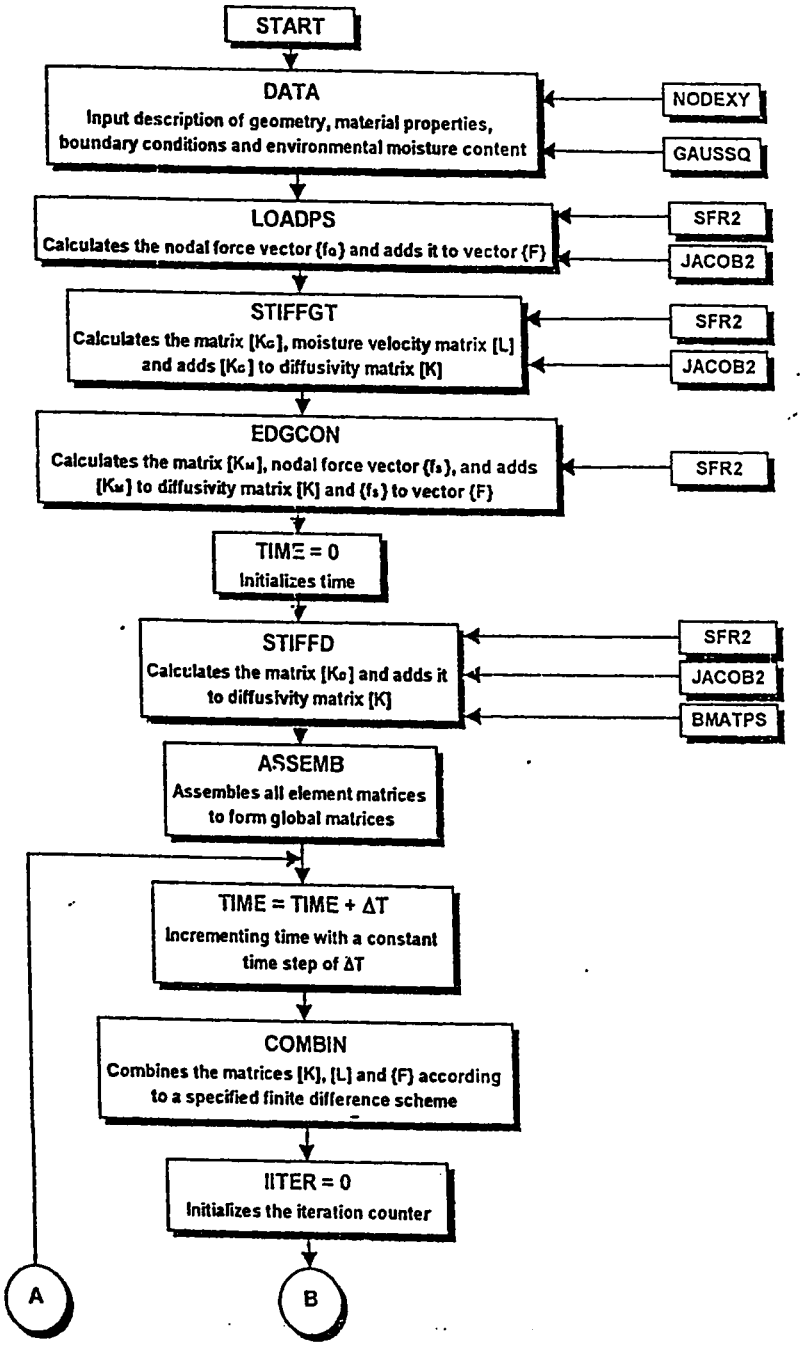

Figure 4.3: Flowchart of Two-Dimensional Moisture Diffusion Program MSTDIFF2

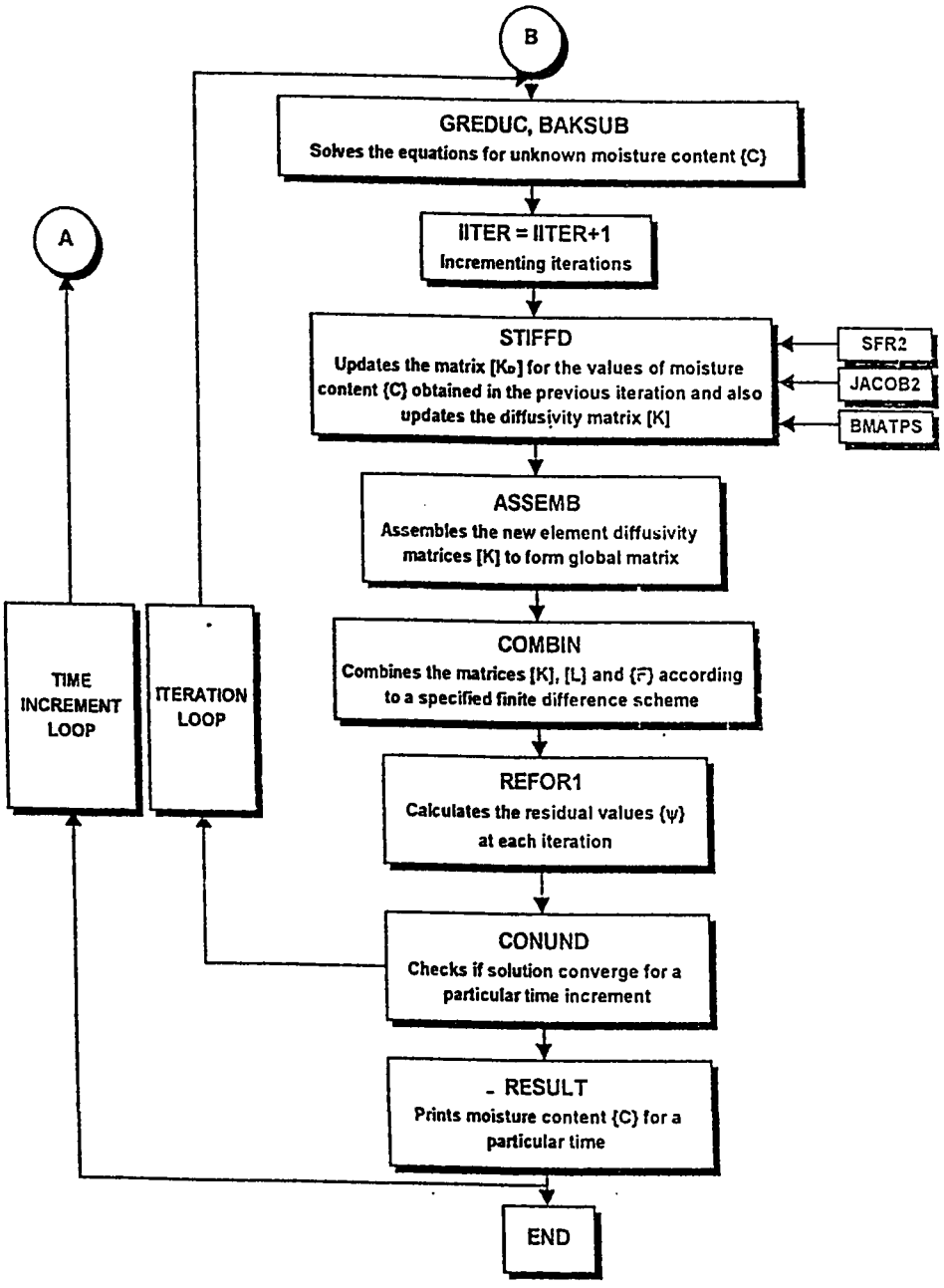

Figure 4.4: Flowchart of Two-Dimensional Moisture Diffusion Program MSTDIFF2 (Continued)

The load vector for a constant thickness (t) is given by

$$\{f_S\} = \int_{-1}^{+1} \int_{-1}^{+1} \left[[B]^T[D]\{\epsilon_{sh}\}\right] t|J|d\xi d\eta \tag{4.2}$$

The shrinkage stresses are determined as

$$\{\sigma\} = \{\sigma_R\} - \{\sigma_S\} \tag{4.3}$$

where $\{\sigma_R\}$ is the stress due to restrained shrinkage and $\{\sigma_S\}$ is the stress due to free shrinakge.

Therefore the stress vector $\{\sigma\}$ is given by

$$\{\sigma\} = [D][B]\{d\} - [D]\{\epsilon_{sh}\} \tag{4.4}$$

4.2.1 Shrinkage Stress Analysis Program STRSRSYS

The execution of the code STRSRSYS can be described as follows:

1. Reads the input data for description of geometry, material properties and boundary conditions.

2. Reads the input data for shrinkage strains in selected elements, along with data for concentrated, gravity and surface loading. It also computes the equivalent nodal forces for each element.

3. Computes the stiffness matrix for each element.

4. Assembles all the element matrices to form global matrices.

5. Computes the nodal displacements using Guass reduction and back substitution routines.

6. Computes the stresses in x- and y-direction, and shear stress at the Guass points from the displacements obtained in step (5).

7. Prints results for displacements, reactions and stresses.

Hence, finally we obtain the stresses in the repaired system due to drying shrinkage of repair material. The flowchart of the computer program STRSRSYS is depicted in Figure 4.5. The input data to the code STRSRSYS, for the shrinkage stress analysis in a repair material/concrete substrate system discussed in Section 6.10, is given in Appendix D.

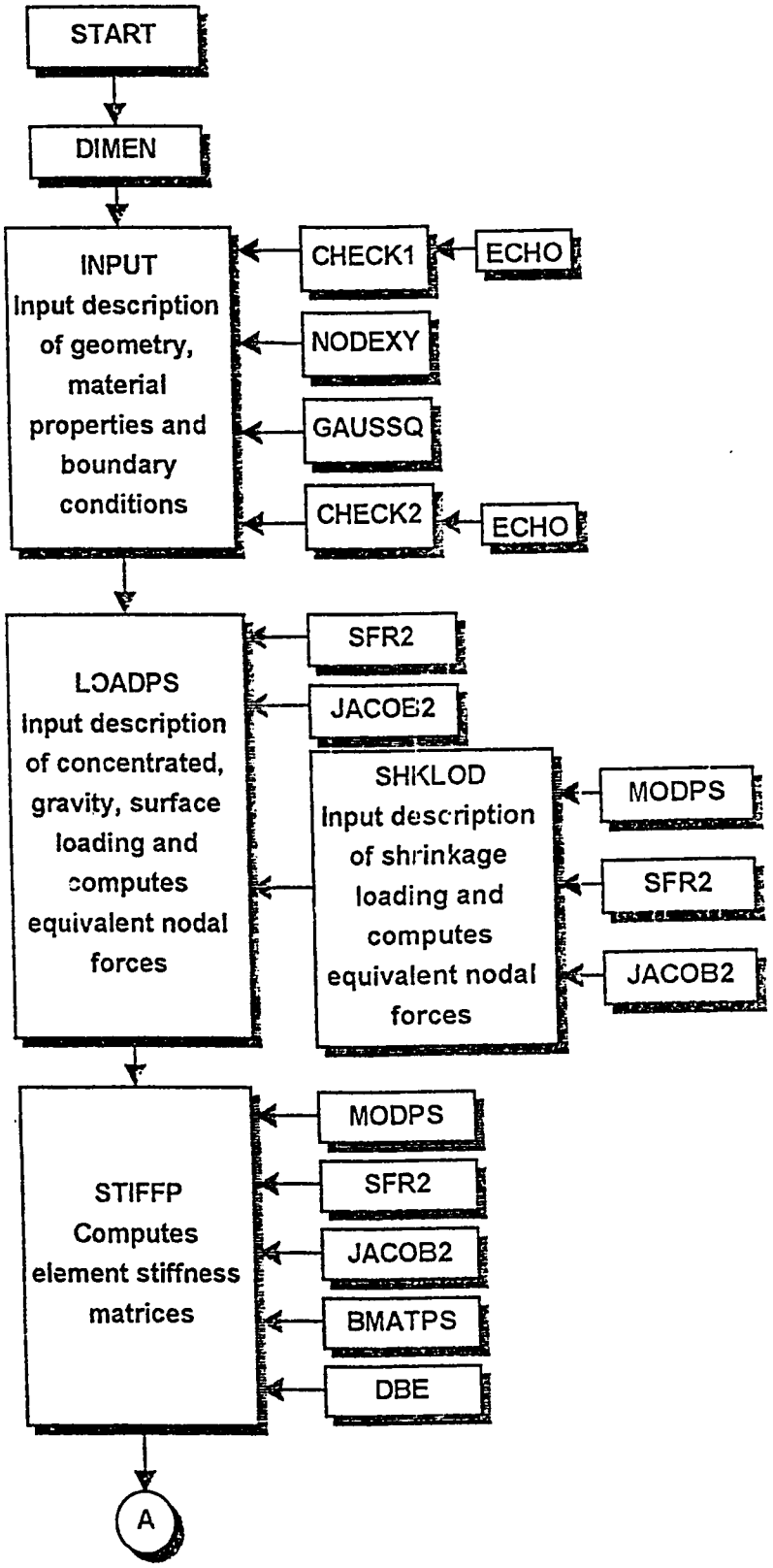

Figure 4.5: Flowchart of Shrinkage Stress Analysis Program STRSRSYS

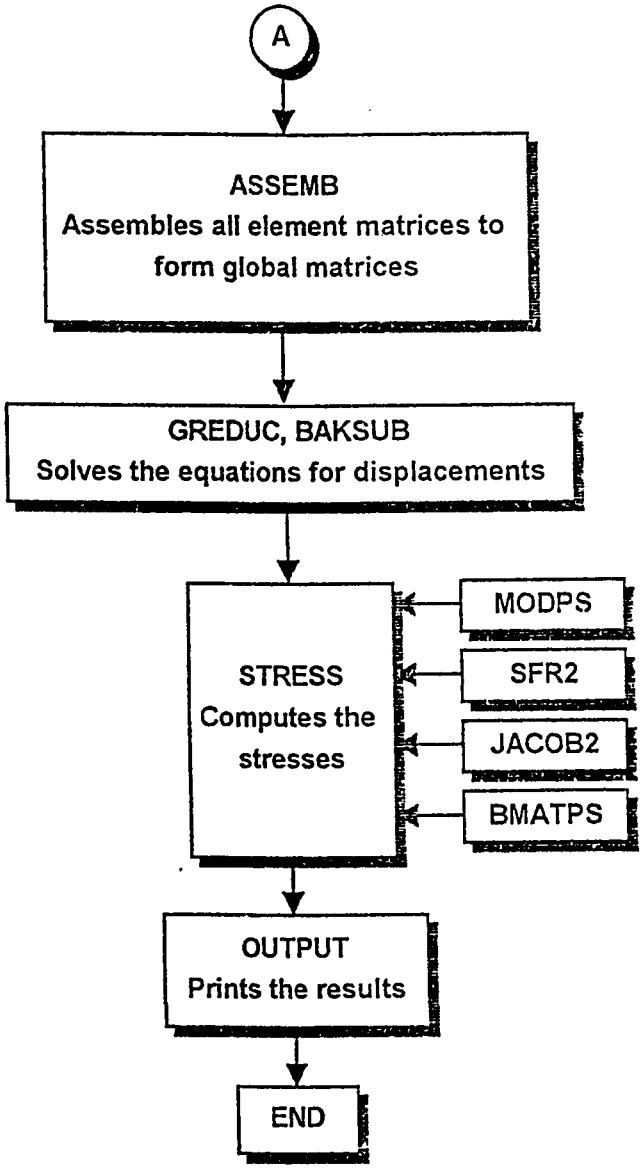

Figure 4.6: Flowchart of Shrinkage Stress Analysis Program STRSRSYS (Continued)

Chapter 5

EXPERIMENTAL PROGRAM

5.1 Materials

5.1.1 Repair Material

The repair material used in this research is a commercially available cementitious mortar. The manufacturer's data sheet claims it to be specially formulated for use in Middle East conditions. It is supplied as a powder to which water is simply added on site. It contains special pre-blended non-shrink cements, graded sands, fillers and chemical additives.

It is used for permanent repairs to all types of concrete and masonry. Its lightweight components and addition of special fillers allow the application of this material to vertical and overhead surfaces.

The repair material has the following properties as given in the manufacturer's data sheet:

1. Compressive strength measured in accordance with BS 4550 is $33 N/mm^2$ at 28 days. The curves showing the variation of compressive strength with water-

powder ratio and curing temperature are given. The curves indicate that, both the water-powder ratio and curing temperature have little effect on ultimate strength and the material can tolerate wide variations in water content and curing temperature.

2. Flexural strength measured in accordance with BS 4551 is $7N/mm^2$ at 28 days.

3. Slant shear bond strength to concrete is $23N/mm^2$ at 28 days tested in accordance with BS 6319 Part 4:1984.

4. Density is $1750kg/m^3$ at 0.18 water-powder ratio.

5. Water permeability is measured in accordance with BS 1881 I.S.A.T. Surface absorbtion at time 10 minutes is $0.18ml/m^2/second$ and at time 2 hours is $0.06ml/m^2/second$.

6. The coefficient of thermal expansion is $7.3X10^{-6}/^oC$.

5.1.2 Coarse Aggregate

The coarse aggregate used, for preparing substrate concrete, in this investigation was brought from Abu-Hadriyah, which is a major source of aggregate supply in the Eastern Province. The crushed limestone aggregate consists mainly of calcite as major mineral (91%) with small quantities of quartz (4%) and dolomite (4%).

The grading of the coarse aggregate was chosen so that it falls within the grading limits of ASTM C 33 for size no.7 with $3/8"(0.375mm)$ maximum size of the aggregate. The adopted grading and the corresponding ASTM limits are shown in Table 5.1.

Table 5.1: Coarse Aggregate Grading According to ASTM C 33

Sieve size	selected%passing	ASTM limits
3/8"	40	40-70
#4	5	0-15
#8	0	0-5

The coarse aggregate was washed thoroughly with water and then dried in the sunlight to remove the dust and impurities from the surface of the aggregate.

5.1.3 Fine Aggregate

The fine aggregate used, for preparing substrate concrete, in this investigation was dune sand brought from Abqaiq road. It consists of quartz, gypsum, calcite and feldspar.

5.1.4 Cement

The cement used for preparing concrete specimens was ASTM C 150 Type I, Ordinary Portland Cement.

5.1.5 Water

Potable water from the laboratory tap was used for preparing and curing the specimens.

5.1.6 Superplasticizer

The superplasticizer used, for preparing concrete specimens, was a commercially available superplasticizer. Its recommended dosage as given in manufacturer's data sheet, is $0.6 - 1.0 litre/100kg$ cement.

5.2 Preparation of Specimens for Measurement of Moisture Loss and Shrinkage Strains in Repair Material

5.2.1 Shapes and Sizes of Specimens

Repair mortar specimens used for the determination of moisture content were of sizes 200x10x40, 80, 120 mm as shown in Figure 5.1. For measurement of free shrinkage, the size of the specimen used was 200x50x10 mm and for apparent shrinkage the size was 200x50x50 mm, as shown in Figure 5.2 and Figure 5.3, respectively.

5.2.2 Mix Design of Repair Material

The mix design adopted for the specimens used for determination of moisture content and free and apparent shrinkage in the repair material was:

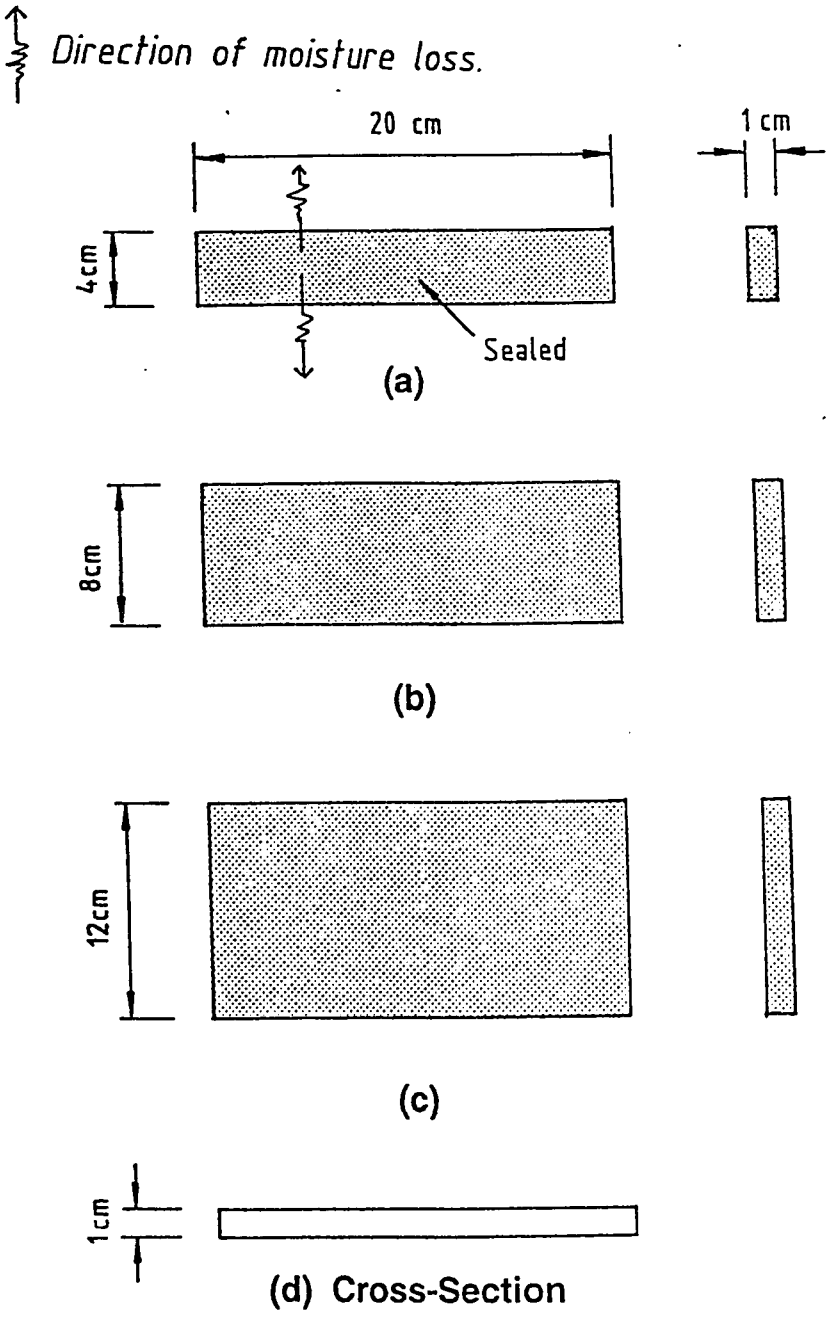

Figure 5.1: Specimens for Measurement of Moisture Loss

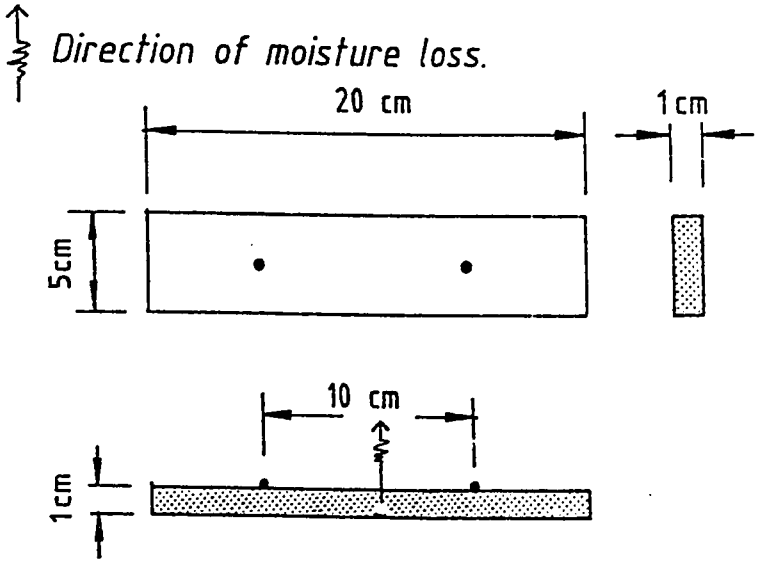

Figure 5.2: Free Shrinkage Specimen

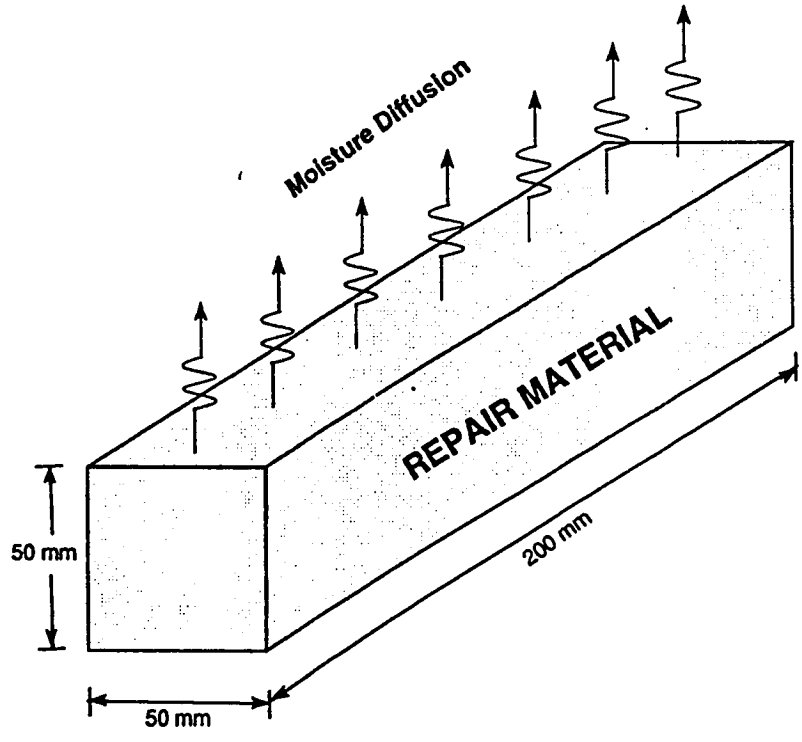

Figure 5.3: Apparent Shrinkage Specimen

Repair material powder	$1750 kg/m^3$
Water-powder ratio	0.18

5.2.3 Mixing of Repair Material

The repair material powder was mixed with water in a bucket. A slow speed drill (500 rpm) with a spiral paddle as shown in Figure 5.4 was used for mixing the powder with water to obtain a smooth mortar.

5.2.4 Casting of Specimens

All the specimens were cast, using the above mix, in the wooden moulds. The moulds were filled with the repair mortar and the mortar was well compacted by hand. The surface was then leveled first with the help of a straight edge and then with the trowel so that a smooth surface is obtained. For the thick specimens (50 mm deep) the moulds were filled in two equal layers and each layer was compacted thoroughly. After the casting was finished, the surfaces of the specimens were covered with polythene bags to prevent evaporation of water from the surface. The polythene bags were removed after 6 hours and the surfaces of the specimens were covered with moist burlap to keep the specimens moist. The specimens were left in the moulds for about 24 hours, thereafter, they were demoulded for sealing.

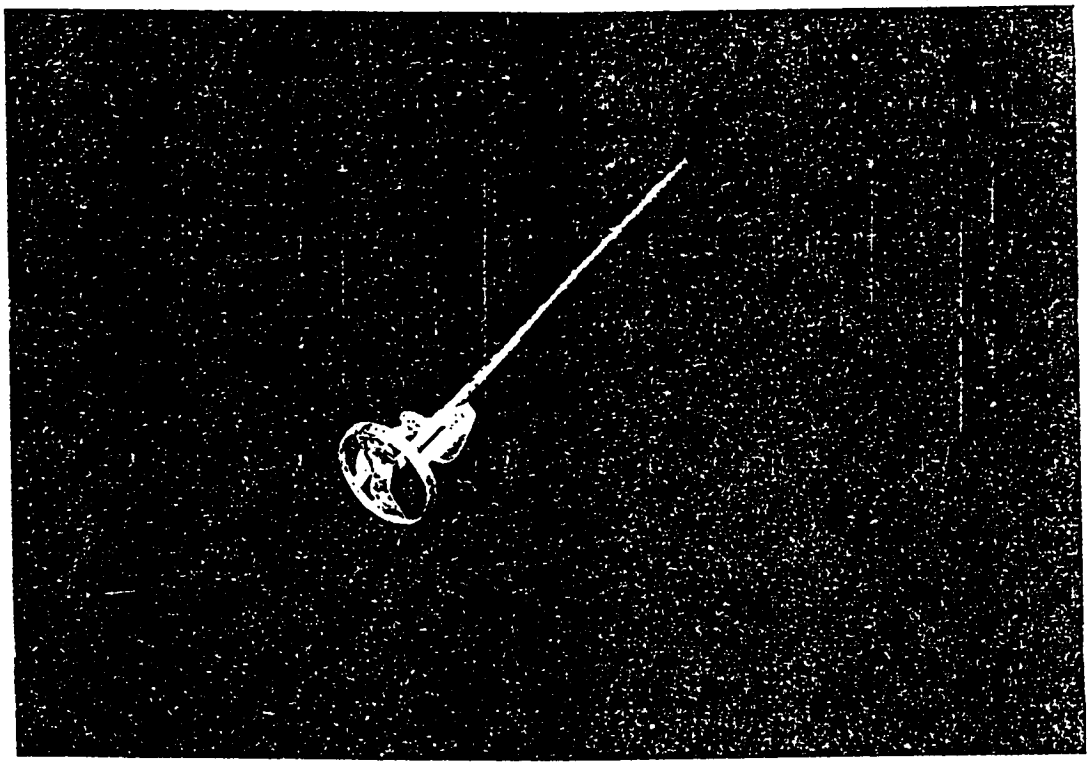

Figure 5.4: Spiral Paddle

5.2.5 Sealing of Specimens

The specimens for determination of moisture content were sealed with paraffin wax on the four sides and the two end sides of 200x10 mm were exposed to the surrounding environment as shown in Figure 5.1.

The specimens for measurement of free and apparent shrinkage were sealed with paraffin wax from all sides except the top surface, as shown in Figure 5.2 and Figure 5.3.

5.3 Preparation of Concrete Specimens

5.3.1 Shapes and Sizes of Specimens

The concrete specimens which were used as a substrate concrete over which repair layer was cast were of sizes 200x50x50 mm, as shown in figure 5.5. Concrete cylinders of size 75x150 mm were used to measure the compressive strength of concrete.

5.3.2 Mix Design

The mix design adopted for concrete specimens was:

Cement content	$356 kg/m^3$
Coarse aggregate/fine aggregate ratio	2
Water/cement ratio	0.40
Superplasticizer	1.0 litre/100 kg Cement

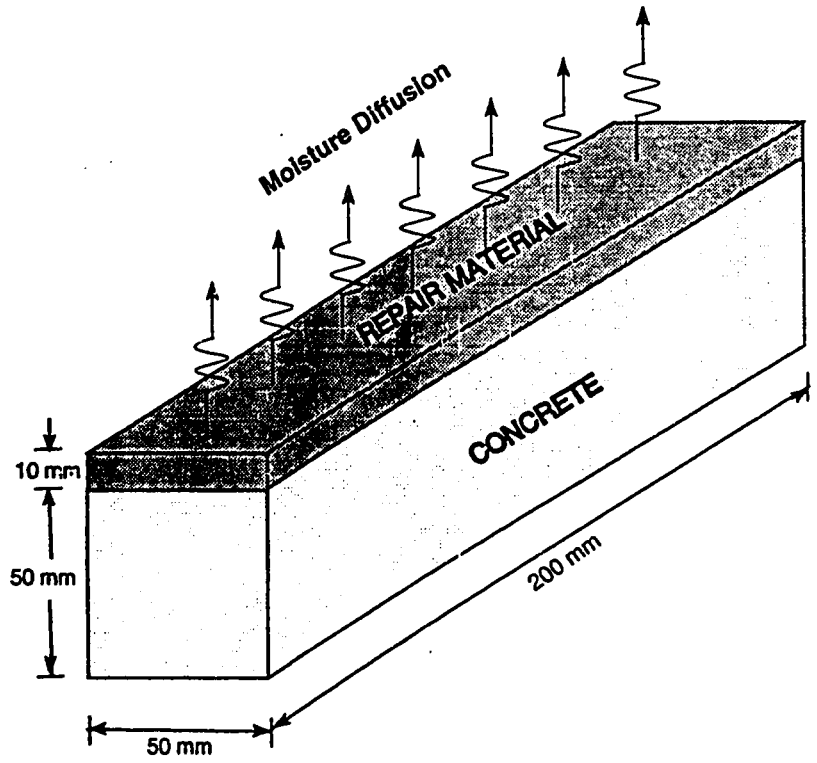

Figure 5.5: Specimen with a Repair Layer Over Concrete Substrate

5.3.3 Mixing Process

Mixing of the cement, coarse aggregate, fine aggregate, water and superplasticizer was carried out using an electrically operated concrete mixer. The superplasticizer was used to obtain the desired workability and was thoroughly mixed with water before adding it to the concrete mixture in the mixer.

5.3.4 Casting of Specimens

Concrete specimens to be used as substrate concrete were cast in the wooden moulds. The moulds were filled in two approximately equal layers and the cylinders were filled in three equal layers. All the moulds were then vibrated using a small laboratory vibrating table. After the casting, the surfaces of the specimens were covered with polythene bags to prevent evaporation of water from the surface. The specimens were left in the moulds for about 24 hours, thereafter, they were demoulded for curing.

5.3.5 Curing of Specimens

All the specimens were moist cured after demoulding by keeping them completely immersed in water for 28 days.

5.3.6 Testing of Concrete Cylinders

Compressive strength test was carried out at the age of 28 days. The cylinders were removed from water and placed in the air inside the laboratory for about two hours and were capped on the uneven top surface. Capping was done using a sulphur compound in accordance with the ASTM C 617. Compressive strength tests were performed on a hydraulically operated compression testing machine.

5.3.7 Stabilization of Concrete Specimens for Shrinkage

Concrete specimens to be used as a substrate concrete were dried in an oven at $80^{o}C$ for about 24 hours after curing. They were then left in the laboratory for 4 months at the laboratory environment to make them dimensionally stable.

5.4 Repair of Concrete Specimens

5.4.1 Surface Preparation

The surface of the concrete was made rough with the help of a chisel and a hammer so that it could develop a good bond with the new repair material. The concrete specimens were then placed in the moulds to cast repair layers of different thickness over them.

5.4.2 Priming

The concrete surface was primed with a priming material supplied by the

manufacturers of the repair material. The priming material used was an epoxy bonding agent so as to prevent the diffusion of moisture into the concrete.

5.4.3 Application of Repair Material

The repair material was mixed as described in Section 5.2.3. The thoroughly mixed repair material was applied to the primed concrete surface and pressed by hands. The pressure exerted by hands ensures good bond between the old concrete and the new repair material. The surface was then leveled first with help of a straight edge and then with the trowel so that a smooth surface is obtained. After the application of repair material, the surfaces of the specimens were covered with polythene bags to prevent evaporation of water from the surface. The polythene bags were removed after 6 hours and the surfaces of the specimens were covered with moist burlap to keep the specimens moist. The specimens were left in the moulds for about 24 hours, thereafter, they were demoulded for sealing.

5.4.4 Sealing of Repaired Specimens

The repaired specimens were sealed with paraffin wax on all the sides except the top surface of 200x50 mm which was exposed to the surrounding environment as shown in Figure 5.5.

5.5 Measurement of Weight Loss

The moisture content at various depths from the drying surface of the repair material was determined in Section 6.1 by measuring the weight changes of the various length specimens shown in Figure 5.1. For measurement of the weight loss, the specimens were kept in controlled ambient conditions with a constant temperature of $35°C$ and $55 \pm 5\%$ relative humidity. The diffusion of moisture from these specimens was one-dimensional as moisture was allowed to diffuse from the two end sides only. Weight changes were measured using a sensitive electronic balance with an accuracy of 0.01 gram. The electronic balance was covered during weight measurements so as to avoid fluctuations in the reading due to the movement of the air.

5.6 Measurement of Shrinkage Strains

The free, apparent and restrained shrinkage strains in the specimens shown in Figures 5.2, 5.3 and 5.5 were measured using a demec guage shown in Figure 5.6. Despite repeated attempts, the use of electrical strain guages gave erroneous results due to lack of proper bond with the 'wet' surface of repair material.

The demec points were attached to the surface of the repair material. The ambient conditions were the same as those discussed in Section 5.5 and the diffusion of moisture was also one-dimensional.

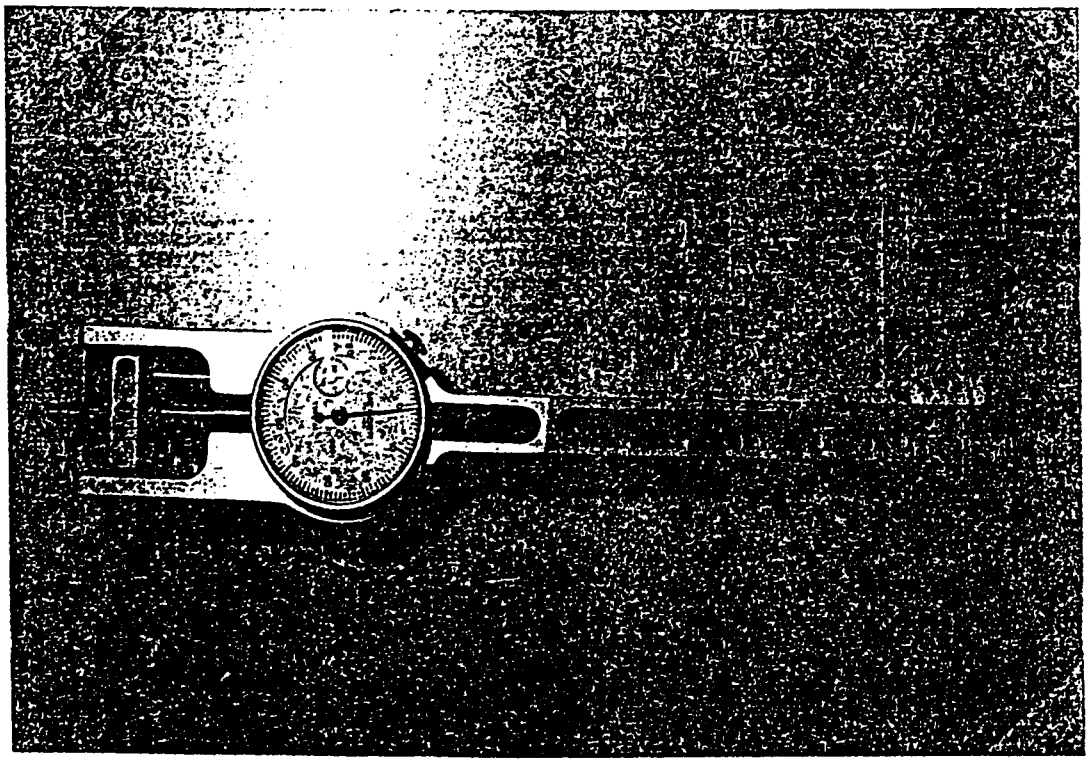

Figure 5.6: Demec Guage

Chapter 6

RESULTS AND DISCUSSION

6.1 Experimental Determination of Moisture Content

If it is assumed that the distribution of moisture at a distance x a from drying surface is the same without regard to the length of the specimen, then the moisture content C(x,t) at time t and at a distance x (x = 1,3,5 cm) is given by the following equation [14]:

$$C(x,t) = \left[1 - \frac{(w_i - w_{i-1})}{W_o(l_i - l_{i-1})S}\right] \times 100 \qquad (6.1)$$

where l_i is length of specimen, w_i is the absolute moisture loss of the specimen (of length l_i) at time t, W_o is diffusible moisture in a unit volume and S is area of drying surface. The diffusible moisture is given by the diffence between the weight of the specimen at the start of drying and its absolute weight on oven drying after the experiment. Derivation of Eqn. 6.1 is given in Appendix A.

The relationship between moisture loss and drying time of the various specimens of different lengths is obtained directly from the experiments as shown in

Figure 6.1. Time-dependent changes in moisture content at depth any x from the drying surface are calculated by Eqn. 6.1. Figure 6.2 shows the moisture loss at different depths for different drying times. According to Figure 6.2, the change in moisture content near the surface of concrete is rapid, but at points slightly deeper inside, the changes are slow.

The distribution of moisture content after 60 days from the start of drying versus depth from the drying surface is given in Figure 6.3. It is very clear from this curve that drying of the repair material is rapid at the surface portion in contact with outside air, and very slow at interior portions.

6.2 Determination of Moisture Diffusivity

The equation for one-dimensional moisture diffusion when the moisture diffusivity K_c is a function of moisture content C is

$$\frac{\partial C}{\partial t} = \frac{\partial}{\partial x}\left[K_c(C)\frac{\partial C}{\partial x}\right] \tag{6.2}$$

Using the Boltzman's transformation [23], C can be expressed in terms of a single variable $\eta = \eta(x,t)$ which is a function of both space and time. Therefore, Eqn. 6.2 is reduced to an ordinary differential equation by the introduction of a new variable, η, where

$$\eta = x/\sqrt{t} \tag{6.3}$$

Thus

$$\frac{\partial C}{\partial x} = \frac{1}{t^{1/2}} \frac{dC}{d\eta} \tag{6.4}$$

and

$$\frac{\partial C}{\partial t} = -\frac{x}{2t^{3/2}} \frac{dC}{d\eta} \tag{6.5}$$

and hence

$$\frac{\partial}{\partial x}\left[K_c(C)\frac{\partial C}{\partial x}\right] = \frac{\partial}{\partial x}\left[K_c(C)\frac{1}{t^{1/2}}\frac{dC}{d\eta}\right] = \frac{1}{t}\frac{d}{d\eta}\left[K_c(C)\frac{dC}{d\eta}\right] \tag{6.6}$$

Substituting Equations 6.5 and 6.6 into Eqn. 6.2 results in

$$-\frac{x}{2t^{3/2}}\frac{dC}{d\eta} = \frac{1}{t}\frac{d}{d\eta}\left[K_c(C)\frac{dC}{d\eta}\right] \tag{6.7}$$

or on using Eqn. 6.3, the above Eqn. 6.7 becomes

$$-\frac{1}{2}\eta\frac{dC}{d\eta} = \frac{d}{d\eta}\left[K_c(C)\frac{dC}{d\eta}\right] \tag{6.8}$$

which is an ordinary differential equation in η.

For the problem of moisture diffusion from inside the material, which is defined by

$$C = 1, \qquad x > 0, \quad t = 0 \tag{6.9}$$

$$C = C_1, \qquad x = 0, \quad t > 0 \tag{6.10}$$

the initial and boundary conditions become

$$C = 1, \qquad \eta = \infty \tag{6.11}$$

$$C = C_1, \qquad \eta = 0 \tag{6.12}$$

Integrating Eqn. 6.8 yields

$$-\frac{1}{2}\int_1^{C_1} \eta dC = \left[K_c(C)\frac{dC}{d\eta}\right]_1^{C_1} \tag{6.13}$$

At C = 1, $\eta = \infty$, we have the condition

$$\frac{dC}{d\eta} = 0$$

and Eqn. 6.13 becomes

$$-\frac{1}{2}\int_1^{C_1} \eta dC = K_c|_{c=c_1} \left.\frac{dC}{d\eta}\right|_{c=c_1} \tag{6.14}$$

and moisture diffusivity K_c at any moisture content C_1 is given as

$$K_c|_{c=c_1} = -\frac{1}{2}\left.\frac{dC}{d\eta}\right|_{c=c_1} \int_1^{C_1} \eta dC \tag{6.15}$$

Therefore, the moisture diffusivity K_c can be determined using Eqn. 6.15 and the changes in moisture content C with distance x and time t, obtained from the experiments.

Variation in moisture content C with depth x from the drying surface and time t is plotted against the variable η as shown in Fig. 6.4. The relationship between the variable η and the moisture content C is expressed in the form given by Penev and Kawamura [15], which is

$$C(\eta) = \left[1 - \frac{p}{p+\eta}\right] \times 100 \tag{6.16}$$

where p is the value of η at 50% moisture loss and is equal to 0.065.

Moisture diffusivity K_c is obtained by substituting for η and $\frac{dC}{d\eta}$ from Eqn. 6.16 into Eqn. 6.15 and integrating the result.. The relationship between the calculated values of diffusivity K_c and moisture content C is shown in Figure 6.5. Diffusivity K_c is calculated in the range of $C = 0.01$ to $C = 0.99$, because K_c cannot be defined at $C = 1$ and 0. However for the purpose of predicting the rate of drying, this range is sufficient, since drying takes place well within it.

It can be inferred from Figure 6.5 that the moisture diffusion from the interior of the repair material is closely related to the moisture content of the repair material. More precisely, in the range of high moisture content, the diffusivity falls sharply with the decrease in moisture content, but with moisture content below 60 to 70%, it may be considered to be more or less constant.

Based on results of Figure 6.5, the relationship between moisture diffusivity K_c and moisture content C is obtained using non-linear regression and is given by Eqn. 6.17.

$$K_c(C) = K_o + a\left(\frac{C}{1-C}\right)^b \tag{6.17}$$

where K_o is diffusivity in oven-dry condition (C = 0%) and equal to 0.1175 cm^2/day, and the regression parameters a and b are 0.05 and 1.878, respectively.

6.3 Determination of Surface factor

A repair mortar specimen, having the dimensions 10cmx2cmx2cm, was ana-

lyzed in which diffusion of moisture was from only one side, as shown in Figure 6.6(a). The analysis was performed using 6 two-noded one-dimensional finite elements, as shown in Figure 6.6(b). Surface factor f was determined by comparing the experimental results of moisture loss with the predicted values using the one-dimensional Finite Element Code MSTDIFF1, for the above mentioned one-dimensional diffusion problem. The values of moisture loss predicted using diffusivity K_c as a function of moisture content C were found to be in good agreement with the experimental values for the value of surface factor $f = 0.3cm/day$, as shown in Figure 6.7. The surface factor f of this repair material is low as compared to that of normal concrete which is $0.55cm/day$ [14].

The effect of variation in surface factor f was studied using different values for f like 0.2, 0.3, 0.4, 0.6, and 1.0. Figure 6.8 shows the predicted values of moisture loss with drying time for different values of f. It is clear from Figure 6.8 that variation of the surface factor f has a little effect on the moisture loss.

6.4 Comparision between Experimental and Computed Values of Moisture Loss

For the one-dimensional moisture diffusion problem in a cementitious repair material, the experimental values of moisture loss at a distance $x = 1cm$ from the drying surface and the predicted values using non-linear moisture diffusion theory are plotted against drying time as shown in fig. 6.7. Also, the moisture loss values

predicted using the linear moisture diffusion theory are shown in Figure 6.7. The value of K_c used in the linear analysis was $0.3cm^2/day$. The prediction of moisture loss using moisture dependent diffusivity is found to be more accurate than that predicted using a constant diffusivity, especially after about 15% of the moisture has been lost.

The high rate of moisture loss, especially in the initial period of drying, is attributed to the high value of diffusivity in that period. Hence, it can be said that the moisture diffusivity K_c is one of the major parameters affecting the moisture loss from a cementitious repair material.

6.5 Effect of Variation in the Relationship Between Diffusivity K_c and Moisture Content C

Different relationships between the diffusivity K_c and moisture content C were tried using different values for the parameters K_o, a and b, as shown in Figure 6.9. The mositure loss values computed using these relationships are shown in Figure 6.10. From Figures 6.9 and 6.10, it is clear that low values of diffusivity K_c specially at high levels of moisture content C reduce moisture loss. The relationship given by curve 2, which has lowest value of the diffusivity K_c, seems to be the most ideal one because moisture loss is very slow from the start of the drying. This reduction of moisture loss in the initial period of drying, reduces the drying shrinkage in

this period as drying shrinkage is highly related to moisture loss. The reduction of drying shrinkage decreases the level of induced stresses in the repair material, which is very important as the material takes time to develop enough strength to resist the induced stresses. Hence, it can be concluded that the control of moisture diffusivity K_c, especially in the initial period of drying, will reduce the induced stresses in the repair material.

6.6 Applications of Two Dimensional Finite Element Model

In order to study the applications of the two-dimensional Finite Element Model. different cases were solved. The cases were selected so as to simulate the practical field conditions of the patch repair to substrate concrete. The cases selected provide information about the variation of moisture content with time in space coordinates for different boundary conditions and also for different thicknesses of the repair mortar over substrate concrete.

Four cases were analyzed as shown in Figure 6.11 The first case is the same which was solved using the one-dimensional Finite Element Model. It is again solved here using two-dimensional Finite Element Model to check the predictability of the two-dimensional Finite Element Model. The second and third cases have the same boundary conditions with a different thickness of the repair layer. The fourth case has the same thickness as of the third case but with different boundary conditions

simulating an encapsulated repair.

All the four cases were analyzed using the experimentally obtained curve for moisture diffusivity K_c shown in Figure 6.5 and the material is assumed to be isotropic so that $K_{cx} = K_{cy}$. The surface moisture transfer coefficient f used is $0.3cm/day$ with the equilibrium moisture content C_e as 50%. The thickness t used is 1cm.

Case I. A repair mortar specimen, having the dimensions 10cmx2cm and very long in the other dimension, is analyzed in which diffusion of moisture is from only one side, as shown in Figure 6.11(a). The cross-section is analyzed using a two-dimensional finite element grid with 21 nodal points and 12 four-noded elements. The time-dependent changes in moisture loss along the distance from the drying surface are presented in Figure 6.14. The moisture loss values obtained were found to be exactly the same as those obtained using the one-dimensional finite element model. Case I served as a verification of the two-dimensional finite element formulation and software coding by comparison to the one-dimensional finite element model which had previously been noted to yield results in close agreement with experimentally obtained values.

Case II. A repair mortar layer cast over concrete substrate, having cross-section 50cmx2cm is analyzed in which the diffusion of moisture is from the top surface and through the sides, as shown in Figure 6.11(b). The repair system is

assumed to be very long in the third direction like, for example, in the case of industrial flooring. Moisture cannot diffuse into the substrate concrete as it is assumed to be sealed at the interface between the concrete and the repair material.

One half of the cross-section is analyzed using a two-dimensional finite element grid with 27 nodal points and 16-four noded elements as shown in Figure 6.13. The time-dependent changes in moisture content are presented in Figures 6.15, 6.16 and 6.17 along the cross sections, A-A,B-B and C-C respectively.

Case III. A repair mortar layer cast over concrete substrate, having cross-section 50cmx5cm is analyzed in which moisture diffusion is from the top surface and through the sides, as shown in Figure 6.11(c). A thicker layer of repair mortar is chosen to get greater variation (gradient) of moisture content through the thickness. One half of the cross-section is analyzed using the two-dimensional finite element grid with 48 nodal points and 35-four noded elements as shown in Figure 6.13. The time-dependent changes in moisture content are presented in Figures 6.18 to 6.22 along the cross sections, A-A, B-B, C-C, D-D and E-E, respectively.

Case IV. A repair mortar layer cast over concrete substrate, having cross-section 50cmx5cm is analyzed in which moisture diffusion is from the top surface only as shown in Figure 6.11(d). One half of the cross-section is analyzed using the two-dimensional finite element grid with 48 nodal points and 35-four noded elements as shown in Figure 6.13. The time-dependent changes in moisture content are presented in Figures 6.23, 6.24, and 6.25 along the cross sections, A-A, B-B and

C-C, respectively.

The results of the cases II and III indicate that the moisture content at a particular time of drying, is high in the interior and there is a significant variation in moisture content at the ends. The variation in moisture content at the ends is due to the diffusion of moisture in two directions *i.e.* through the top surface and the end, showing the effect of two-dimensional moisture diffusion. The diffusion of moisture in the central portion is predominantly through the top surface and hence the moisture content in this region is almost constant. Comparision of the results of cases II and III indicate that the moisture loss is less in thick repair layers. The mositure content in the case IV is constant, that is, it does not vary along the length at a particular drying time since the mositure diffusion is one-dimensional, through the top surface only. Therefore it can be concluded that in the case of patch repairs the mositure diffusion is predominantly one-dimensional and even when the ends are exposed to drying a major portion of the repair has one-dimensional moisture diffusion.

6.7 Relationship Between Moisture Loss and Free Shrinkage Strains

Free shrinkage strains obtained from the experiments are plotted against the drying time as shown in Figure 6.26. It can be inferred from Figure 6.26 that the

strains increase rapidly during the initial drying period and as the drying progresses the increase in strains is slow and it reaches a constant or ultimate value at the end of 28 days.

To obtain a relationship between free shrinkage strains and moisture loss, the free shrinkage strains are plotted against the experimentally determined moisture loss values (determined in Section 6.1) at a depth $x = 1cm$ from the drying surface, as shown in Figure 6.27. According to Figure 6.27 the relationship between moisture losses and free shrinkage strains is not linear. Thus it is not possible to predict directly the free shrinkage strains by moisture loss for this repair material, as has been the trend for shrinkage modelling in ordinary concrete [11, 13]. The actual relationship between free shrinkage strains and moisture loss, which is non-linear, is expressed by the following expression based on a regression model

$$(\epsilon_{sh})_M = \frac{M^{2.5}}{195 + M^{2.5}} (\epsilon_{sh})_{ult} \tag{6.18}$$

a form similar to the ACI equation for variation of shrinkage with time [24]. In the above equation, ϵ_{sh} represents the free shrinkage strain, M the %-loss of moisture starting from 0%, and $(\epsilon_{sh})_{ult}$ the ultimate free shrinkage strain, which is taken as 0.0016.

The Eqn. 6.18 enables the prediction of free shrinkage strains for different values of moisture loss for this particular repair material.

6.8 Variation of Apparent Shrinkage along the Depth

Apparent shrinkage strains at depth x from the drying surface are plotted against the drying time as shown in the Figure 6.28. It appears from this Figure that the apparent shrinkage strain at and in the neighborhood of the drying surface increases rapidly at the early stage of drying. However, as the depth from the drying surface increases the increase in shrinkage strains is slow. This phenomenon is very much similar to that of moisture diffusion.

Figure 6.28 also shows that the apparent shrinkage strains at the drying surface are very much close to the free shrinkage strains obtained using $1cm$ thick specimen. However, as the distance from the drying surface increases, the strains decrease which shows the effect of the internal restraint provided by the material. Figure 6.29 depicts the apparent shrinkage strains against local moisture losses at depth $x = 1cm$ and $x = 3cm$ from the drying surface. According to Figure 6.29 the moisture losses do not vary linearly with the apparent shrinkage strains for both the cases, *i.e.* in the neighborhood of the drying surface and deeper inside the material. This relationship between apparent shrinkage strains and moisture losses differs from that of concrete in which this relationship is expressed by a straight line in the neighborhood of the drying surface [14].

6.9 Comparision Between Free and Restrained Shrinkage Strains

Figure 6.30 presents a comparison between the free and restrained shrinkage strains. Both free and restrained shrinkage strains were measured using $10mm$ thick repair material specimens. In the restrained shrinkage specimen, shrinkage of the repair layer was restrained by the substrate concrete. Due to the very small thickness of the repair layer, the effect of restraint provided by the substrate concrete is high in this case and thus the restrained shrinkage strains are low compared to the free shrinkage strains. Shrinkage cracking was found in the repair material due to the high free shrinkage strain.

6.10 Shrinkage Stresses in Repair Material/Substrate Concrete System

Free shrinkage strains ϵ_{sh} are used as the input to the finite element code STRSRSYS to find the stresses due to restrained shrinkage of the repair material in the repair material/concrete substrate system. A thin repair layer of size 200 x 50 x 10 mm cast over a concrete substrate of size 200 x 50 x 50 mm as shown in Figure 5.5 is analyzed for shrinkage stresses.

A 24-element mesh with 8-noded plane stress elements shown in Figure 6.31 is used to model the repair material/concrete substsrate system. The effect of shrinkage along the width and thickness of the repair layer is considered negligible, as they

are very small compared to the length, and is ignored by this model. The analysis carried out in this study is linear elastic. The bond between the repair material and the substrate concrete is assumed to be perfect. The data relating the elastic and mechanical properties of the repair material is taken from Ref. [25] and that of substrate concrete is obtained from the tests performed on concrete cylinders and is given in Table 6.1.

Table 6.1: Properties of Repair Material and Concrete Substrate

Properties	Concrete substrate	Repair material
Compressive Strength	40MPa	25MPa
Tensile Strength	4MPa	3MPa
Modulus of Elasticity	30,000MPa	14,000MPa
Poisson's ratio	0.2	0.2

Figure 6.32 shows the predicted values of tensile stresses due to restrained shrinkage at the top surface of the repair layer in the repaired system. The tensile stress values calculated using the experimentally measured shrinkage strains in a corresponding restrained overlay/substrate system are also shown in the Figure 6.32. The predicted values of restrained shrinkage stresses are in good agreement with the stress values calculated using the experimentally measured shrinkage strains.

Figure 6.33 presents the tensile and shear stresses in the repair material, close to the interface of the repair material and concrete substrate system. It is clear from Figure 6.33 that the maximum tensile stress occurs at the center and the maximum shear stress occurs at the ends. The variation of shrinkage stresses along the depth

of the repaired system is shown in Figure 6.34. It indicates that the repair material is subjected to tensile stresses and the substrate concrete is subjected to compressive stresses.

These results show very high tensile and shear stress values in the repair material compared to the permissible maximum stress of 3MPa. This will lead to cracking of the repair material at the center and debonding at the ends. The high stress in the repair material/concrete substrate system is attributed to the high free shrinkage strains in the repair material.

6.11 Effect of Variation in Thickness of Repair Layer on Shrinkage Stresses

As the thickness of the repair layer over concrete substrate increases, there is a variation in the shrinkage stresses developed in the repair material. Analysis of the shrinkage stress is carried out by varying the thickness of the repair layer to $20mm$ with free shrinkage strain of the repair material as the input data to the finite element code STRSRSYS. A 28-element mesh with 8-noded plane stress elements is used to model the repair material/concrete substsrate system. The effect of shrinkage along the width and depth of the repair layer is considered negligible and is ignored by this model. The bond between the repair material and the substrate concrete is assumed to be perfect.

Figure 6.35 shows the variation of shrinkage stresses in the repair material close to the interface. It is clear from this Figure that the tensile stresses decrease and shear stresses increase as the thickness of the repair layer over a concrete substrate is increased. This shows that the restraint provided by the concrete substrate has an important role in the development of shrinkage stresses in a repair system.

6.12 Determination of Allowable Ultimate Shrinkage Strain

The allowable ultimate shrinkage strain in the repair material to avoid cracking, *i.e.* which causes tensile stresses within the permissible limits, is determined by using different values of ultimate shrinkage strains ranging from 200 microstrains to 1500 microstrains. Figure 6.36 shows the maximum tensile stress values for different ultimate shrinkage strains in the repaired system with $10mm$ thick repair layer over $50mm$ thick concrete substrate. The allowable shrinkage strain was found to be 0.0003 causing a maximum tensile stress of 3.0 MPa which is equal to the tensile strength of the repair material. Figure 6.37 depicts the tensile and shear stresses in the repair material, close to the interface due to ultimate shrinkage strain of 0.0003. Thus, for the repair material/concrete substrate system considered, the ultimate shrinakge strian should not exceed 0.0003 to avoid cracking and delamination of the repair material due to drying shrinkage of the repair material.

6.13 Effect of Variation in Modulus of Elasticity of the Repair Material on Shrinkage Stresses

The modulus of elasticity was found to vary significantly for different repair materials used for concrete repairs. The effect of variation in the modulus of elasticity of the repair material E_r on shrinkage stresses is studied by varying it from 10,000 MPa to 45,000 MPa. Elastic modulus of concrete substrate E_s used is 30,000 MPa. The stresses are calculated in a repaired system with $10mm$ thick repair layer over $50mm$ thick concrete substrate using a shrinakge strain of 0.0003 in the repair layer. Figure 6.38 shows the variation of maximum tensile stress with the modular ratio (E_s/E_r), *i.e.* the ratio of elastic modulus of the concrete substrate E_s to the elastic modulus of the repair material E_r. The lower the elastic modulus of the repair material, higher will be the modular ratio (E_s/E_r). The results indicate that the lower the elastic modulus of the repair material, the lower are the stresses developed in the repaired system.

6.14 Effect of Variation in Poisson's Ratio of the Repair Material on Shrinkage Stresses

For two-dimensional elastic analysis, it is necessary to study the effect of variation in Poisson's ratio of the repair material on shrinkage stresses. Poisson's ratio was found to vary within a small range of 0.15 to 0.25 for different repair materials used for concrete repairs as given in Ref. [8]. Stresses are calculated in a

repaired system with $10mm$ thick repair layer over $50mm$ thick concrete substrate using a shrinakge strain of 0.0003 in the repair layer. Poisson's ratio of repair material is varied within the known range of 0.15 to 0.25 and for concrete substrate a value of 0.2 is used. Figure 6.39 depicts the variation of maximum tensile stress with the ratio ν_s/ν_r *i.e.* Poisson's ratio of the concrete substrate to the Poisson's ratio of the repair material. It is seen that Poisson's ratio has almost no effect on the maximum tensile stress. Thus, it can be stated that Poisson's ratio has a little effect on the stresses induced in the repaired system.

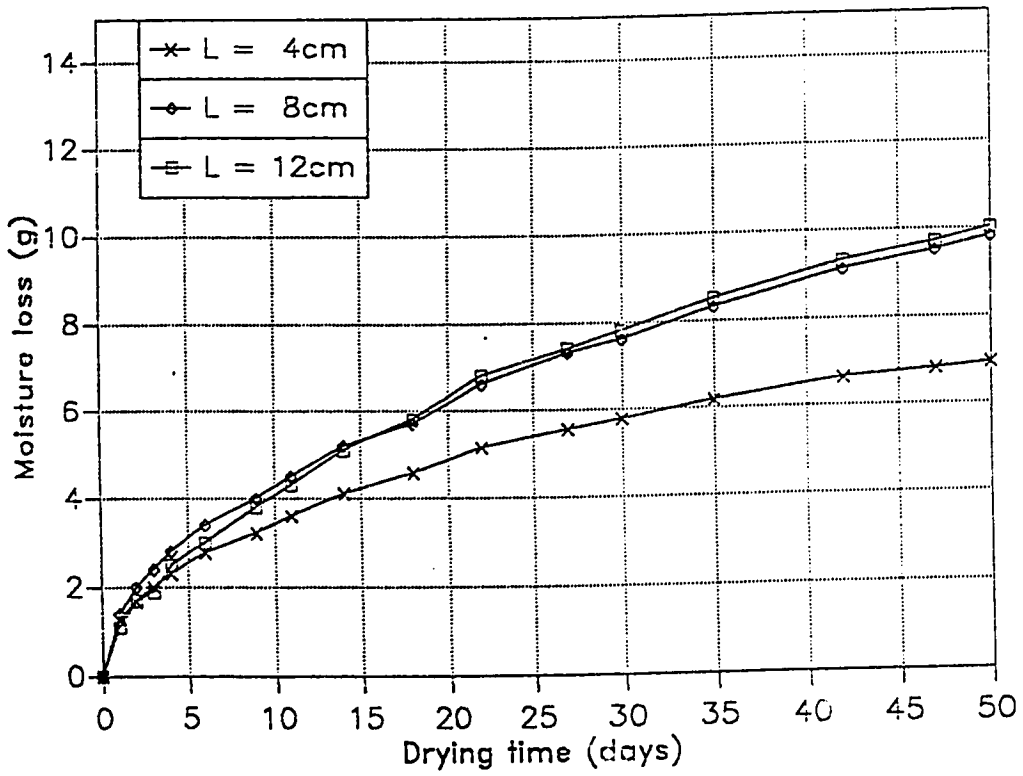

Figure 6.1: Relationship Between Moisture Loss and Drying Time

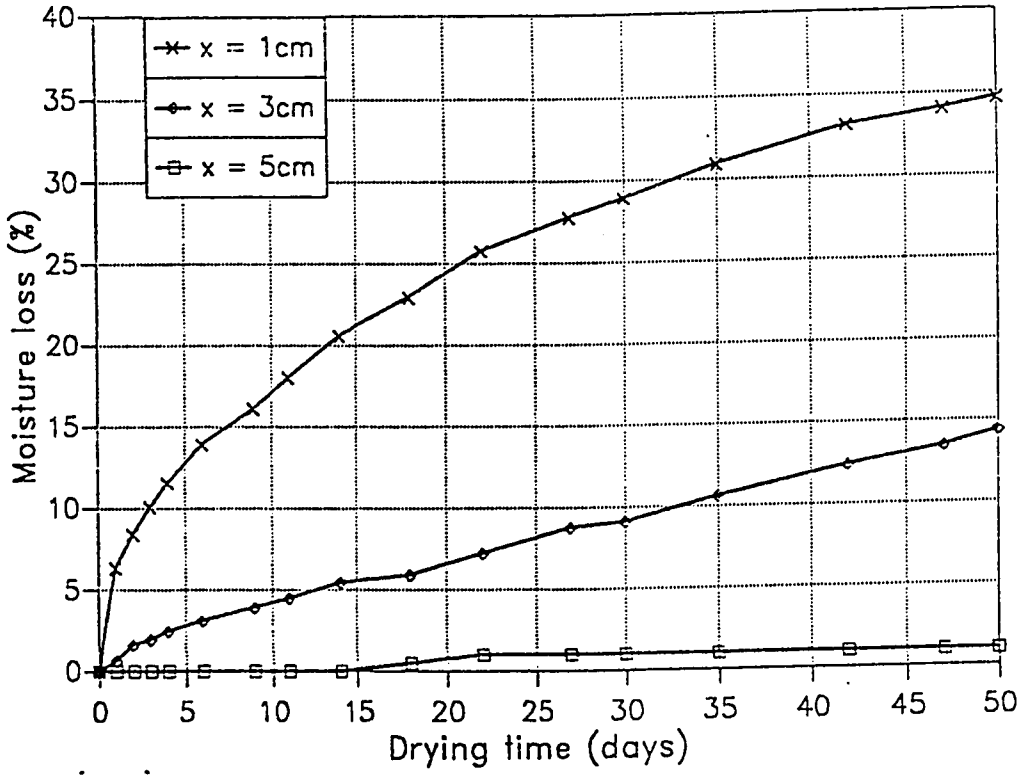

Figure 6.2: Moisture Loss vs Drying Time at Different Depths from Drying Surface

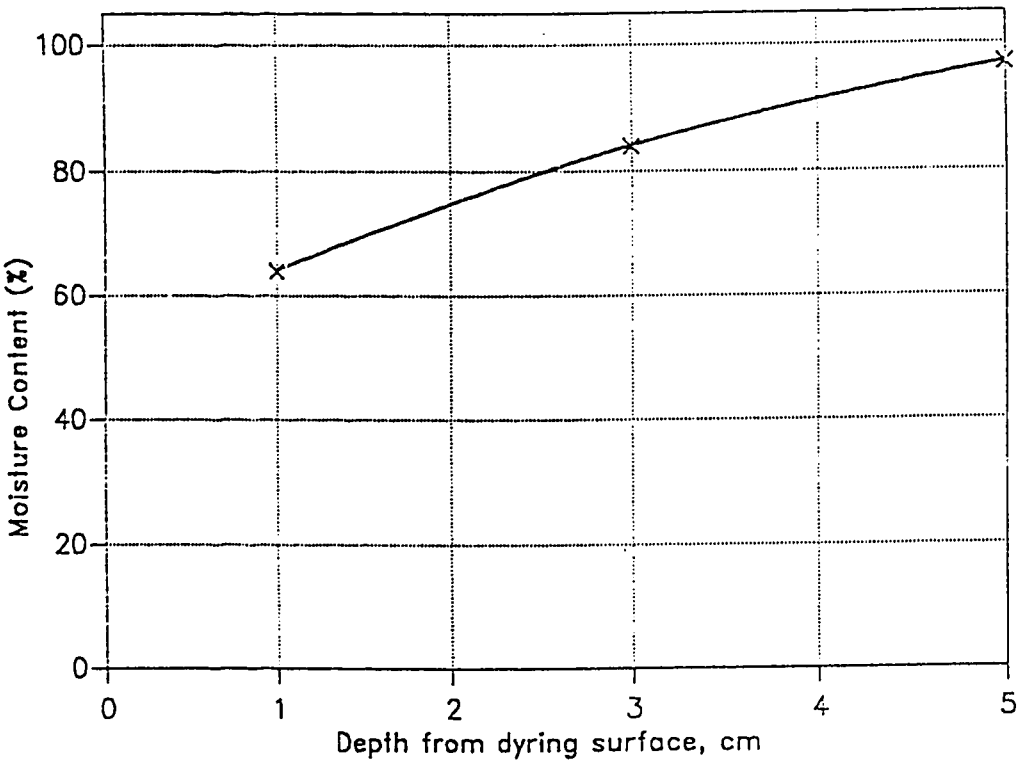

Figure 6.3: Moisture Content at Different Depths from Drying Surface at 60days

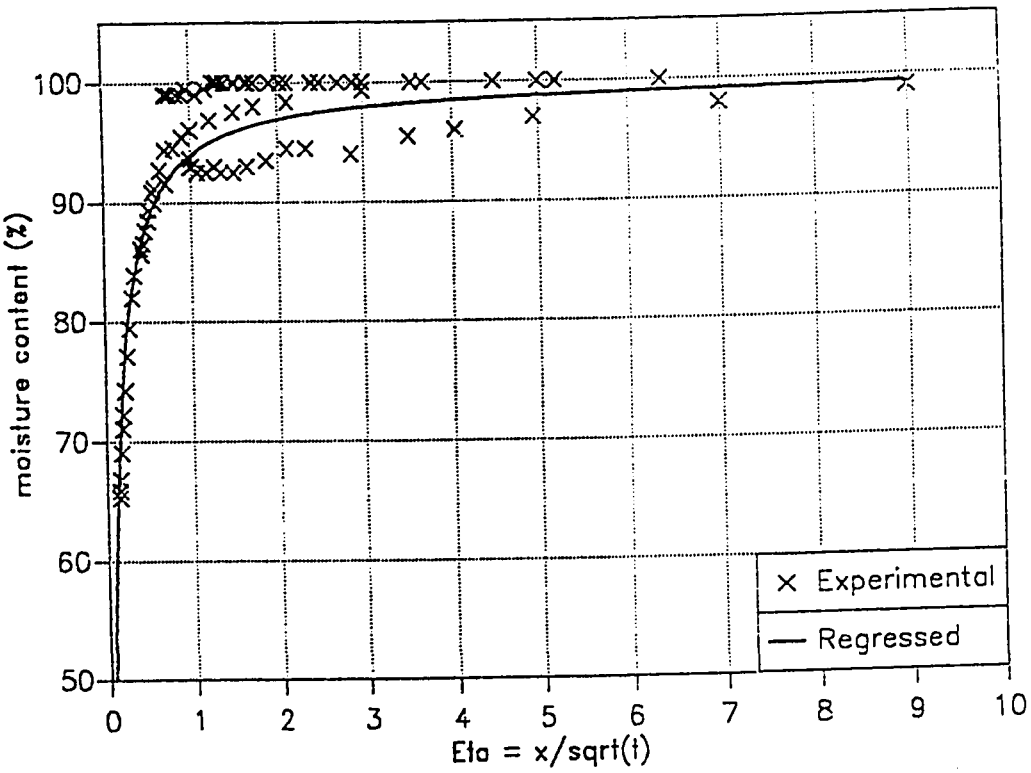

Figure 6.4: Moisture Content vs η

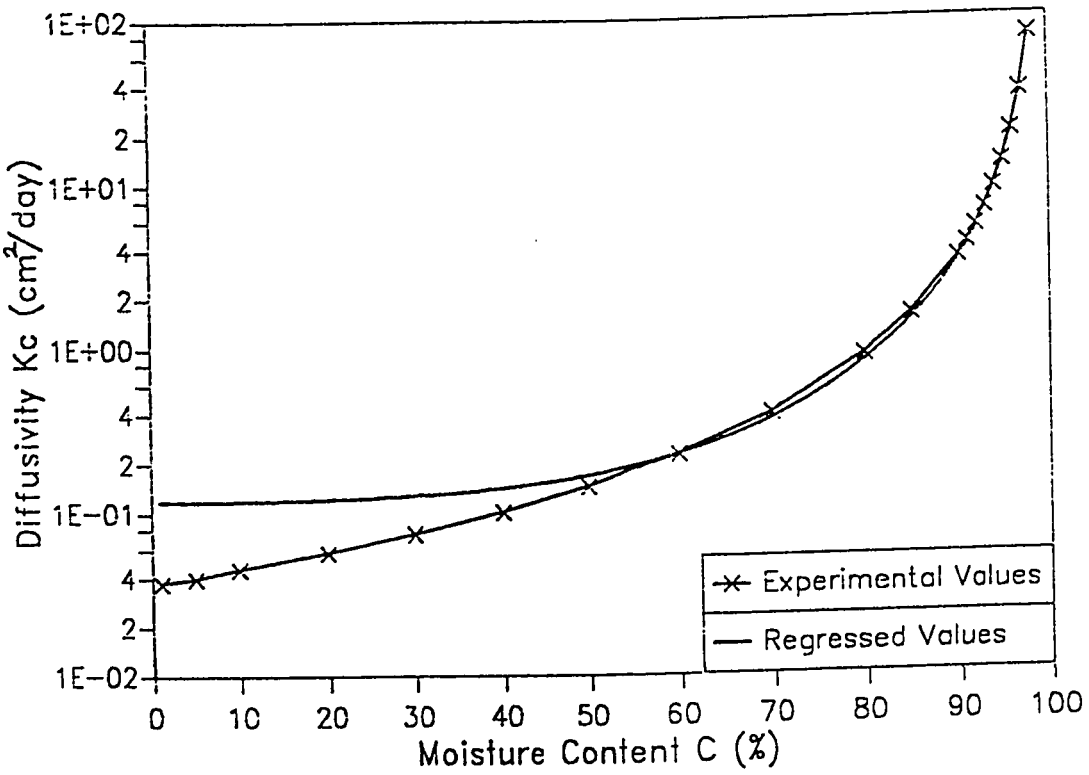

Figure 6.5: Relationship Between Moisture Content C and Diffusivity K_c

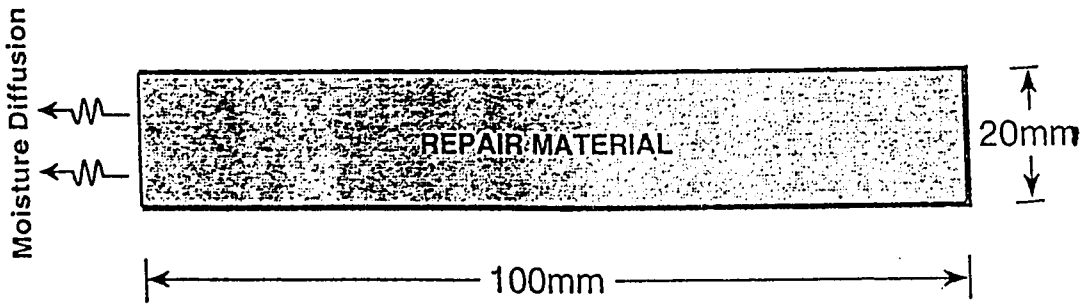

(a)

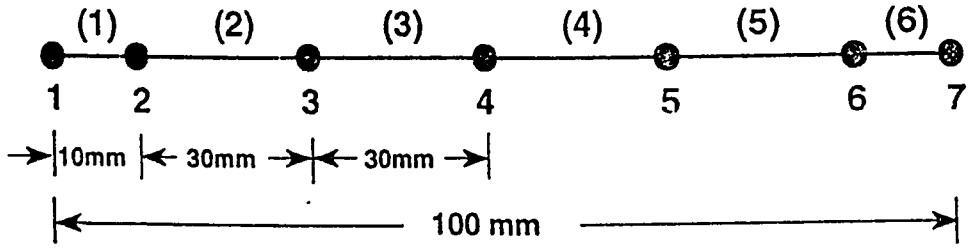

(b) Finite Element Discretization

Figure 6.6: Problem Solved Using One-Dimensional Finite Element Model

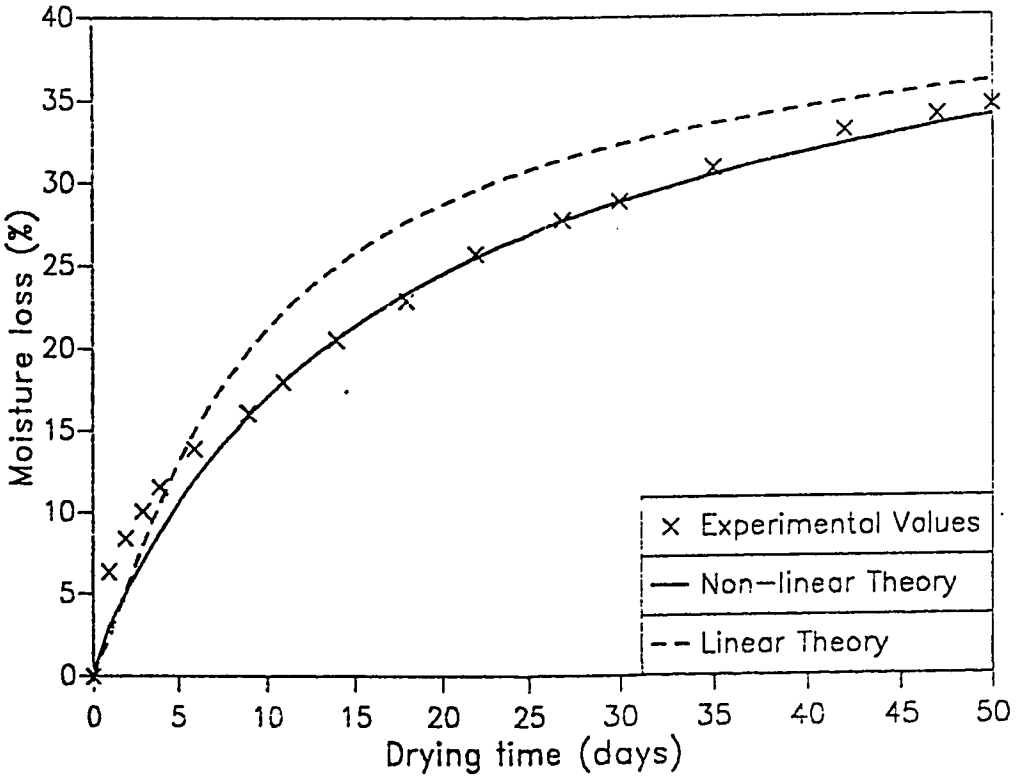

Figure 6.7: Experimental and Predicted Values of Moisture Loss at $x = 1cm$ from the Drying Surface

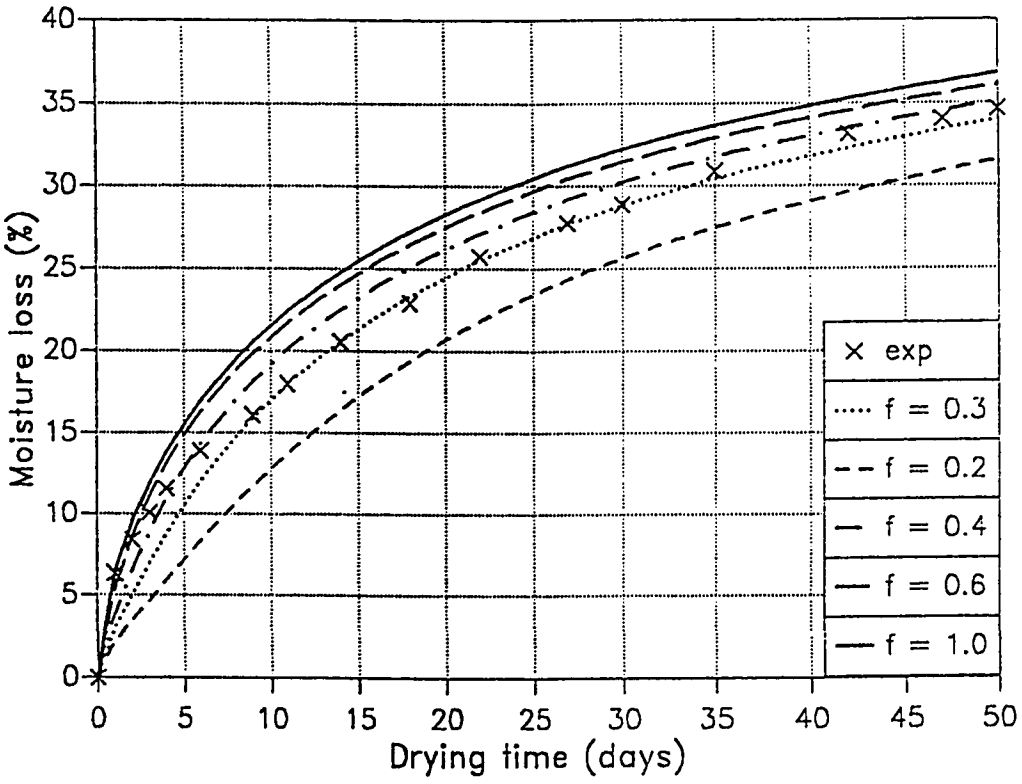

Figure 6.8: Effect of Variation in Surface Factor f on Moisture Loss Predictions

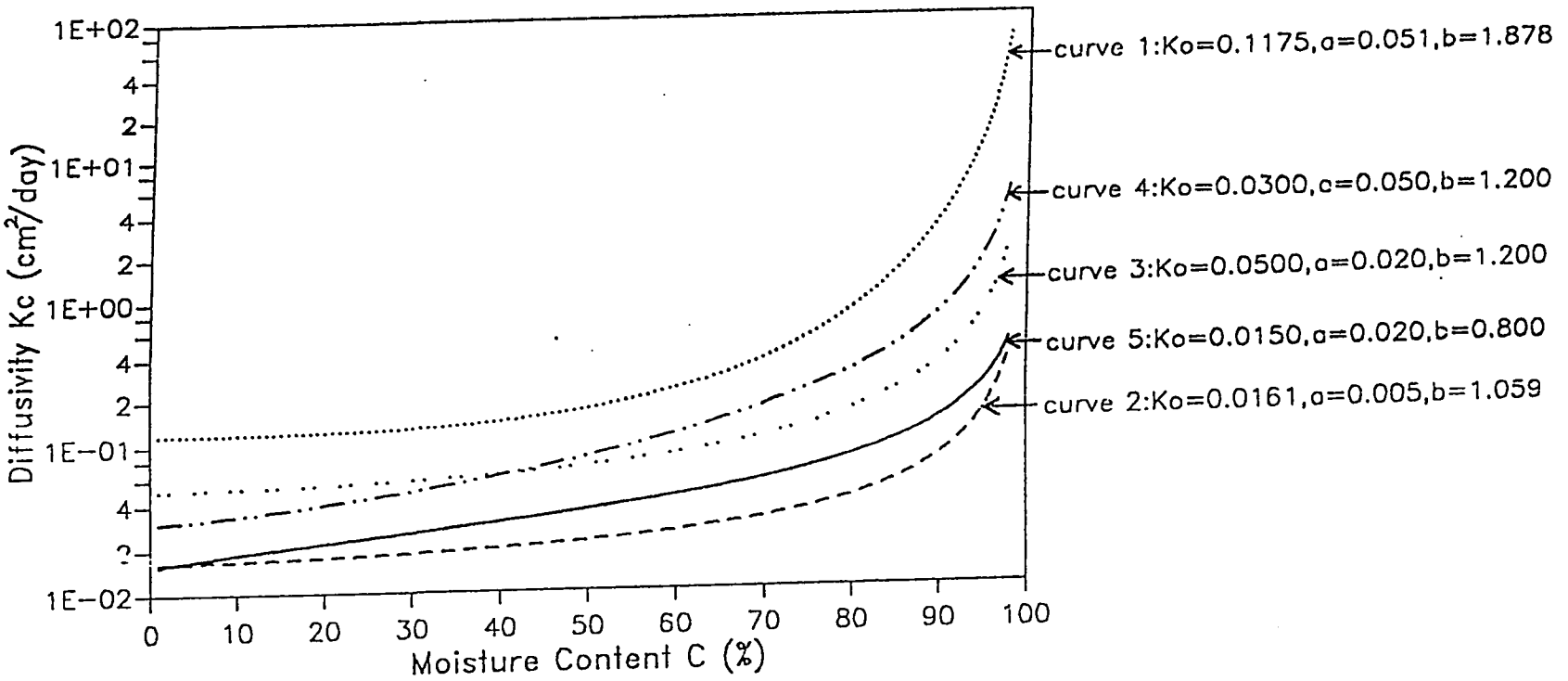

Figure 6.9: Relationships Between Diffusivity K_c and Moisture Content C for Different Values of K_o, a and b

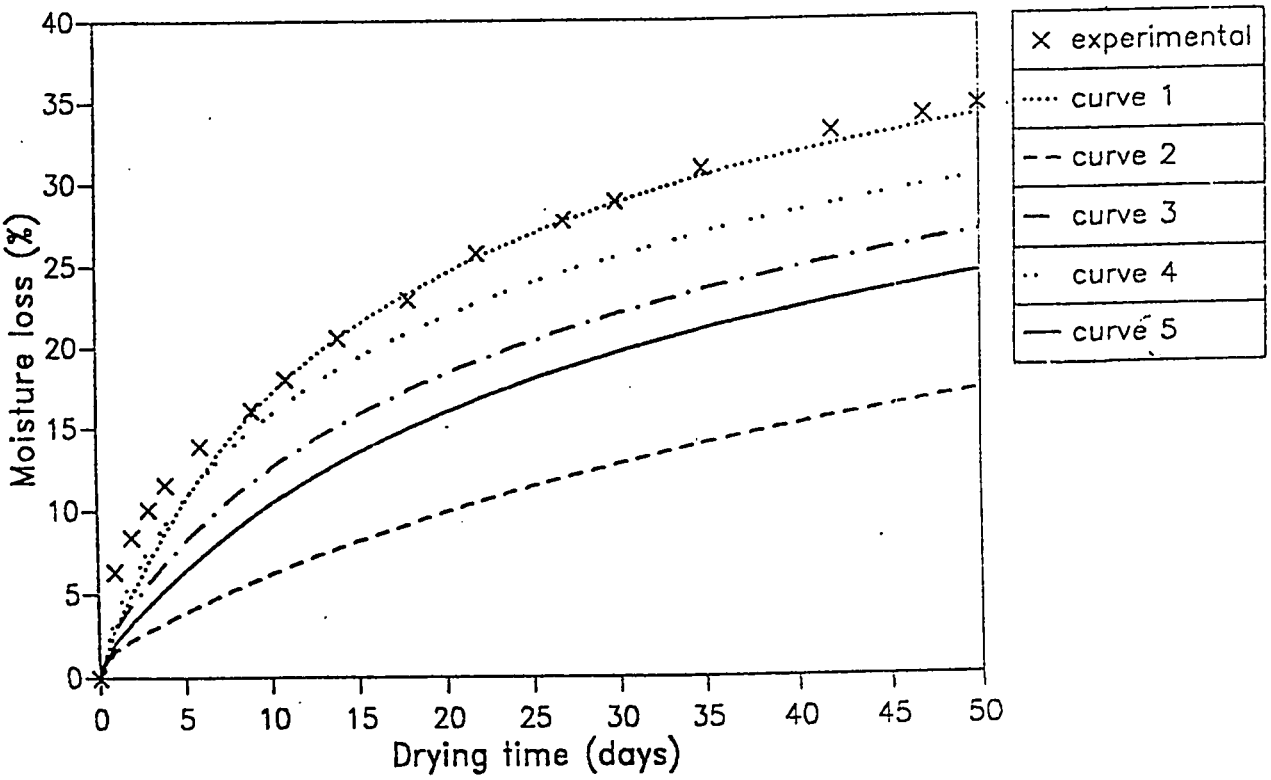

Figure 6.10: Moisture Loss Predictions for Different Relationships Between Diffusivity K_c and Moisture Content C

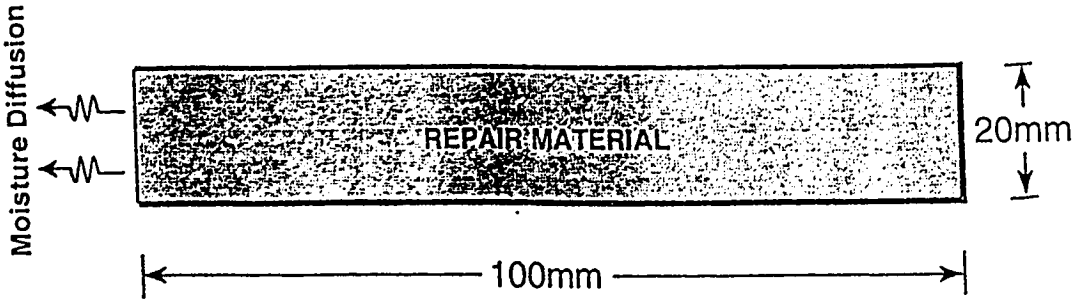

(a) Case I

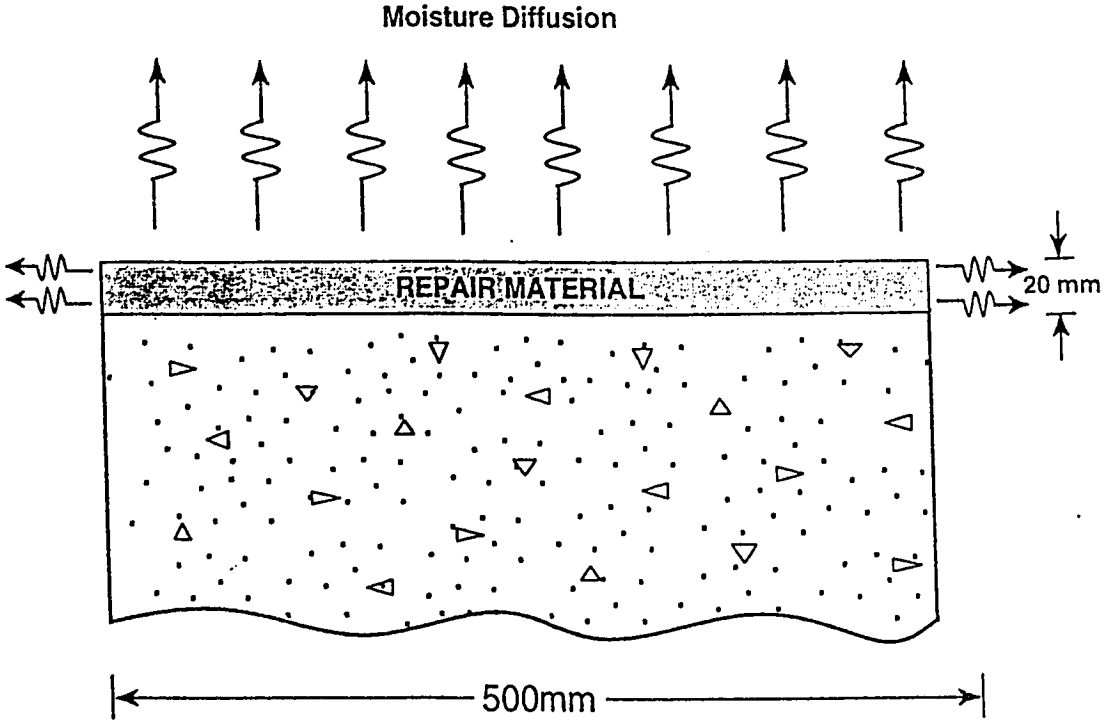

(b) Case II

Figure 6.11: Cases Solved Using Two-Dimensional Finite Element Model

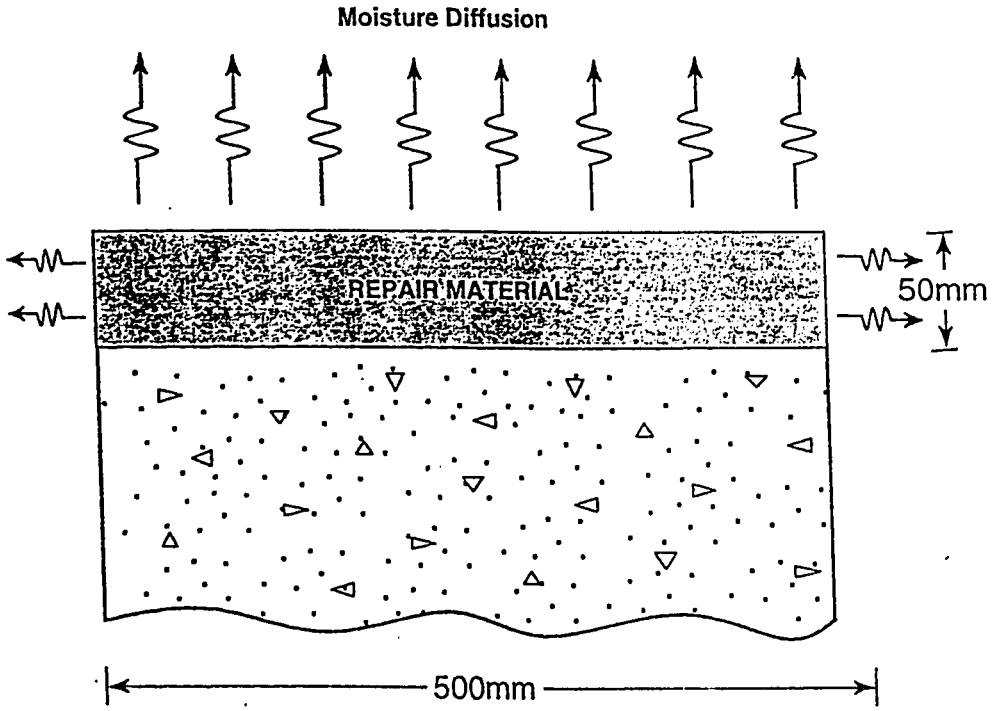

(c) Case III

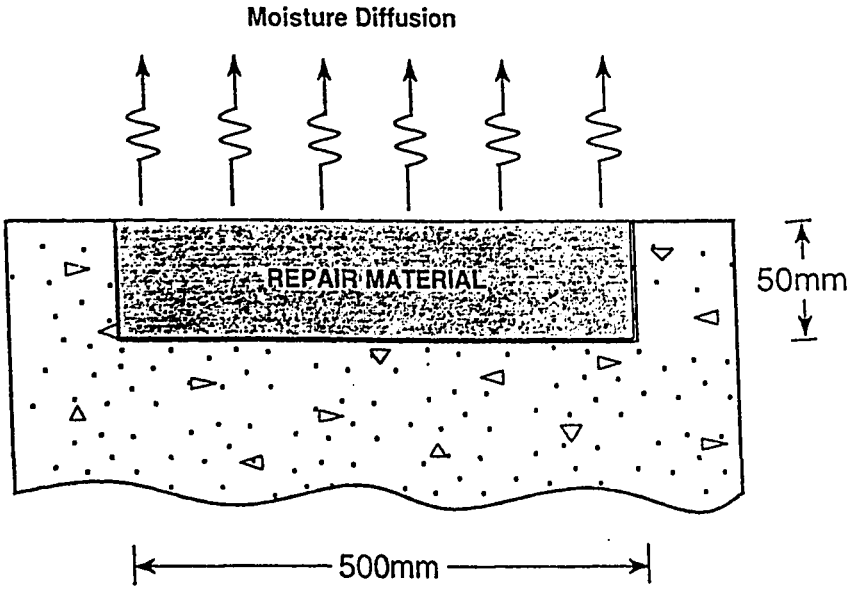

(d) Case IV

Figure 6.12: Cases Solved Using Two-Dimensional Finite Element Model (Continued)

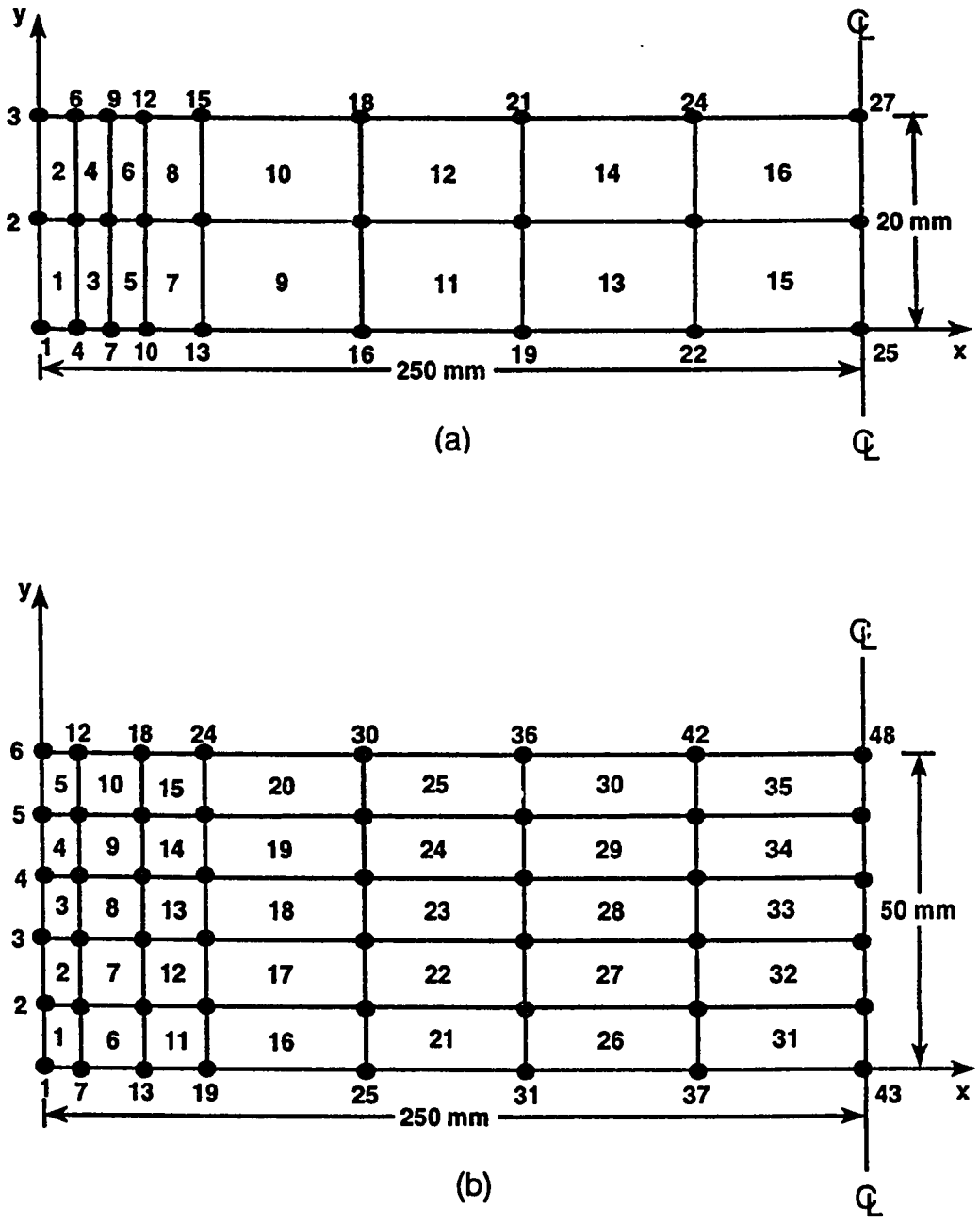

Figure 6.13: Finite Element Discretization (a)20mm Thick Repair Layer (b)50mm Thick Repair Layer

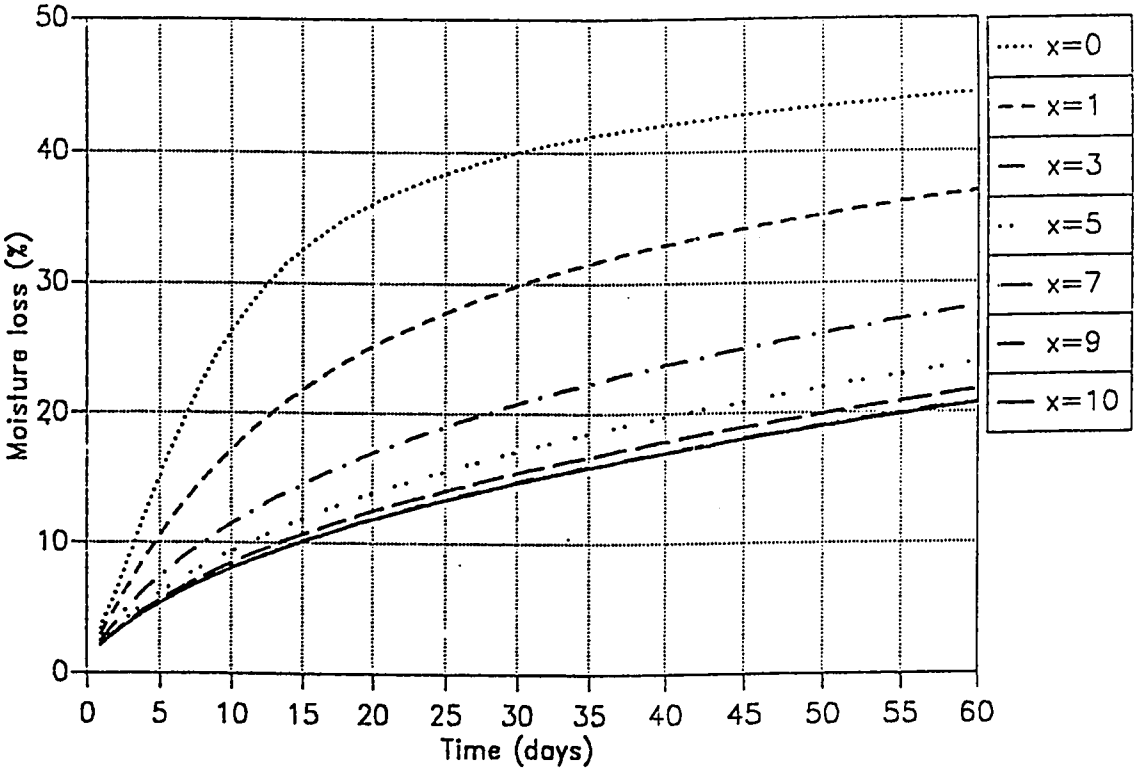

Figure 6.14: Time-Dependent Changes in Moisture Loss Along the Distance from the Drying Surface(Case I)

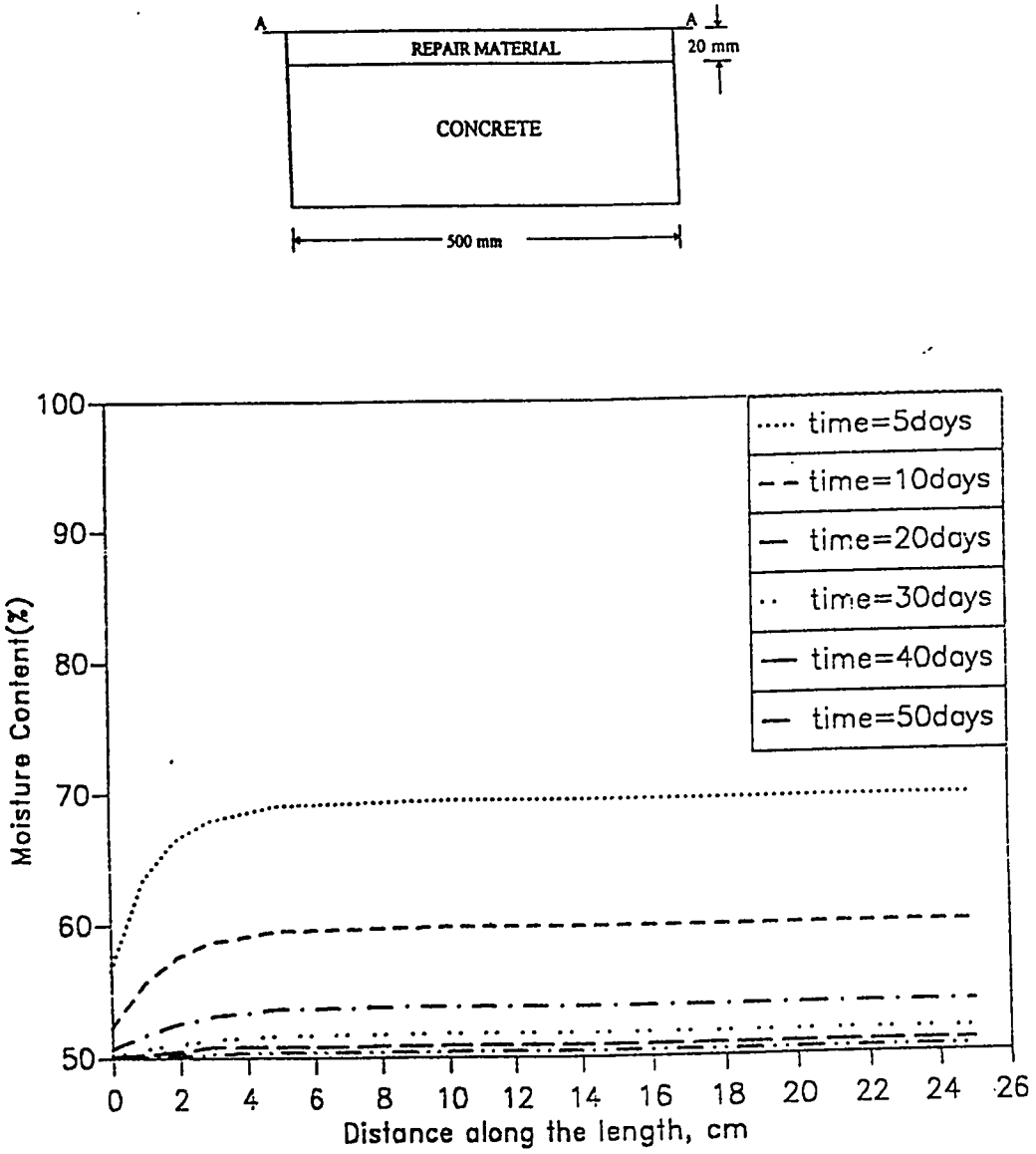

Figure 6.15: Time-Dependent Changes in Moisture Content at Section A-A(Case II)

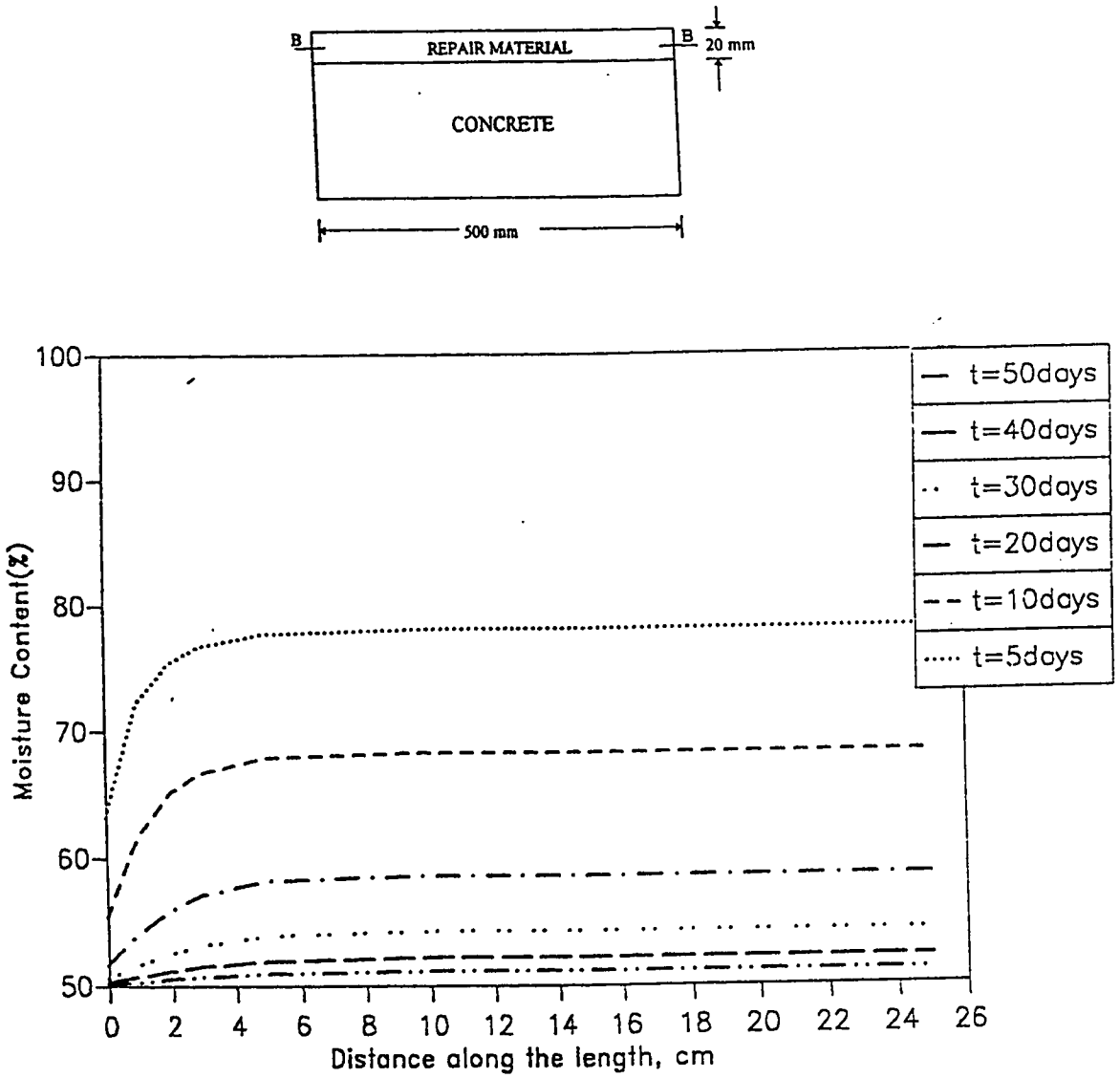

Figure 6.16: Time-Dependent Changes in Moisture Content at Section B-B(Case II)

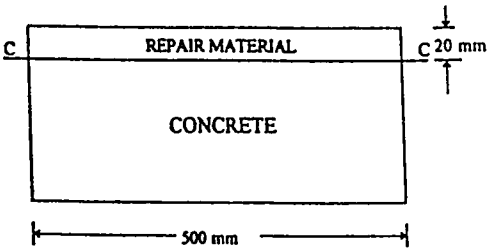

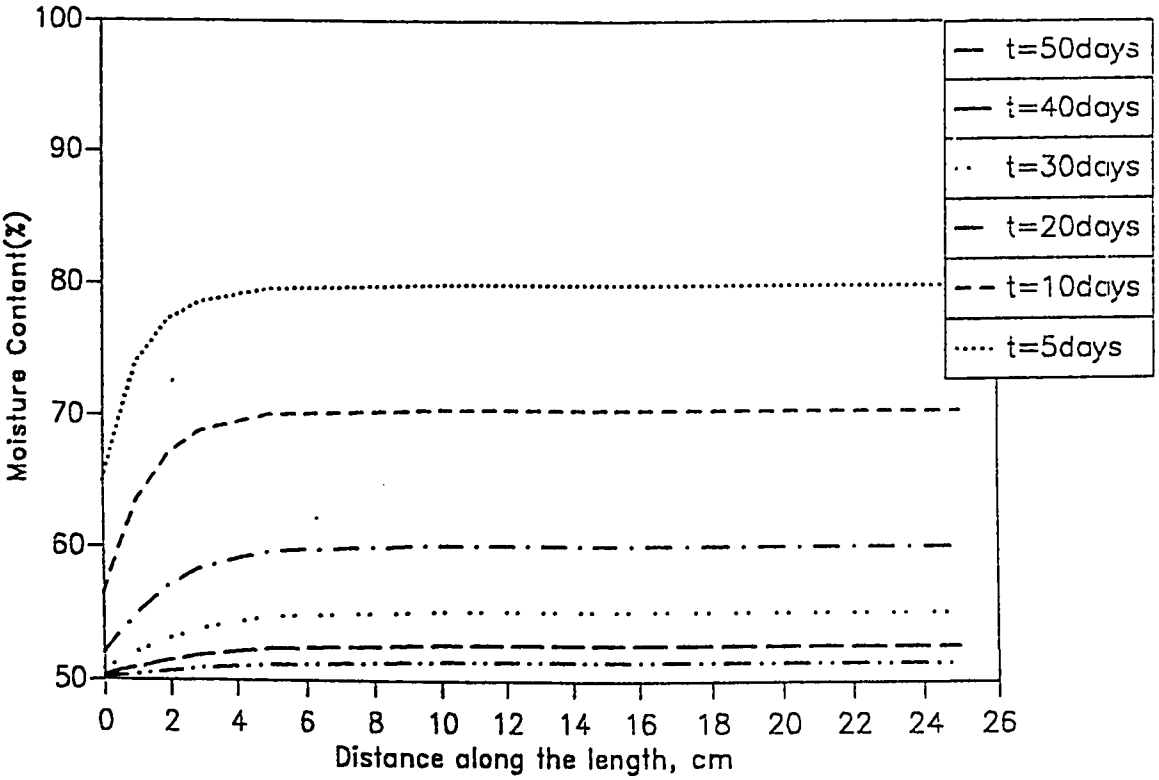

Figure 6.17: Time-Dependent Changes in Moisture Content at Section C-C(Case II)

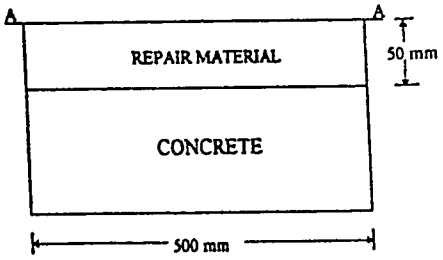

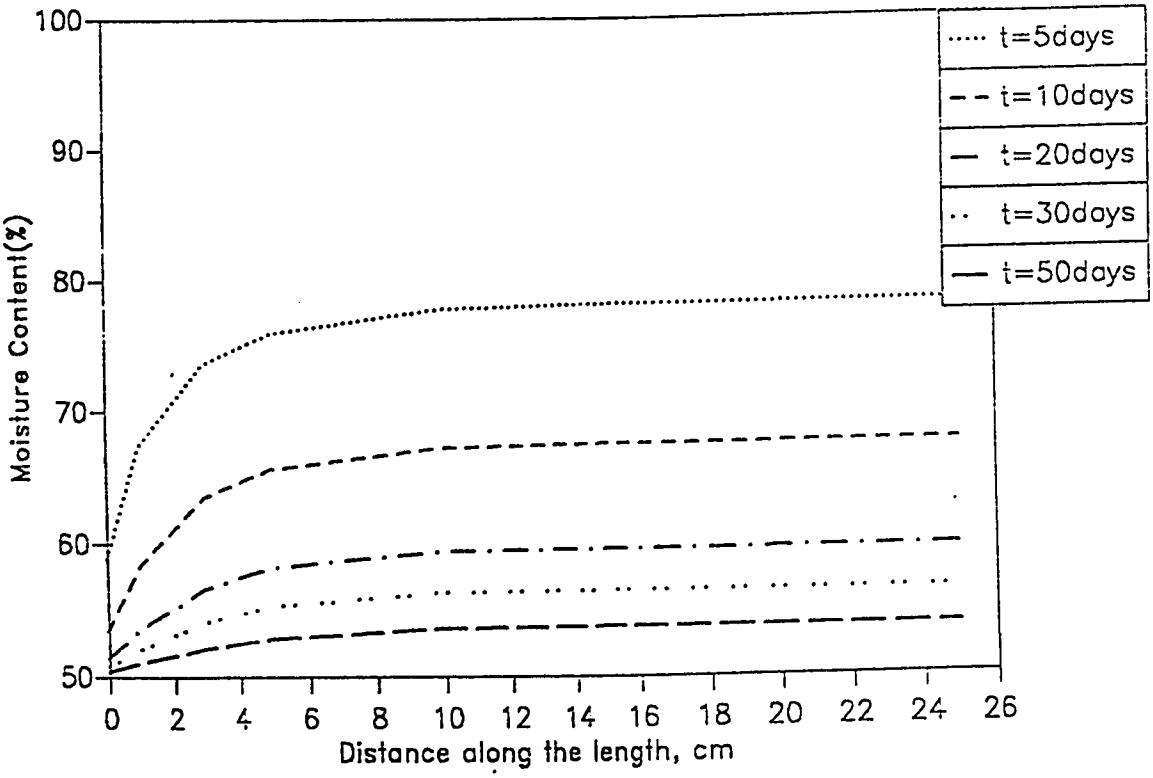

Figure 6.18: Time-Dependent Changes in Moisture Content at Section A-A(Case III)

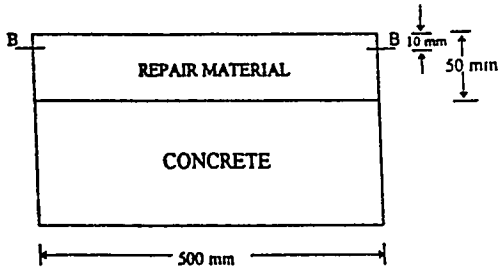

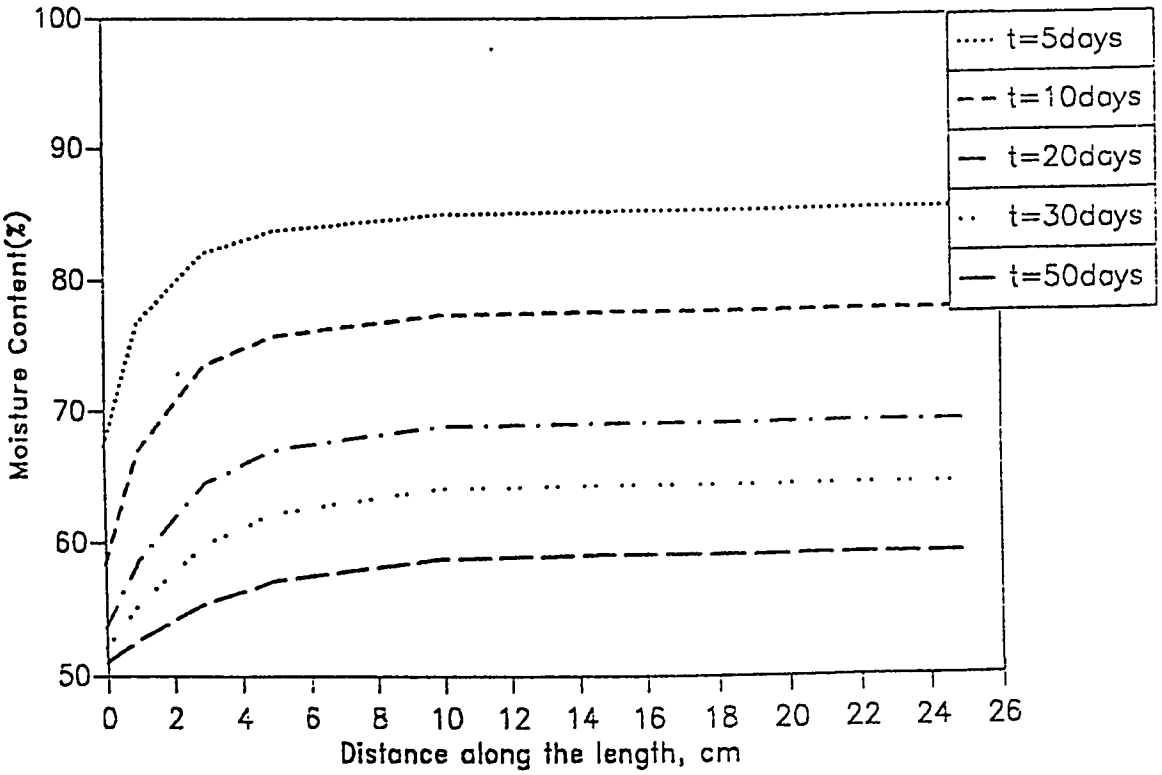

Figure 6.19: Time-Dependent Changes in Moisture Content at Section B-B(Case III)

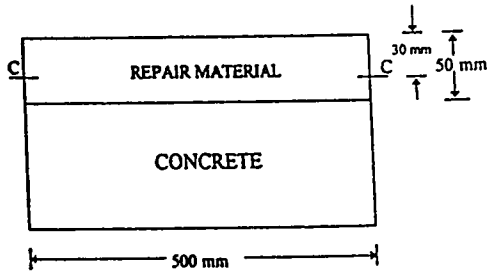

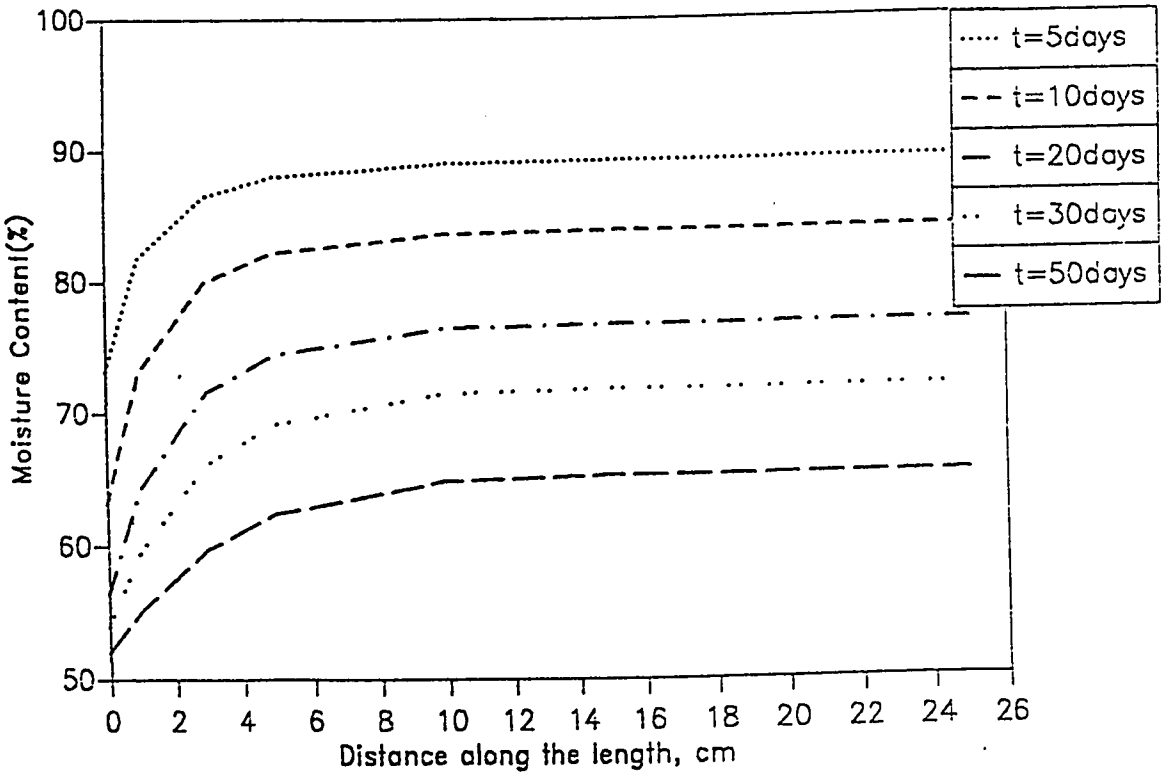

Figure 6.20: Time-Dependent Changes in Moisture Content at Section C-C(Case III)

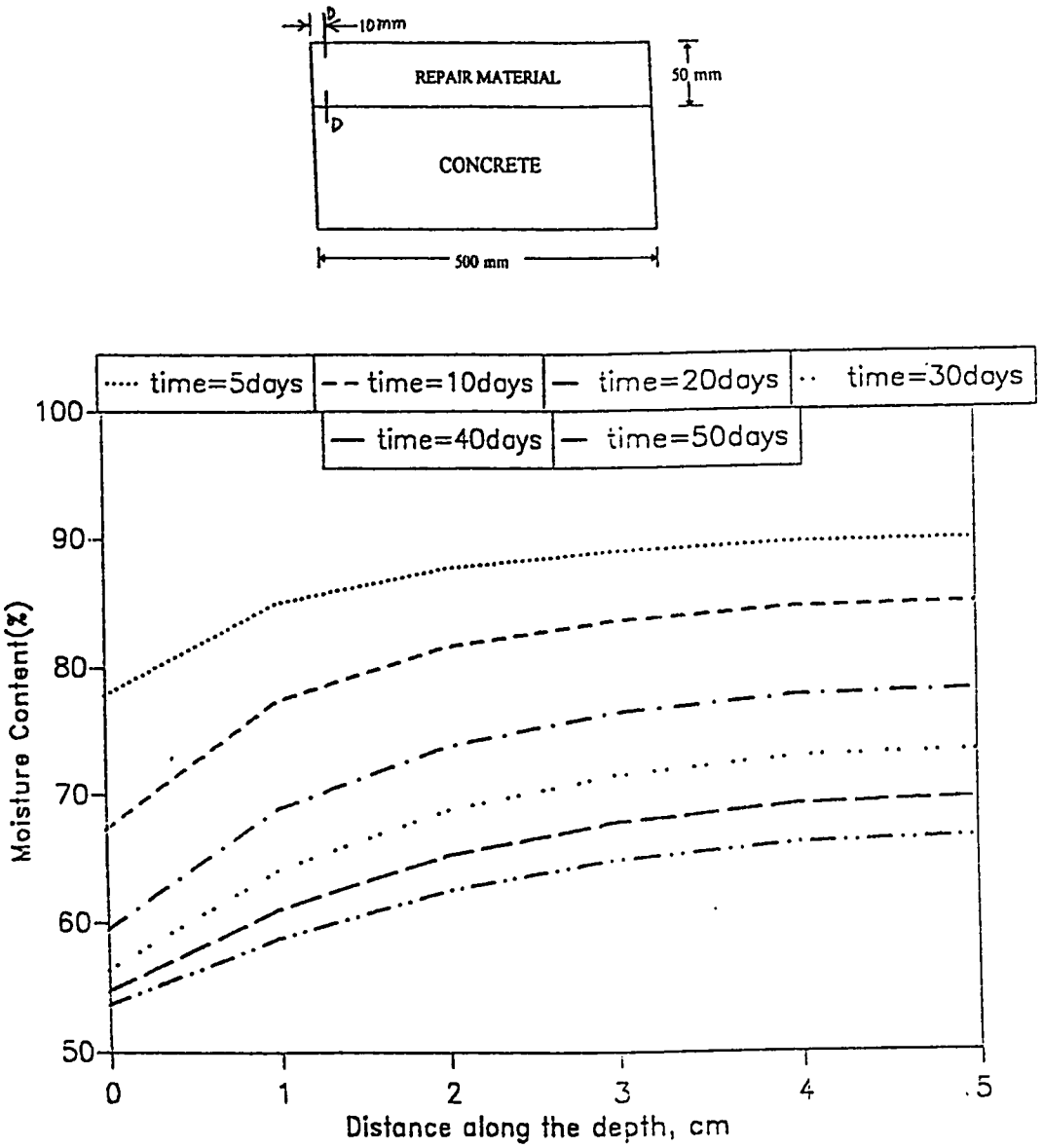

Figure 6.21: Time-Dependent Changes in Moisture Content at Section D-D(Case III)

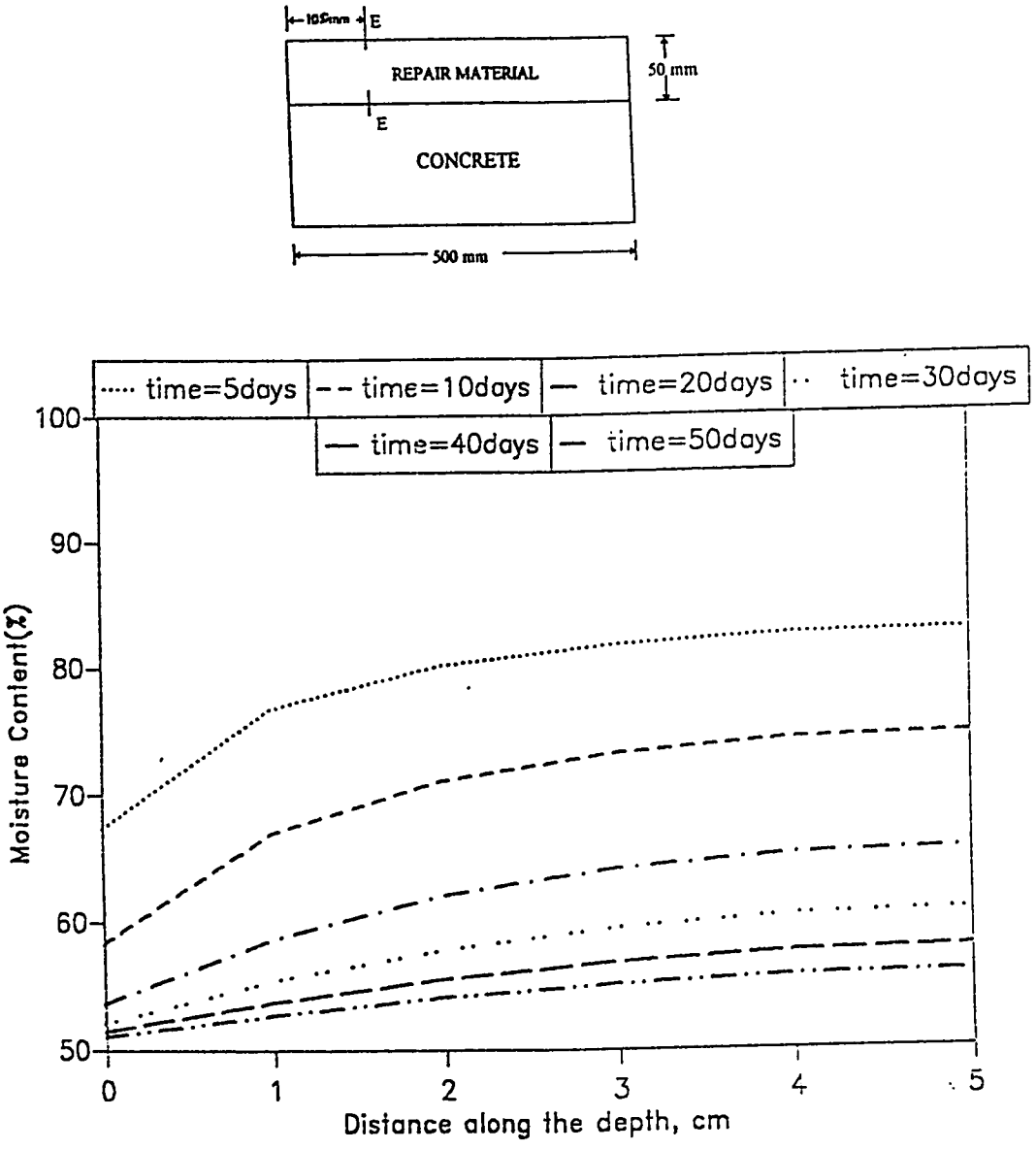

Figure 6.22: Time-Dependent Changes in Moisture Content at Section E-E(Case III)

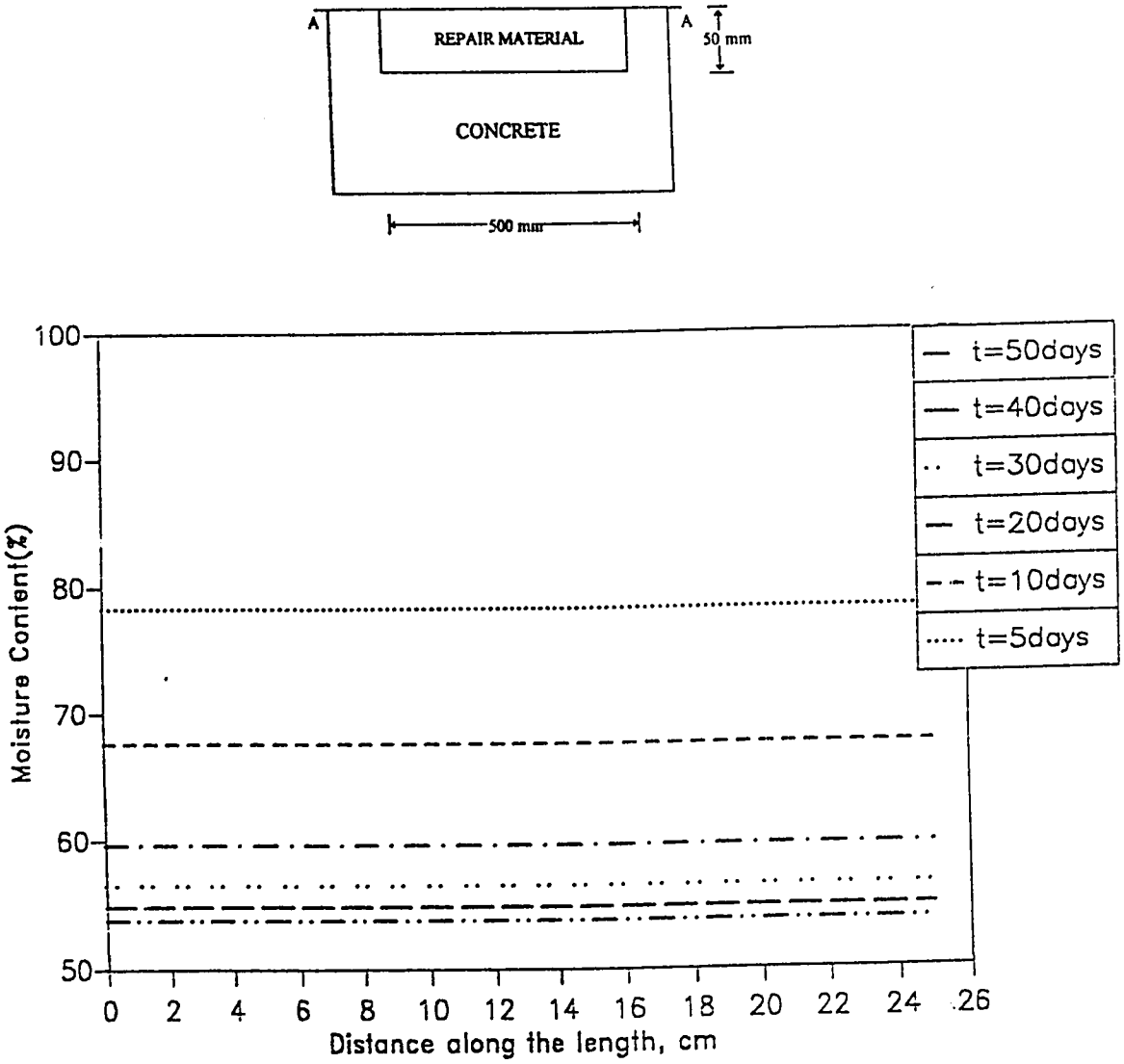

Figure 6.23: Time-Dependent Changes in Moisture Content at Section A-A(Case IV)

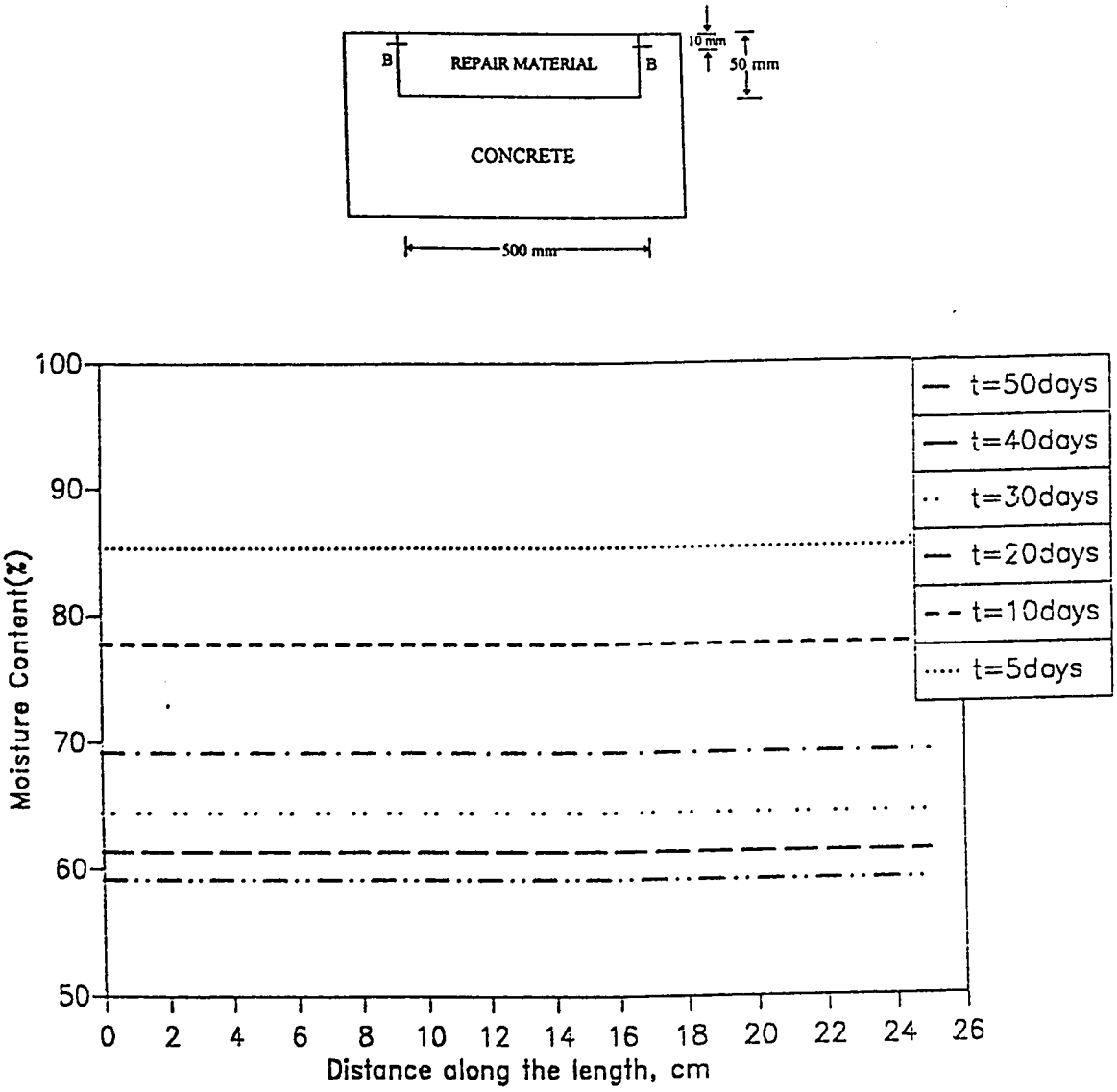

Figure 6.24: Time-Dependent Changes in Moisture Content at Section B-B(Case IV)

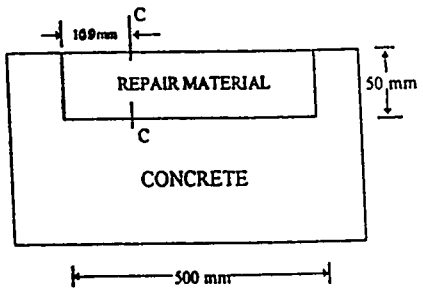

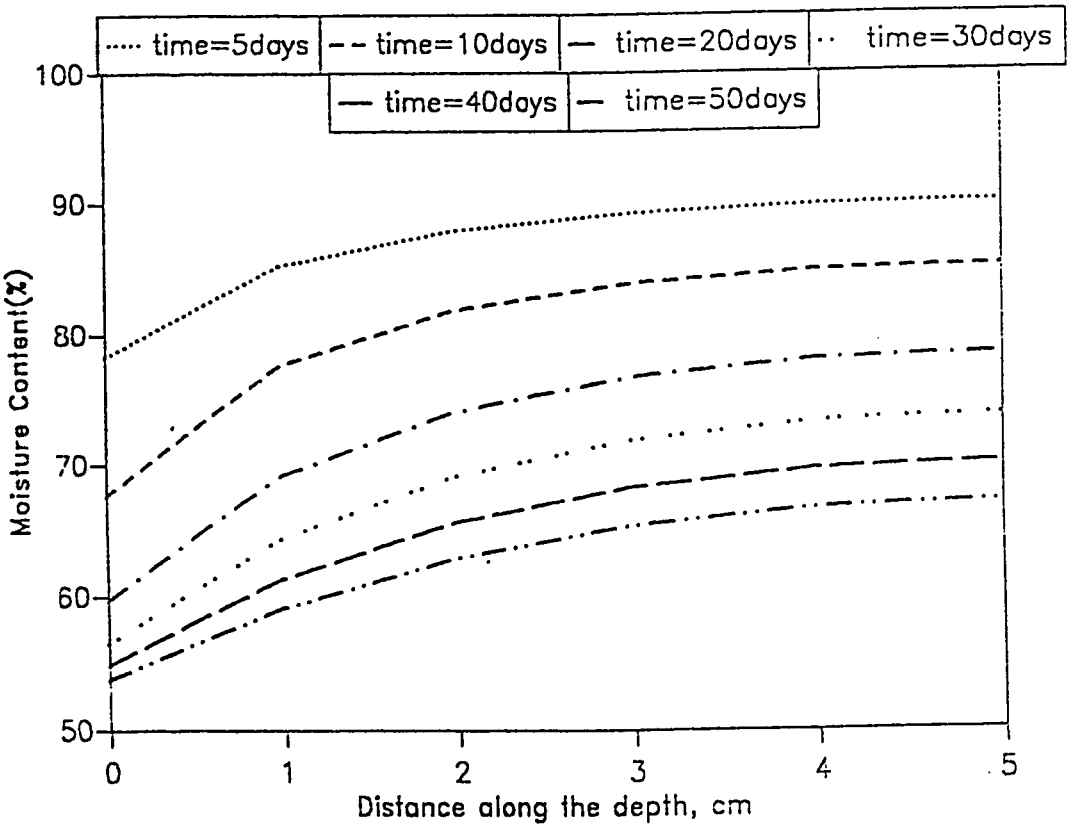

Figure 6.25: Time-Dependent Changes in Moisture Content at Section C-C(Case IV)

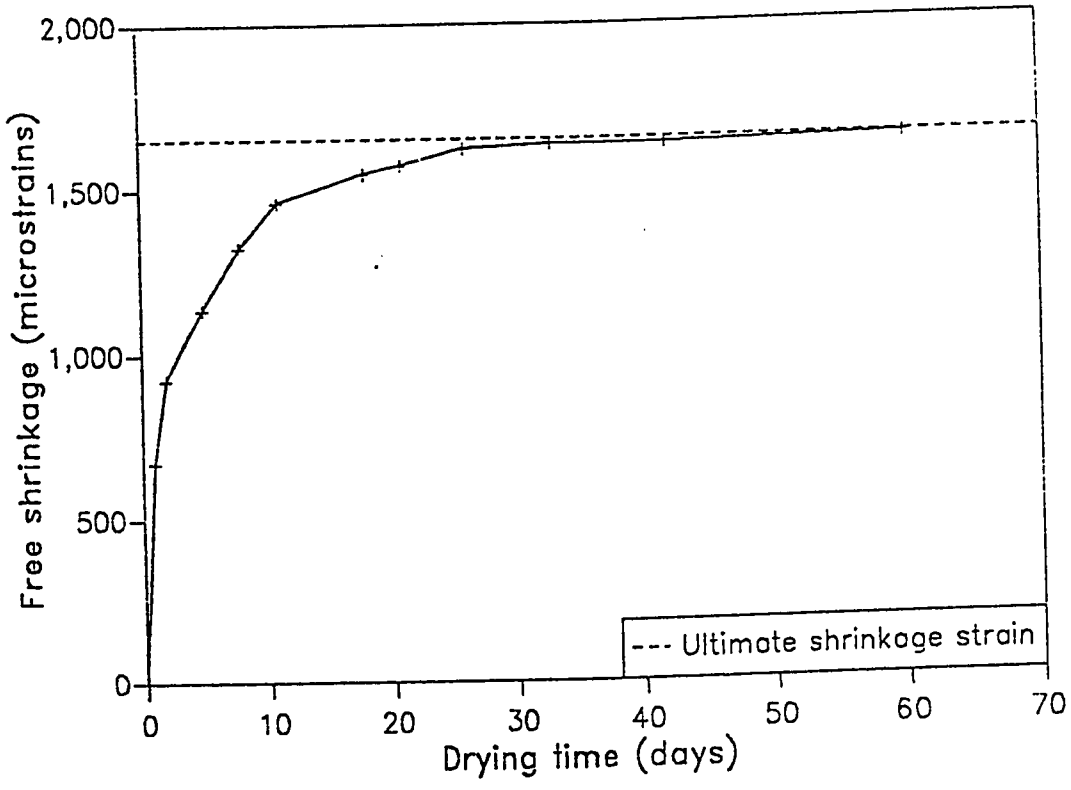

Figure 6.26: Free Shrinkage Strains vs Drying Time

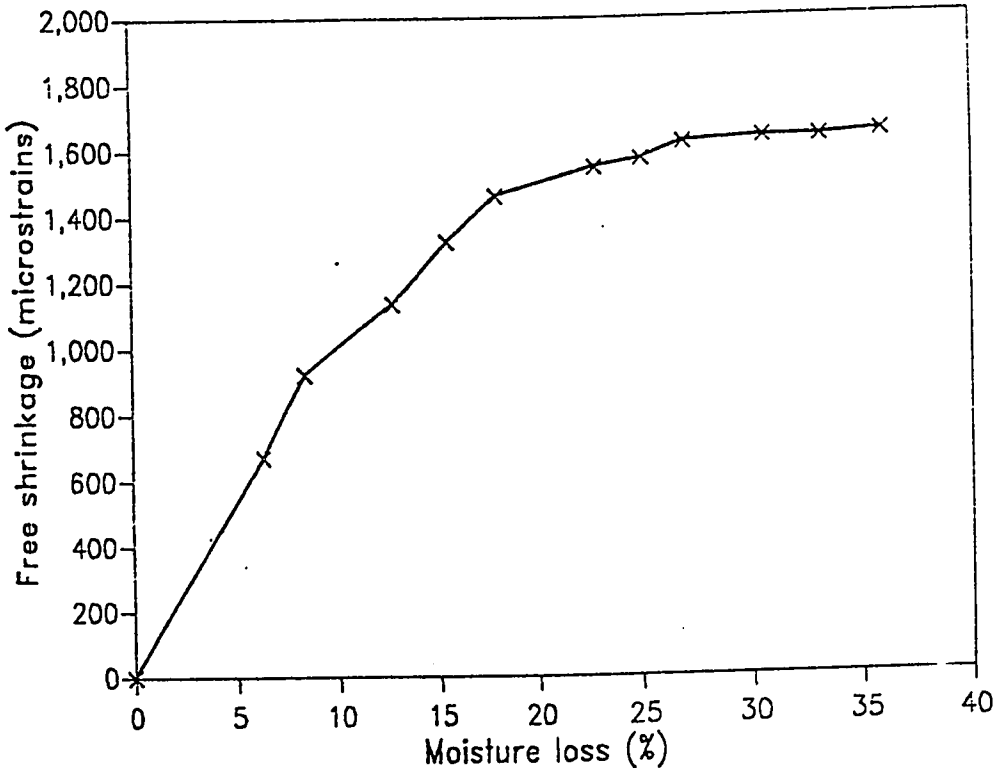

Figure 6.27: Relationship Between Free Shrinkage Strains and Moisture Loss

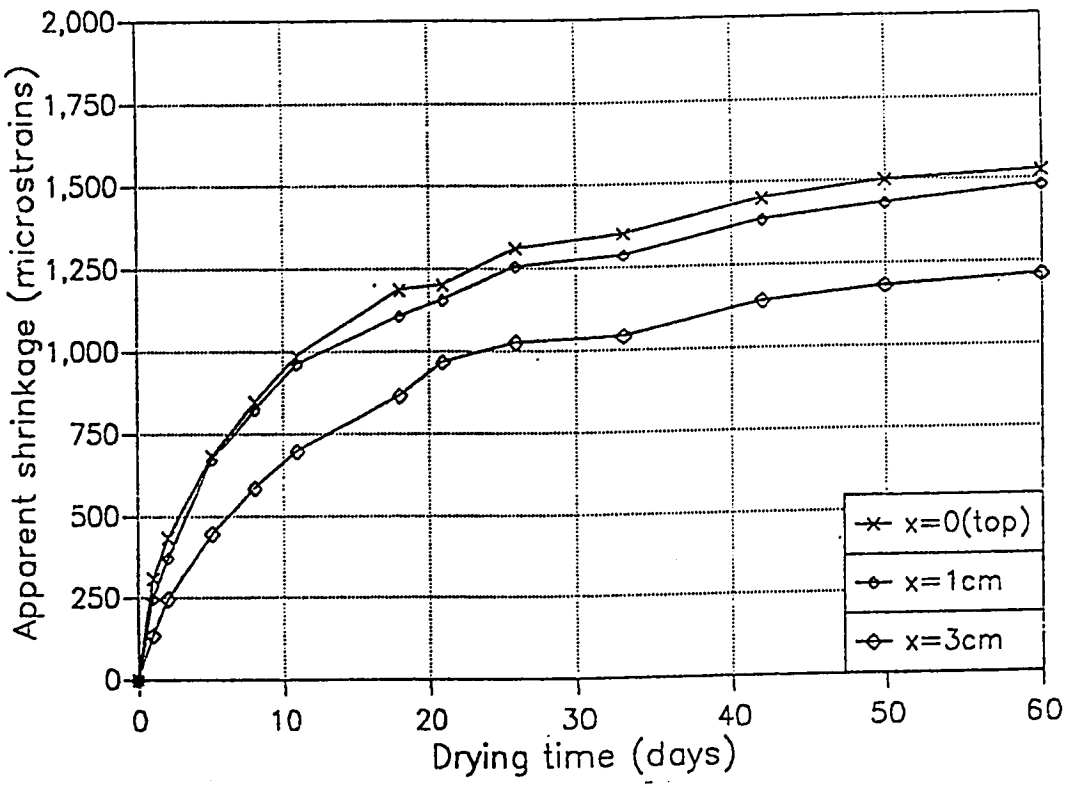

Figure 6.28: Apparent Shrinkage Strains Vs Drying Time

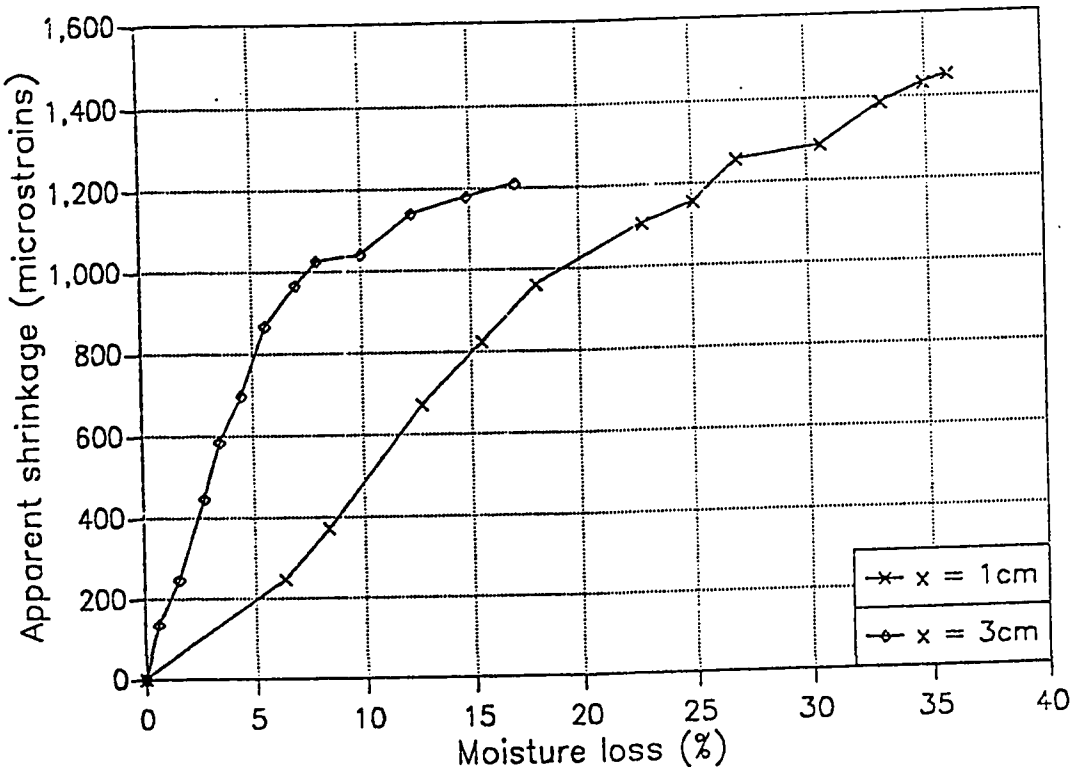

Figure 6.29: Relationship Between Apparent Shrinkage Strains and Moisture Loss

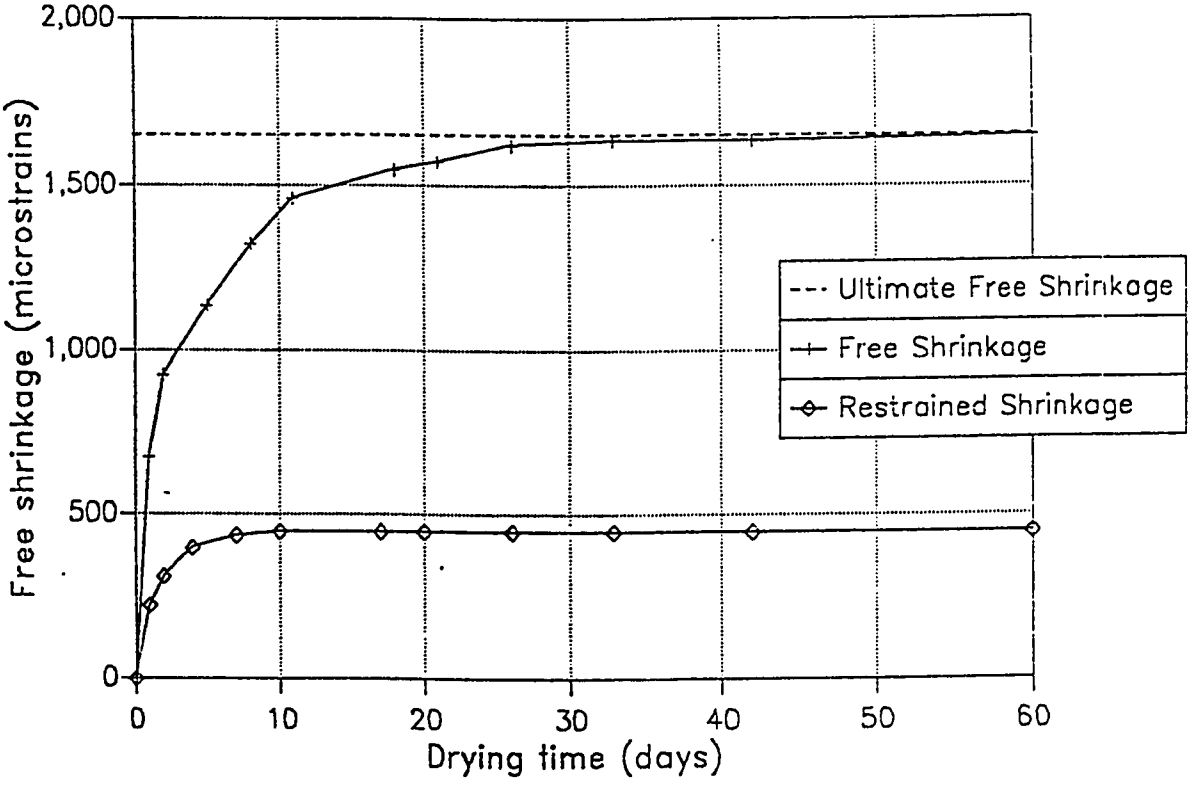

Figure 6.30: Comparision Between Free and Restrained Shrinkage Strains

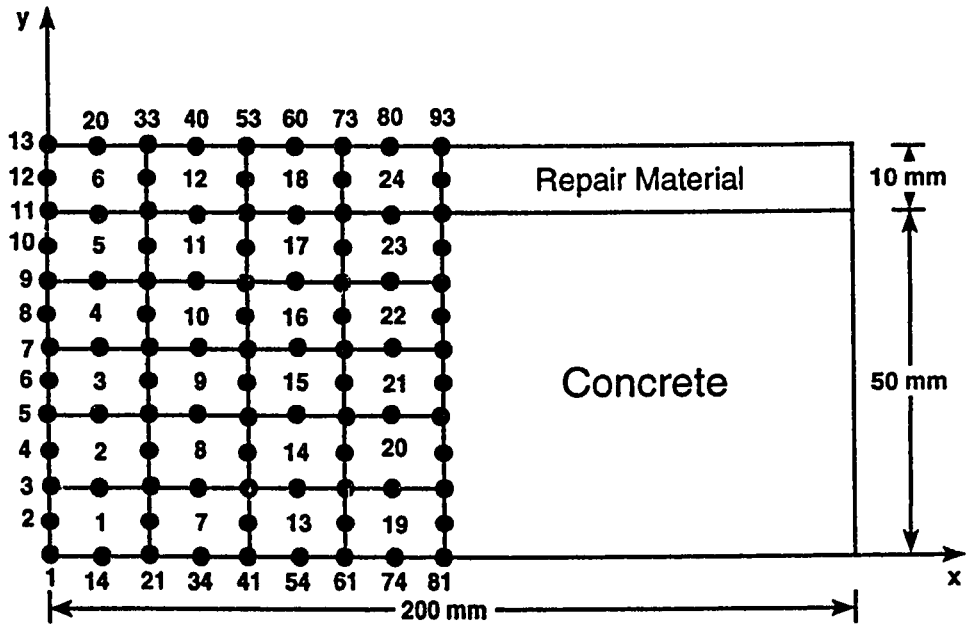

Figure 6.31: Finite Element Discretization Using 8-Noded Elements

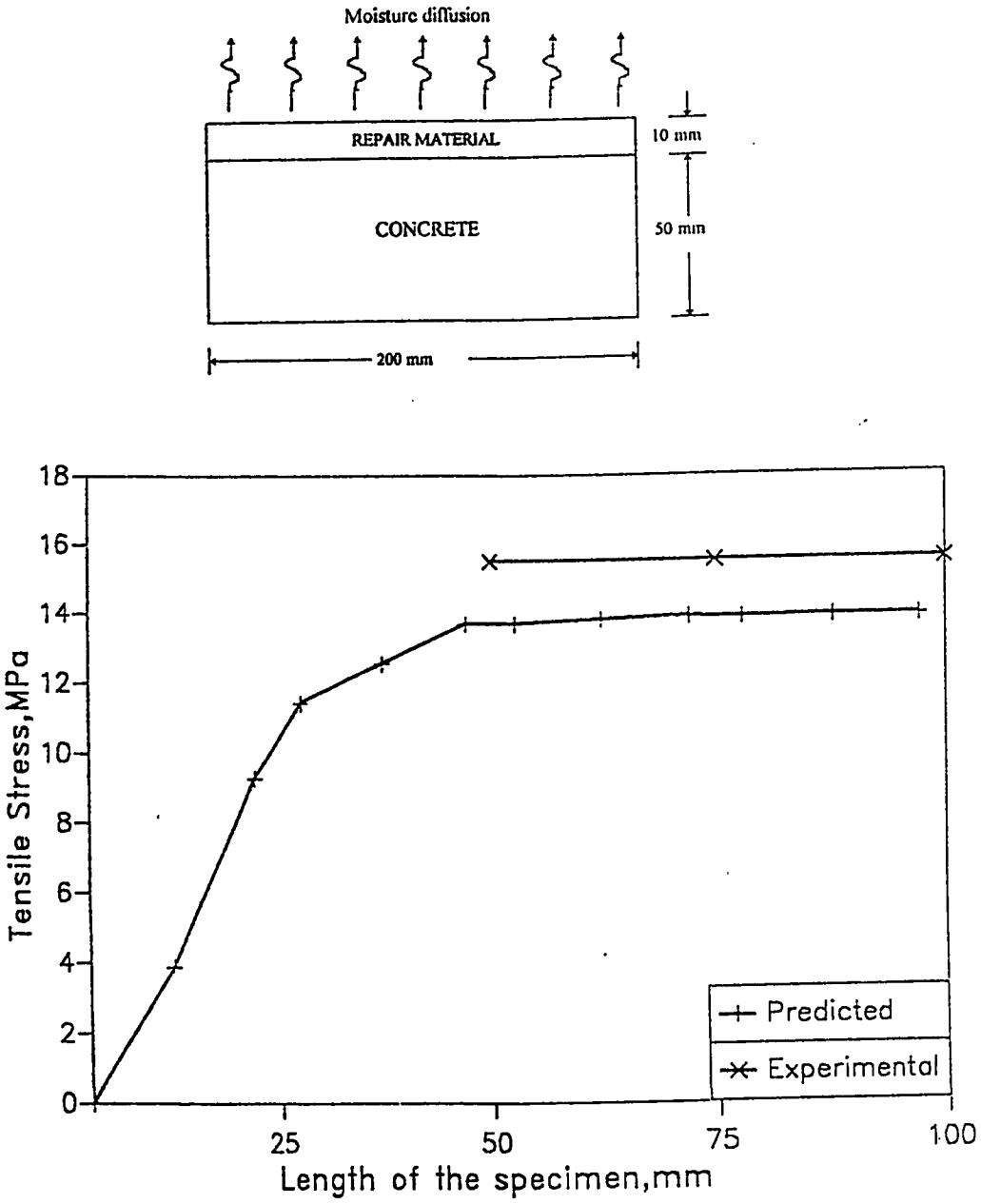

Figure 6.32: Comparision Between Predicted and Calculated Values of Shrinkage Stresses

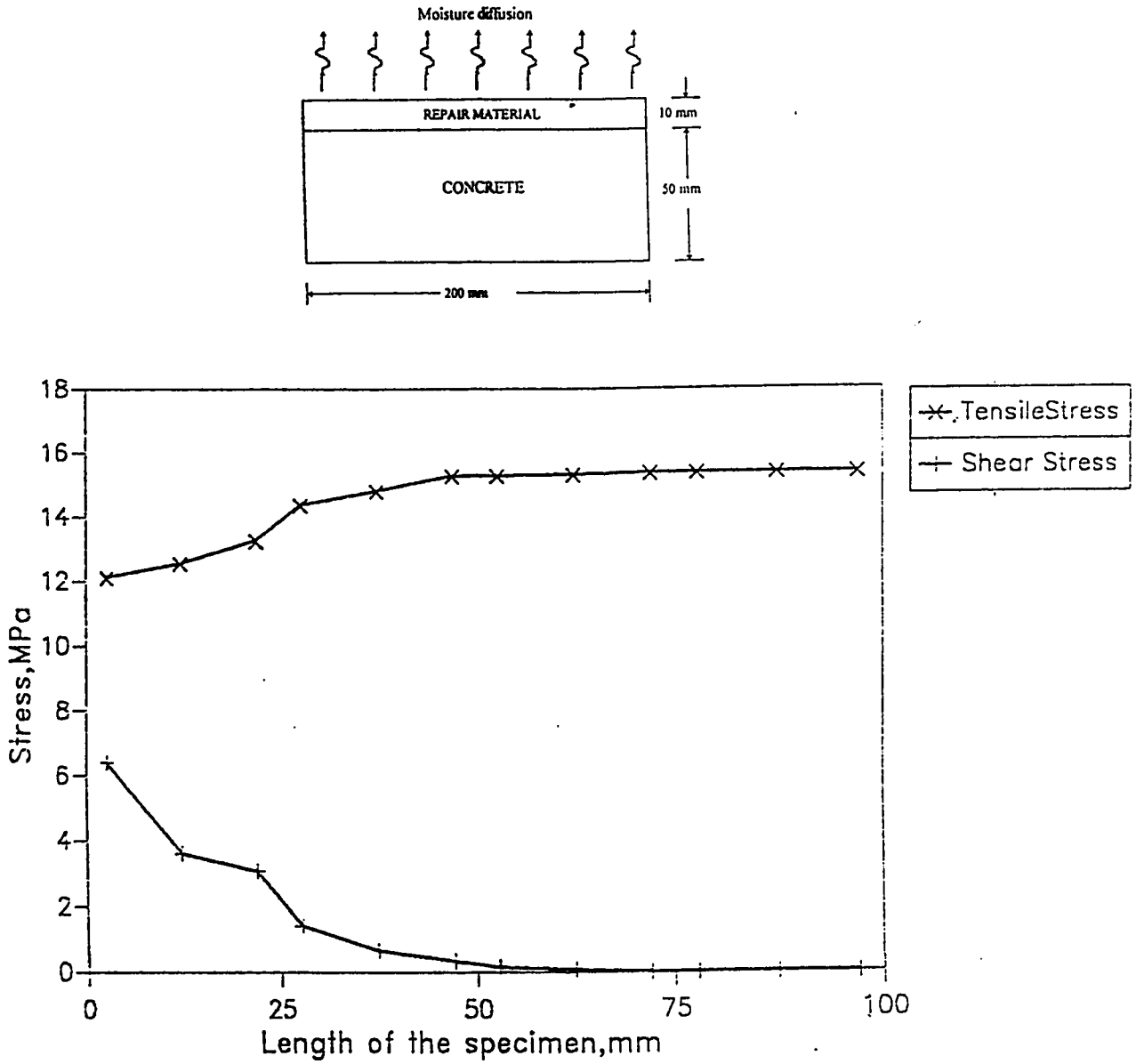

Figure 6.33: Shrinkage Stresses at the Interface in the Repair Material (Due to Shrinkage Strain of 0.0015)

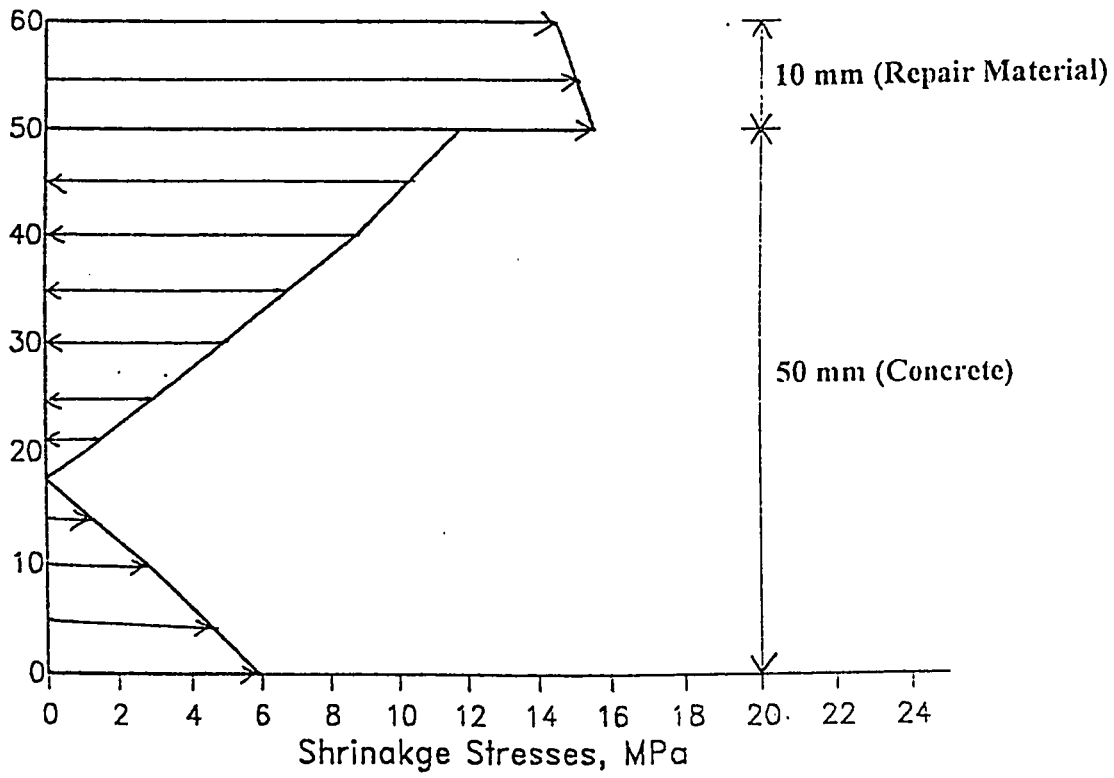

Figure 6.34: Variation of Shrinkage stresses Along the depth of the Repaired Section (Due to Shrinkage Strain of 0.0015)

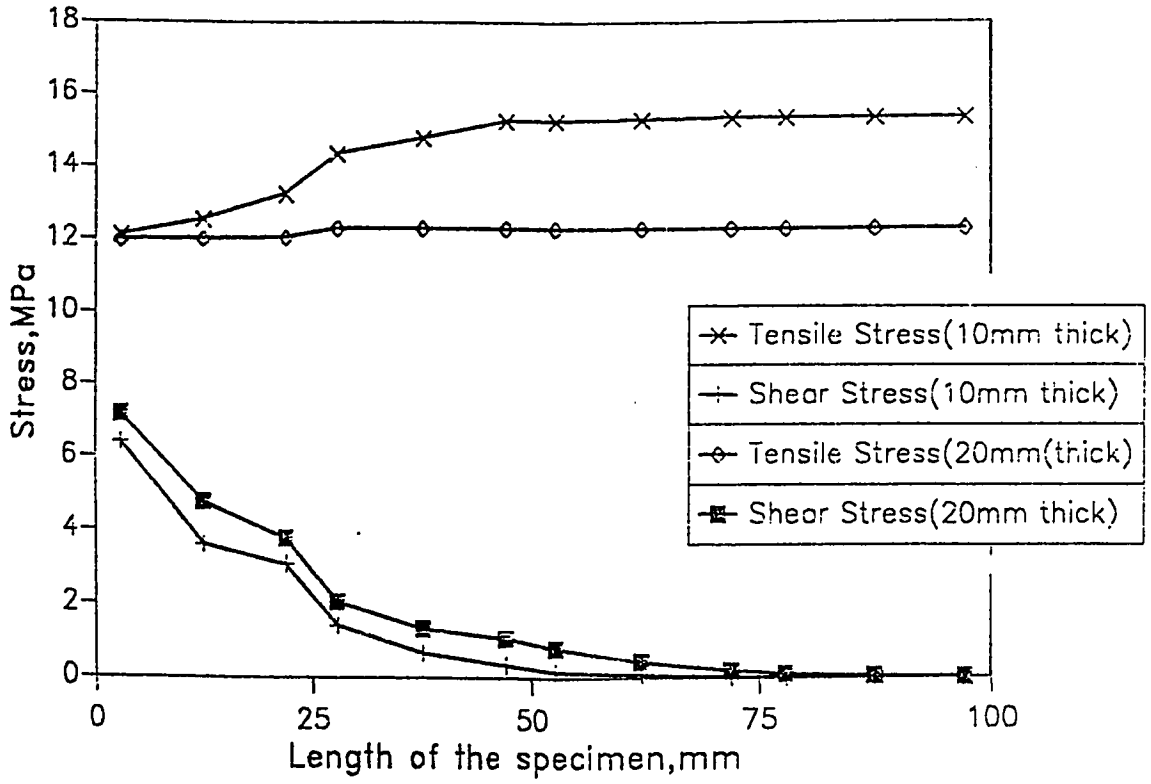

Figure 6.35: Shrinkage Stresses at the Interface in the Repair Material (Due to Shrinkage Strain of 0.0015)

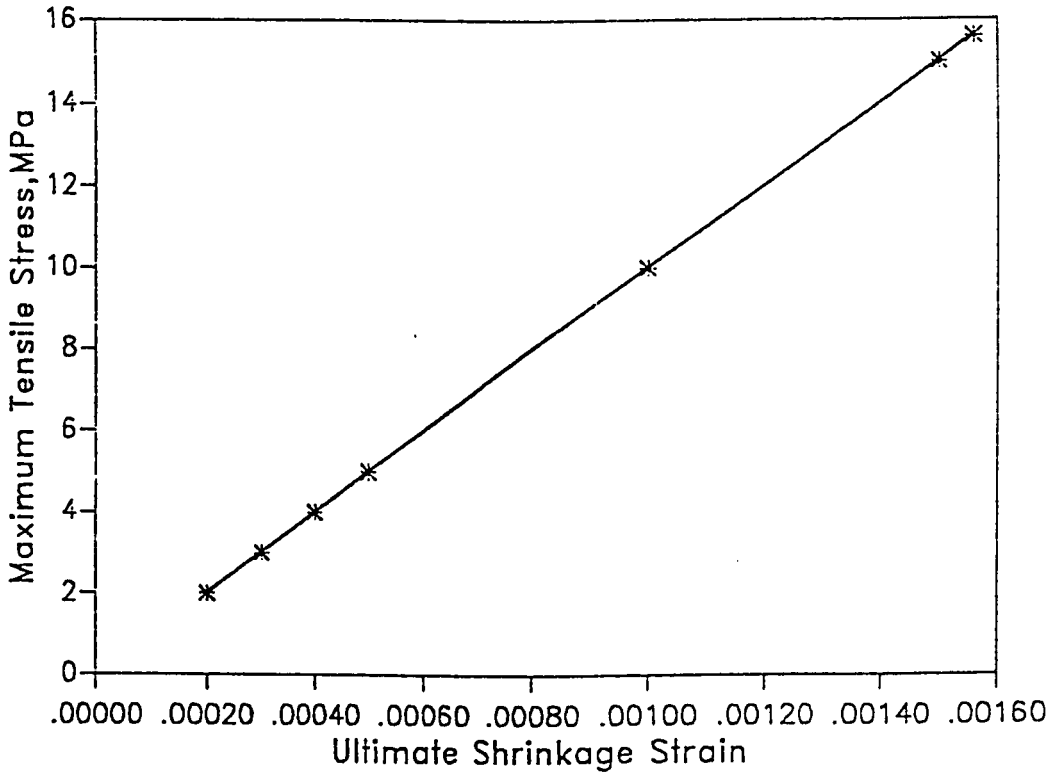

Figure 6.36: Variation of Maximum Tensile Stress with Ultimate Free Shrinkage Strain

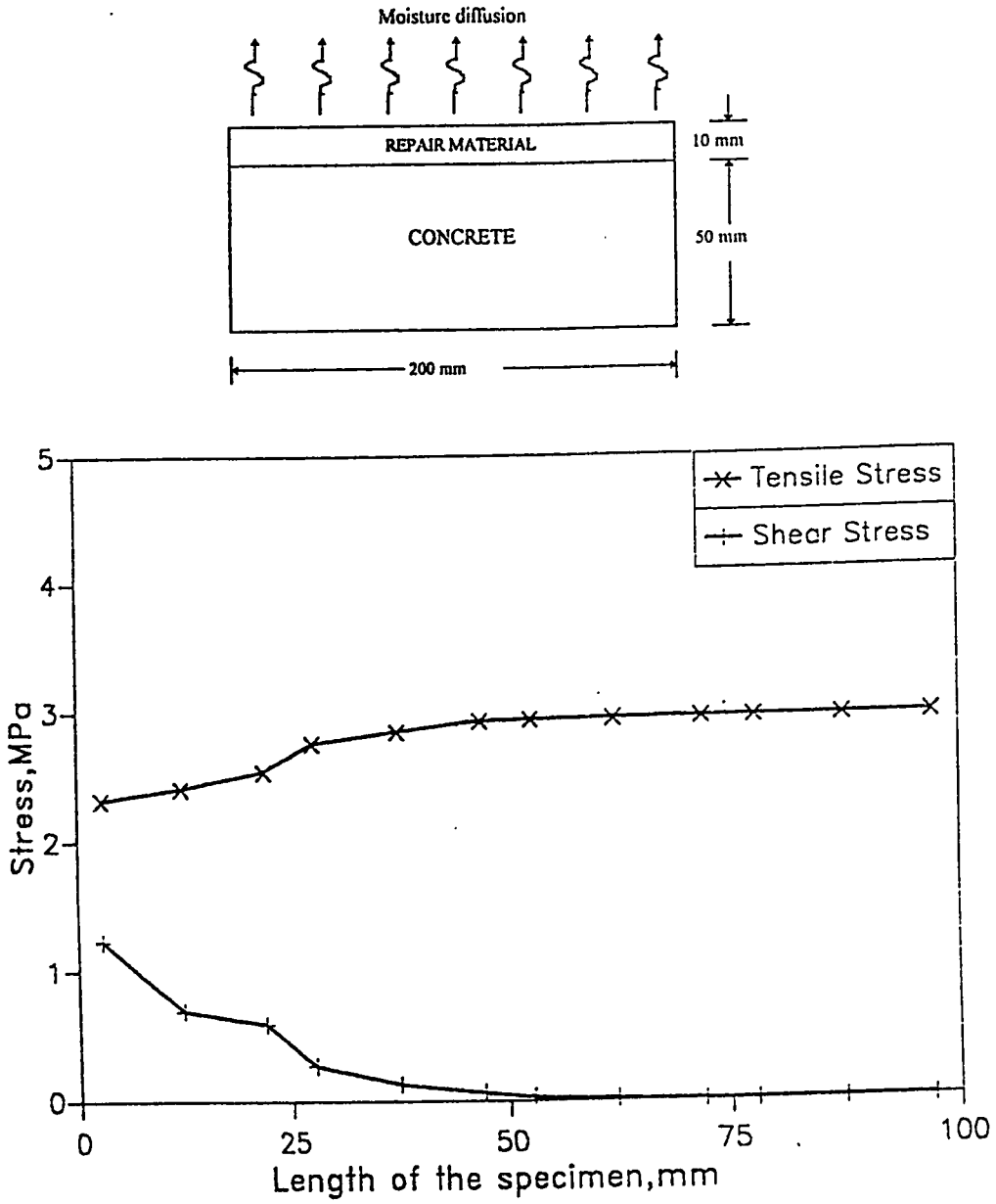

Figure 6.37: Shrinkage stresses at the Interface in the Repair Material (Due to Shrinkage Strain of 0.0003)

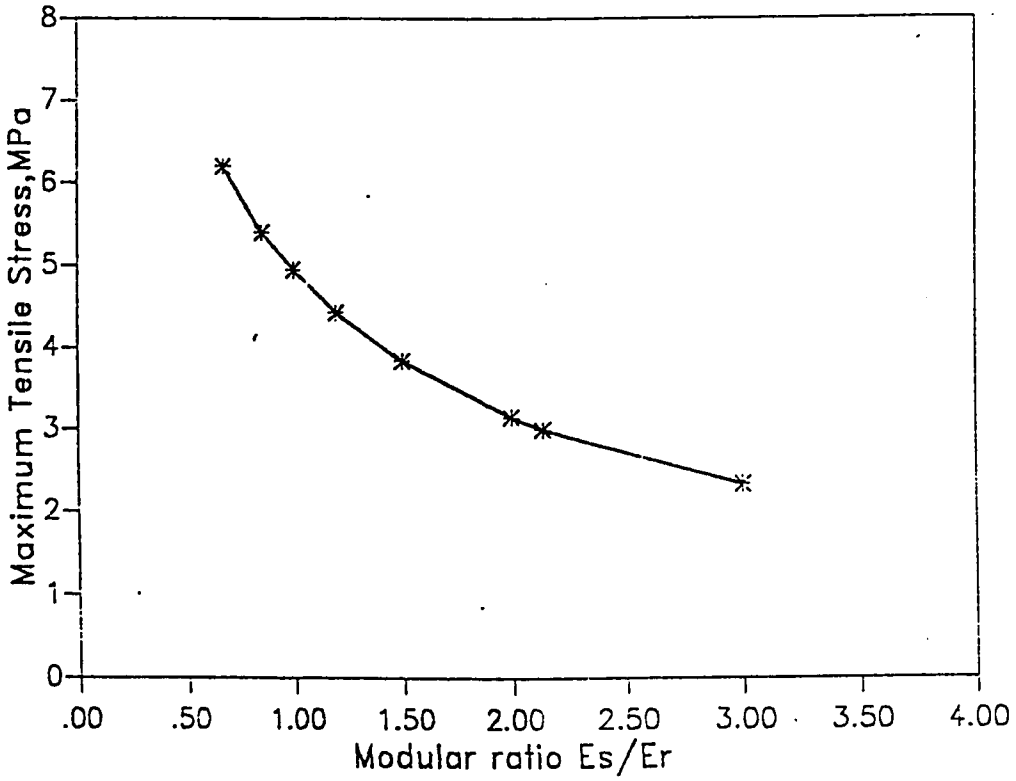

Figure 6.38: Variation of Maximum Tensile Stress with Modular Ratio E_s/E_r (Stress due to Shrinkage Strain of 0.0003)

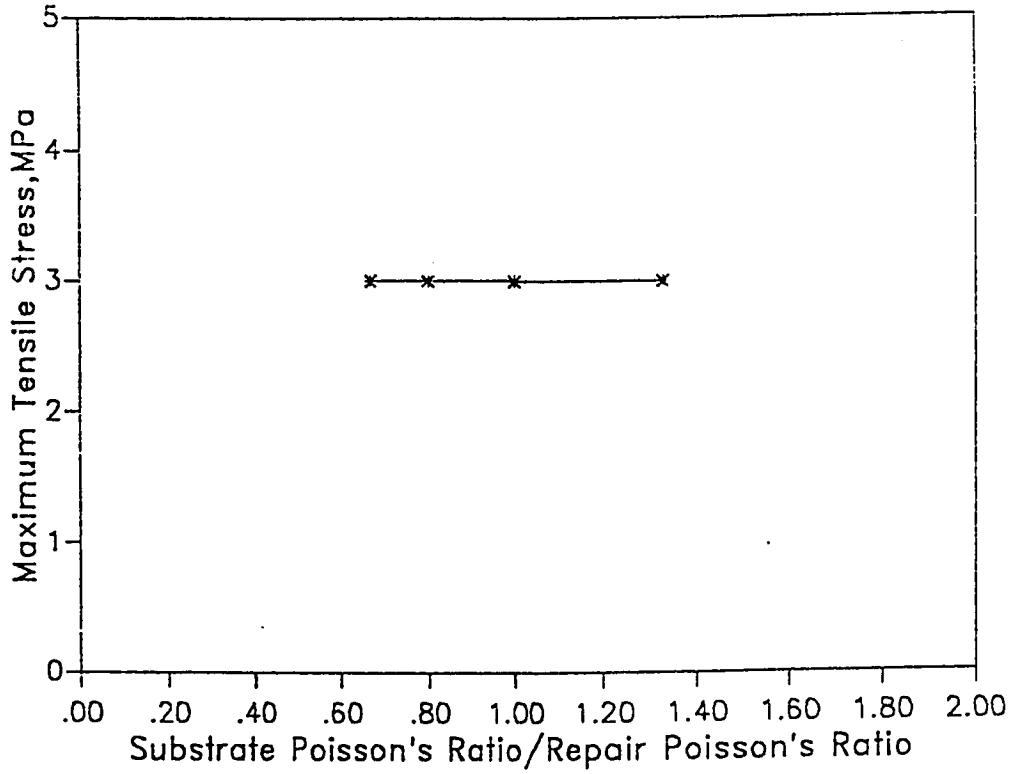

Figure 6.39: Variation of Maximum Tensile Stress with the Ratio ν_s/ν_r (Stress due to Shrinkage Strain of 0.0003)

Chapter 7

CONCLUSIONS AND RECOMMENDATIONS

7.1 Conclusions

The main conclusions drawn from this study can be summarized as follows :

1. The moisture diffusivity K_c governs the moisture diffusion from a cementitious repair material and it is highly moisture dependent. At high levels of moisture content or in the initial period of drying, diffusivity K_c is very high and it decreases rapidly as the moisture content decreases.

2. The moisture loss from the repair material, predicted by the use of the moisture dependent diffusivity K_c, is in better agreement with the experimental data, than the one predicted by the use of a constant diffusivity K_c.

3. The relationship between the moisture loss and free shrinkage strain is not linear, the strain increases rapidly during the initial drying period and as the drying progresses, it slows down and reaches a constant or ultimate value.

4. The non-linear variation of free shrinkage with moisture loss, renders questionable the present practice of predicting free shrinkage strain in ordinary concrete directly by modelling the shrinkage diffusion equation.

5. The actual relationship between free shrinkage strain and moisture loss for the repair material used in this study is expressed by a form similar to the ACI equation for variation of shrinkage with time.

6. The ultimate free shrinakge strain of the repair material had the most significant effect on the level of induced stresses in the repair overlay/substrate concrete system.

7. The higher the ultimate free shrinkage strain in the repair material, the higher are the induced tensile and shear stresses in the repair layer.

8. The maximum tensile stress occurs in the repair layer close to the repair/substrate interface. If the maximum tensile stress exceeds the tensile strength of the repair material it will lead to distress and cracking in the repair layer.

9. The maximum shear stress occurs in the repair layer close to the repair/substrate interface, especially at the ends of the repair layer, which will lead to delamination of the repair layer if the maximum shear stress exceeds the shear strength of the repair material.

10. The restraint provided by the concrete substrate had a significant effect on the

level of induced stresses. The tensile stresses were found to decrease with the increase in the thickness of the repair layer, whereas the shear stresses were found to increase.

11. An acceptable range of ultimate free shrinkage strain for the repair material used in this study is

$$\epsilon_{sh} \leq 0.0003$$

which would lead to shrinkage restraint tensile and shear stresses in the repair material to be within limiting or less than the ultimate values.

12. The elastic modulus of the repair material had a significant effect on the level of induced stresses, *i.e.* the higher the elastic modulus of the repair material the higher are the induces stresses.

7.2 Recommendations

7.2.1 Design of Durable Concrete Repairs

The following recommendations are made with regard to the design of durable repairs using cementitious repair mortars

1. The repair engineer needs to pay special attention to the following:

   (a) the ultimate free shrinkage strain of the repair material (ϵ_{sh});

   (b) the diffusivity K_c of the repair material;

   (c) the modulus of elasticity E_r of the repair material; and

(d) the degree of restraint exerted by the concrete substrate

in order to minimize the probability of failure either by:

- tension cracking of the repair material; or by
- delamination at the interface of repair layer and hardened concrete substrate

2. Materials engineers need to design repair mixes such that:

   (a) diffusivity K_c is low, its gradient with respect to moisture content should not be excessive, especially at high levels of moisture content.

   (b) Control of K_c will lead to lower ultimate levels of free shrinkage strain.

3. Special attention must be paid to the conditions of curing, as ambient humidity affects the ultimate level of free shrinkage strain through the evaporative boundary condition. Use of curing compounds would have a beneficial effect in reducing loss of moisture, especially in the early stages where concrete has not attained maturity.

4. Fibres can be used to improve the tensile strength of repair material and also the proper preparation of contact surface between the repair layer and concrete substrate will lead to an increase in the interface shear strength.

5. Creep has a beneficial effect on reducing tensile stresses in repair layer. However, efforts should be made to use repair materials with a low modulus of

elasticity E, which is specially critical in the early stages of strength development of the repair layer.

6. Recommendations suggested for a concrete repair system to minimize stresses due to drying shrinkage can also be adopted to reduce shrinkage stresses that result in a new two-tier concrete slab system where fresh concrete is poured over a pre-cast unit in order to achieve a composite section without use of formwork.

7.2.2 Future Work

The following recommendations are made with regard to future research work in the area of shrinkage in repaired concrete

1. Further experimental work should be carried out with properly designed specimens so as to obtain more accurate relationships between: (i) diffusivity K_c and moisture content C; and (ii) free shrinkage ϵ_{sh} and moisture loss M, for different repair materials and under different environmental conditions.

2. A non-linear computational model should be developed to model the stresses induced due to drying shrinkage which can predict cracking and delamination with time.

3. The effect of creep on stress relaxation should be considered in the stress analysis along with the early age properties like tensile strength, creep coefficient

and modulus of elasticity of the repair material.

Bibliography

[1] Emmons P. H and A. M. Vaysburd. "Factors affecting the durability of concrete repair: The contractor's viewpoint". *Construction and Building Materials*, 8(1):5–16. 1994.

[2] Emmons P. H, Vaysburd. A. M, and J. E. McDonald. "A rational approach to durable concrete repairs". *Concrete International*, 15(9):40–45, September 1993.

[3] Emberson N. K and G. C. Mays. "Significance of property mismatch in the patch repair of structural concrete, part 1: properties of repair systems". *Magazine of Concrete Research*, 42(152):147–160, September 1990.

[4] Yuan Y. S and M. Marosszeky. "Major factors influencing the performance of structural repair". In *Evaluation and Rehabilitation of Concrete Structures and Innovations in Design, ACI. SP 128-50*, pages 819–837. Detroit, 1992.

[5] Yuan Y. S and M. Marosszeky. "Analysis of corroded reinforced concrete sections for repair". *Journal of Structural Engineering*, 117(7):2018-2034, July 1991.

[6] Emmons P. H, Vaysburd. A. M, and J. E. McDonald. "Concrete repair in the future turn of the century - any problems?". *Concrete International*, 16(3):42–49. March 1994.

[7] Emmons P. H and A. M. Vaysburd. "The total system concept - necessary for improving the performance of repaired structures". *Concrete International*, 17(3):31–36, March 1995.

[8] Emberson N. K and G. C. Mays. "Design of patch repairs: Measurements of physical and mechanical properties of repair systems for satisfactory structural performance". In *Protection of Concrete. ed. by Dhir,R.K. and Green,J.W.*, pages 937–954. E.& F.N.Spon, London, 1990.

[9] Edward M. R and B. S. Martin. "Selection criteria for concrete repair materials". *Concrete International*, pages 46–49, September 1989.

[10] Carlson R. W. "Drying shrinkage of large concrete members". *Proceedings Of the American Concrete Institute*, 33:327–336, January-February 1937.

[11] Pickett G. "Shrinkage stresses in concrete". *Journal Of the American Concrete Institute*, 17(3 & 4):165–204 & 361–398, January & February 1946.

[12] Becker N. K and C. Macinnis. "A theoretical method for predicting the shrinkage of concrete". *Journal Of the American Concrete Institute*, 69:652–657, September 1973.

[13] Iding R and B. Bresler. "Prediction of shrinkage stresses and deformations in concrete". In *Fundamental Research on Creep and Shrinkage of Concrete, ed. by Wittmann. F.H.*, pages 341–352. Martinus Nijhoff Pub., The Hague, 1982.

[14] Sakata K. "A study on moisture diffusion in drying and drying shrinkage of concrete". *Cement and Concrete Research*, 13(2):216–224. 1983.

[15] Penev D and M. Kawamura. "Moisture diffusion in soil-cement mixtures and compacted lean concrete". *Cement and Concrete Research*, 21(1):137–146. 1991.

[16] Concrete Society Working Party. "Non-structural cracks in concrete". Technical Report 22. The Concrete Society, December 1982.

[17] Malhas F. A. "The effect of drying shrinkage on the bond strength between repair mortars and concrete". In *Proc. Second ASCE-SAS Regional Conference and Exhibition 'Save The Environment'. Beirut. Lebanon.* pages 589–603. November 1995.

[18] Segerlind L. J. "*Applied Finite Element Analysis*". John Wiley & Sons, Inc., New York. 1984.

[19] Bathe K. J and M. R. Khoshgoftaar. "Finite element formulation and solution of nonlinear heat transfer". *Nuclear Engineering and Design*, 51:389–401, 1979.

[20] Hinton E and D. R. J. Owen. "*Finite Element Programming*". Academic Press, London. 1977.

[21] Owen D. R. J and E. Hinton. "*Finite Elements in Plasticity: Theory and Practice*". Pineridge Press Limited, Swansea, U.K., 1986.

[22] Logan D. L. "*A First Course in the Finite Element Method*". PWS-KENT Publishing Company, Boston, U.S.A, 1992.

[23] Crank J. "*The Mathematics of Diffusion*". Oxford at the Clarendon Press, 1975.

[24] ACI Committee 209. "Prediction of creep, shrinkage and temperature effects in concrete structures". Technical report, ACI Manual of Concrete Practice. 1994.

[25] Al-Ustath A. "Evaluation of repair materials with emphasis on crack injection repair". Master's thesis, King Fahd University of Petroleum and Minerals, Dhahran. KSA, 1990.

[26] Sakata K, Nishigaki. M, and O. Kuramoto. "Finite element analysis of non-linear moisture transfer problems in concrete". Technical Report 4, Reports of Research and Development. Okayama University Computer Center, March 1980.

[27] Lyness J. F, Owen D. R. J, and O. C. Zienkiewicz. "The finite element analysis of engineering systems governed by a non-linear quasi harmonic equation". *Computers and Structures*, 5:65-79, 1975.

[28] Bloom R and A. Bentur. "Free and restrained shrinkage of normal and high-strength concretes". *ACI Materials Journal*, 92(2):211-217. March-April 1995.

[29] Mehta P. K. "*CONCRETE: Structure, Properties and Materials*". Prentice-Hall, Inc., New Jersey, 1986.

[30] Warner J. "Selecting repair materials". *Concrete Construction*, pages 865-871, October 1984.

[31] Birkeland H. W. "Differential shrinkage in composite beams". *Journal of the American Concrete Institute*, 31(11):1123-1136. May 1960.

[32] Pigeon M and F. Saucier. "Durability of repaired concrete structures". In *Advances in Concrete Technology, ed. by Malhotra. V.M.*, pages 741-773. CANMET-Canada Centre for Mineral and Energy Technology, Canada, 1992.

[33] Staynes B. W and T. A. Willway. "The composite behaviour and delamination of thin surface overlays and repairs - identification and measurement of controlling parameters ". In *Proc. 5th International Congress on Polymers in Concrete. Brighton. U.K.*, pages 301-304. September 1987.

[34] Ignatiev N and S. Chatterji. "On the mutual compatibility of mortar and concrete in composite members". *Cement and Concrete Composites*, 14:179-183, 1992.

[35] Decter M. H and M. J. Humphrey. "Primary properties of cementitious repair mortars to achieve long-term durability". In *Proc. 4th International Conference on Deterioration and Repair of Reinforced Concrete in Arabian Gulf, Bahrain*, pages 855-872, October 1993.

[36] Dcctcr M. H and R. W. Lambc. "New materials for concrete repair - development and testing". In *Proc. of the International RILEM/CSIRO/ACRA Conference on Rehabilitation of Concrete Structures, Melbourne, Australia*, 1992.

Appendix A

Derivation of Equation for Moisture Content C at a Distance x from the Drying Surface

Consider a porous body of length l_i with a diffusible moisture W_o per unit volume as shown in Figure A.1. If it is sealed along the four sides of the length and moisture is allowed to diffuse from the two ends, then the moisture flux at the centre of length l_i is given as

$$q_i = W_o l_i S - w_i \tag{A.1}$$

where S is the area of drying surface and w_i is moisture loss in the body. Similarly, the moisture flux at the centre of another porous body of length l_{i-1} shown in Figure A.1 is given as

$$q_{i-1} = W_o l_{i-1} S - w_{i-1} \tag{A.2}$$

where w_{i-1} is moisture loss in the body of length l_{i-1}.

Now consider a control volume, which is common to both bodies, with length from $\frac{l_{i-1}}{2}$ to $\frac{l_i}{2}$ as shown in Figure A.1. The moisture flux flowing into this control

volume is $\frac{q_i}{2}$ and the moisture flux flowing out of this control volume is $\frac{q_{i-1}}{2}$. The moisture content $C(x_i, t)$ at any distance x_i from the drying surface of a body of length of l_i, expressed as percentage of initial diffusible moisture, is given as

$$C(x_i,t) = \left[\frac{\frac{1}{2}(W_o l_i S - w_i) - \frac{1}{2}(W_o l_{i-1} S - w_{i-1})}{W_o\left(\frac{l_i}{2} - \frac{l_{i-1}}{2}\right) S}\right] * 100$$

$$= \left[\frac{W_o S(l_i - l_{i-1}) - w_i + w_{i-1}}{W_o S(l_i - l_{i-1})}\right] * 100 \qquad \text{(A.3)}$$

Therefore

$$C(x_i,t) = \left[1 - \frac{(w_i - w_{i-1})}{W_o S(l_i - l_{i-1})}\right] * 100 \qquad \text{(A.4)}$$

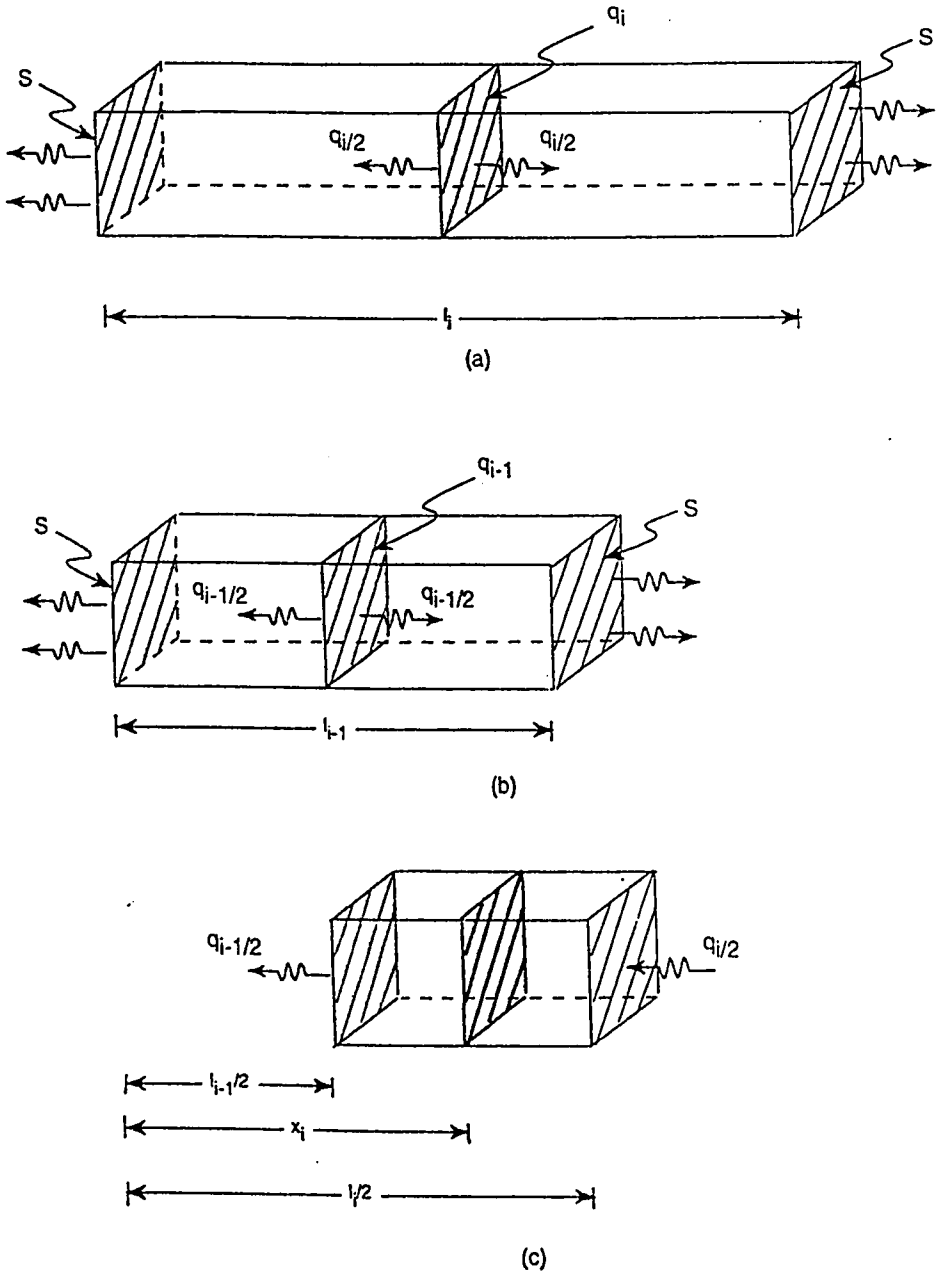

Figure A.1: Moisture Diffusion in Bodies of Lengths (a) l_i, (b) l_{i-1} and (c) Control Volume

Appendix B

Input Data to the Code MSTDIFF1

```
INPUT DATA FOR ONE-DIMENSIONAL MOISTURE DIFFUSION PROBLEM
NPOIN NELEM NBOUN NMATS NPROP DTIME NINCS MDIFF IFORM AMCONT TOLER
  7     6     0     1     4    1.0   50     4     2    0.99  0.01
MATERIAL PROPERTIES
MATNO    AREA    PERI   SFACT   CEQLB
  1      20.0    0.0    1.00    0.50
DIFFUSIVITY PARAMETERS
DCOFO   CONSTA  CONSTB
0.1175  0.0509   1.878
ELEMENT CONNECTIVITY DATA
ELEMENT  I   J   MATNO
   1     1   2     1
   2     2   3     1
   3     3   4     1
   4     4   5     1
   5     5   6     1
   6     6   7     1
NODAL COORDINATES
NODE  COORD
 1     0.0
 2     1.0
 3     3.0
 4     5.0
 5     7.0
 6     9.0
 7    10.0
PRESCRIBED NODAL MOISTURE CONTENT
NODE  CODE  VALUE
CODE FOR END INSULATION
LEFT   RIGHT
 1       0
```

Appendix C

Input Data to the Code MSTDIFF2

```
INPUT DATA FOR TWO-DIMENSIONAL MOISTURE DIFFUSION PROBLEM
NPOIN NELEM NNODE NBOUN NMATS NPROP IFORM DTIME NINCS MDIFF AMCONT TOLER
 27    16     4     0     1     4     1    1.0    5     4    0.98  0.01
MATERIAL PROPERTIES
MATNO     BM      BS       G       Q
  1      0.30    0.15     0.30    0.15
DIFFUSIVITY PARAMETERS
DCOFO   CONSTA  CONSTB
0.1175  0.0509   1.878
ELEMENT CONNECTIVITY DATA
ELEMENT  I   J   K   M   MATNO
   1     1   4   5   2     1
   2     2   5   6   3     1
   3     4   7   8   5     1
   4     5   8   9   6     1
   5     7  10  11   8     1
   6     8  11  12   9     1
   7    10  13  14  11     1
   8    11  14  15  12     1
   9    13  16  17  14     1
  10    14  17  18  15     1
  11    16  19  20  17     1
  12    17  20  21  18     1
  13    19  22  23  20     1
  14    20  23  24  21     1
  15    22  25  26  23     1
  16    23  26  27  24     1
  NODAL COORDINATES
  NODE  X-DIR   Y-DIR
   1     0.00    0.00
   2     0.00    1.00
   3     0.00    2.00
   4     1.00    0.00
   5     1.00    1.00
```

```
 6      1.00     2.00
 7      2.00     0.00
 8      2.00     1.00
 9      2.00     2.00
10      3.00     0.00
11      3.00     1.00
12      3.00     2.00
13      5.00     0.00
14      5.00     1.00
15      5.00     2.00
16     10.00     0.00
17     10.00     1.00
18     10.00     2.00
19     15.00     0.00
20     15.00     1.00
21     15.00     2.00
22     20.00     0.00
23     20.00     1.00
24     20.00     2.00
25     25.00     0.00
26     25.00     1.00
27     25.00     2.00
PRESCRIBED NODAL MOISTURE CONTENT
NODE  CODE  VALUE
CODE FOR SURFACE INSULATION
TOP    BOTTOM
 0       0
NUMBER OF CONVECTING EDGES
NEDGE
 10
LOCATION OF CONVECTING EDGES
ELEM  NODEI  NODEJ   ICODE
 1      2      1       4
 2      3      2       4
 2      6      3       3
 4      9      6       3
 6     12      9       3
 8     15     12       3
10     18     15       3
12     21     18       3
14     24     21       3
16     27     24       3
```

Appendix D

Input Data to the Code STRSRSYS

```
INPUT DATA FOR SHRINAKGE STRESS ANALYSIS
NPOIN NELEM NVFIX NTYPE NNODE NMATS NGAUS NSTRE
  93   24    13     1     8     2     3     3
ELEMENT CONNECTIVITY DATA
ELEMENT MATNO  I   J   K   L   M   N   O   P
   1      1    1  14  21  22  23  15   3   2
   2      1    3  15  23  24  25  16   5   4
   3      1    5  16  25  26  27  17   7   6
   4      1    7  17  27  28  29  18   9   8
   5      1    9  18  29  30  31  19  11  10
   6      2   11  19  31  32  33  20  13  12
   7      1   21  34  41  42  43  35  23  22
   8      1   23  35  43  44  45  36  25  24
   9      1   25  36  45  46  47  37  27  26
  10      1   27  37  47  48  49  38  29  28
  11      1   29  38  49  50  51  39  31  30
  12      2   31  39  51  52  53  40  33  32
  13      1   41  54  61  62  63  55  43  42
  14      1   43  55  63  64  65  56  45  44
  15      1   45  56  65  66  67  57  47  46
  16      1   47  57  67  68  69  58  49  48
  17      1   49  58  69  70  71  59  51  50
  18      2   51  59  71  72  73  60  53  52
  19      1   61  74  81  82  83  75  63  62
  20      1   63  75  83  84  85  76  65  64
  21      1   65  76  85  86  87  77  67  66
  22      1   67  77  87  88  89  78  69  68
  23      1   69  78  89  90  91  79  71  70
  24      2   71  79  91  92  93  80  73  72
 NODAL COORDINATES
 NODE  X-COORD  Y-COORD
  1      0.00     0.00
  3      0.00    10.00
  5      0.00    20.00
  7      0.00    30.00
```

9	0.00	40.00
11	0.00	50.00
13	0.00	60.00
21	25.00	0.00
23	25.00	10.00
25	25.00	20.00
27	25.00	30.00
29	25.00	40.00
31	25.00	50.00
33	25.00	60.00
41	50.00	0.00
43	50.00	10.00
45	50.00	20.00
47	50.00	30.00
49	50.00	40.00
51	50.00	50.00
53	50.00	60.00
61	75.00	0.00
63	75.00	10.00
65	75.00	20.00
67	75.00	30.00
69	75.00	40.00
71	75.00	50.00
73	75.00	60.00
81	100.00	0.00
83	100.00	10.00
85	100.00	20.00
87	100.00	30.00
89	100.00	40.00
91	100.00	50.00
93	100.00	60.00

PRESCRIBED NODAL DISPLACEMENTS

NODE	ICODEX	ICODEY	VALUEX	VALUEY
81	1	0	0.0	0.0
82	1	0	0.0	0.0
83	1	0	0.0	0.0
84	1	0	0.0	0.0
85	1	0	0.0	0.0
86	1	0	0.0	0.0
87	1	0	0.0	0.0
88	1	0	0.0	0.0
89	1	0	0.0	0.0
90	1	0	0.0	0.0
91	1	0	0.0	0.0
92	1	0	0.0	0.0
93	1	0	0.0	0.0

MATNO	PROPERTIES			
	E	NU	T	CODESH
1	30000.0	0.2	50.0	0.0
2	14000.0	0.2	50.0	1.0

CODE FOR LOADING TYPE

IPLOD	IGRAV	IEDGE	ISHRK
0	0	0	1

PRESCRIBED NODAL SHRINKAGE STRAINS

NODE	STRAIN
11	-0.0003
12	-0.0003
13	-0.0003
19	-0.0003
20	-0.0003
31	-0.0003
32	-0.0003
33	-0.0003
39	-0.0003
40	-0.0003
51	-0.0003
52	-0.0003
53	-0.0003
59	-0.0003
60	-0.0003
71	-0.0003
72	-0.0003
73	-0.0003
79	-0.0003
80	-0.0003
91	-0.0003
92	-0.0003
93	-0.0003

OUTPUT PARAMETERS

3

VITAE

- Mohammed Asad
- Born in 1970 at Hyderabad, India.
- Permanent Address :

  H.No.10-3-291/1/G/1

  Vijayanagar Colony

  Hyderabad 500057, INDIA.
- Received Bachelor of Engineering (**B.E.**) degree in Civil Engineering from Osmania University, Hyderabad, India in August 1991.
- Received Master of Science (**M.S.**) degree in Civil Engineering with specialization in Structures from KFUPM, in December 1995.